01 Jan 1971

Damping capacity of a model steel structure

Dixon Rea

R. W. Clough

Jack G. Bouwkamp
Missouri University of Science and Technology

DAMPING CAPACITY OF A MODEL STEEL STRUCTURE

–Dixon Rea, R. W. Clough, J. G. Bouwcamp

Earthquake Engineering Research Center
College of Engineering
University of California–Berkeley

Committee of Structural Steel Producers • Committee of Steel Plate Producers

american iron and steel institute

150 East 42nd Street, New York, N.Y. 10017

JANUARY, 1971

EARTHQUAKE ENGINEERING RESEARCH CENTER

DAMPING CAPACITY OF A MODEL STEEL STRUCTURE

by

DIXON REA

R. W. CLOUGH

J. G. BOUWKAMP

A Report to

American Iron and Steel Institute, New York

College of Engineering

University of California
Berkeley, California

December 1969

Committee of Structural Steel Producers • Committee of Steel Plate Producers

american iron and steel institute

150 East 42nd Street, New York, N.Y. 10017

ABSTRACT

The damping capacities of seven model steel structures, each consisting of a heavy steel platform supported on four columns, have been determined from forced vibration tests. The vibrations were produced by an eccentric-mass vibration generator, and the amplitudes ranged from small displacements up to slightly greater than yield displacement. The tests were terminated at the higher amplitudes once fatigue cracks formed in any of the joint welds in the columns.

For vibration amplitudes up to a critical amplitude slightly less than yield displacement, the damping factors of the structures were constant, independent of amplitude, and ranged between .15 and .25% for different structures. At vibration amplitudes greater than the critical amplitude, the damping factors of the structures became functions of amplitude. For example, the damping factor of one test structure increased from .15 to 1.2% as the displacement amplitude increased from 1.1 to 1.4 inches. The last structure tested revealed that a few cycles of vibration at amplitudes greater than the critical amplitude would increase these values slightly.

Finally, the results summarized above are compared with the results of: (i) experimental work conducted by Lazan; (ii) reversed loading tests conducted on cantilever beams of similar construction to those tested in the work described in this report; and (iii) experimental work conducted by Hanson.

TABLE OF CONTENTS

Page

LIST OF FIGURES

LIST OF TABLES

CHAPTER 1

INTRODUCTION

1.1 Background

The more energy a structure dissipates while vibrating, the less strength it requires to withstand a prescribed earthquake ground motion. Therefore, the ability to estimate damping capacity of a structure in its design stages should lead to more efficient design for earthquake forces. The damping capacity of a structure vibrating at small amplitudes can be estimated if a dynamic test has been conducted already on a similar structure. The results from a number of dynamic tests are available, e.g. (1)* and (2).

Even if it were economically feasible to subject a real structure to vibration amplitudes large enough to cause structural damage, existing vibration generators lack sufficient power to do so. In order to determine the damping capacity of real structures vibrating at large amplitudes (in the case of steel structures, amplitudes large enough to cause yielding in a number of members) an alternative approach is required. One approach is to determine experimentally the energy dissipation capacity of individual elements of real structures vibrating at large amplitudes and then use the results to predict the damping capacities of real structures analytically.

Such an approach seems readily applicable to steel frame structures. Hanson has already performed tests (3) in which a model steel structure consisting of a platform supported on four columns, was vibrated by means of

---

*Numbers in parentheses refer to References listed in Appendix 1.

eccentric-mass vibration generators (4). The columns which were designed so that large plastic deformations could be produced with the power available from the machines, were fabricated by welding a short length of structural steel I-section to each end of a length of tubular section, see Fig. 1.1. The vibration of the structure caused bending about the weak axes of the I-sections' webs.

The tests described in this report were performed on model steel structures which also consisted of a platform supported on four columns. However, the columns were fabricated entirely from lengths of I-sections. Thus, they were a reasonable representation of elements in full-scale steel structures, even though, due to power limitations, only small zones of plastic deformations might be formed in them during the tests.

The vibration amplitudes of the structures tested ranged from small displacements up to amplitudes slightly greater than yield displacement. The damping capacities of the structures were determined in this range. Generally, a rapid increase of damping capacity was observed at amplitudes near the yield displacement. This increase of damping capacity is discussed in relation to the results of tests performed by Lazan (5, 6) and Hanson (3, 7), and also is related to the results obtained from reversed bending tests on cantilever beams (8) similar to those tested in the work described in the report.

1.2 Acknowledgment

The authors would like to express their appreciation to the American Iron and Steel Institute, New York, for sponsoring the research work described in this report. Also, the contributions of S. Cherem and M. K. Kaul, graduate research assistants, are gratefully acknowledged.

CHAPTER 2

EXPERIMENTAL APPARATUS

2.1 Test Structures

The design of the test structures employed in this study was governed by a number of factors. First, the natural frequency of the vibration mode which would be excited by the vibration generator had to lie in the range 2 to 7 cps (the optimum frequency range for the vibration generator). In addition, the natural frequencies of all other vibration modes had to be kept well separated from the natural frequency of that mode. Second, it was necessary that the major source of energy dissipation should result from the inelastic behavior of the structural steel; energy dissipation in joints and energy transmission to the ground, etc., were to be minimal. Finally, the structures were to be fabricated from standard steel sections, and were required to be small enough so the power available from the vibration generators would be sufficient to cause local plastic deformations.

The above factors resulted in a test structure consisting of a heavy steel platform supported by four steel columns as shown in Fig. 2.1. The vibration generators were bolted to the top of the platform (Figs. 2.1 and 2.2) so that they would act with the platform as a rigid body. The rigid platform contained most of the mass in the system, and it had three significant degrees of freedom; the motion of the center of gravity of the mass could be defined essentially by two mutually perpendicular translational coordinates and one rotational coordinate, all in the horizontal plane. The four columns provided the platform with resistance to motion in these degrees of freedom.

The rectangular platform had overall plan dimensions of 10 ft x 7 ft, see Fig. 2.3 Two 10 x 12 WF beams formed the longer sides of the

platform. The WF beams were cross-connected by four 6 ft lengths of rectangular tubing welded to their webs and the undersides of their top flanges. The two outer lengths of rectangular tubing had outside dimensions of 8 in x 3 in and their center-lines were located 6 in from the ends of the WF beams. The two inner lengths of rectangular tubing had outside dimensions of 6 in x 6 in and were spaced equally between the outer lengths. Four 10 ft lengths of 6 in x 2 in channel sections were welded across the tops of the rectangular tubing and ran the length of the platform, Fig. 2.3.

The columns, consisting basically of top and base plates butt-welded to a length of steel section, were attached to the platform by pin connections and fixed at the base to a 2 ft thick concrete floor slab. The pin connections were formed by fitting a trunnion axis assembly to a self-aligning ball bearing housed in a pillow block, see Fig. 2.4(a). The pillow blocks were bolted to the top plate of the column and the trunnion axis assemblages bolted to the underside of the platform. The base plates of the columns were bolted to 2-1/2 in thick attachment plates, Fig. 2.4(b), which in turn were prestressed to the floor slab by 1-1/2 in diameter rods.

The first type of column, A.1, was fabricated from a length of 4 x 4 WF 13 lb section and had an overall length of 7 ft-0 in as shown in Fig. 2.5(a). The top plates, Fig. 2.5(b), were 6 x 6 x 1/2 in with two threaded holes provided for bolting to the pillow blocks. The base plates were 8 x 8 x 1/2 in with four clearance holes for 3/4 in bolts, Fig. 2.5(c). The clearance holes matched the threaded holes in the heavy attachment plates described previously, and thus the base plates could be bolted to the attachment plate as shown in Fig. 2.6.

Design details of column type A.1 were varied to obtain types A.2, A.3 and A.4. Type A.2 was the same as A.1 except for two trapezoidal straps, Fig. 2.5(d), which strengthened the joint between the steel section and the base plate. The tests conducted on the first test structure, assembled with two columns of type A.1, and two of type A.2, showed that the trapezoidal straps improved considerably the fatigue strength of the joint. The joint's fatigue strength was increased further by making the straps parabolic, Fig. 2.5(e), instead of trapezoidal. Parabolic straps were then used in the fabrication of column types A.3 and A.4. Column type A.3 differed from the other columns in having 4 x 4 M 10 lb sections instead of 4 x 4 WF 13 lb sections. Type A.3 was made only once when there was difficulty in obtaining WF sections.

The first five test structures assembled made use of columns of types A.1, A.2, A.3 and A.4, as indicated in Table 2.1 (this table also summarizes the design details of these columns). During these tests all four columns of the structure were subjected to the same dynamic stresses. In order to reduce the number of columns used in later tests, two dummy columns were fabricated. The dummy columns were attached to the foundation attachment plates as well as to the platform by means of pinned connections. Thus they were not subject to cyclic stress and did not suffer any fatigue damage; only two new columns were required for each test. Test structures No. 6 and 7 made use of the dummy columns as shown in Fig. 2.7.

Two types of columns, B.1 and B.2, were used in test structures No. 6 and 7. These types were 5 ft-4 1/2 in in overall length and were fabricated from lengths of 4 x 4 WF 13 lb sections. (The overall length of columns of types B.1 and B.2 was made 5 ft-4 1/2 in so the columns would be

identical to specimens undergoing cyclic load tests in a complementary research project sponsored by the National Science Foundation). They both made use of parabolic straps and type B.1, Fig. 2.8(a), was identical to type A.4 except for the length of standard steel section. Type B.2 was identical to type B.1 except it had an 8 in long reduced section in each flange starting 1 1/2 in above the parabolic straps. The 4 in wide flanges were tapered from both ends of the 8 in section to leave a section 3 in wide and 5 in long in the middle, see Fig. 2.8(b) and Fig. 2.6. The purpose of this reduced section was to induce the yielding to occur at places away from welds, where the yielding had occurred during the tests on the previous structures. The design details of column types B.1 and B.2 are also summarized in Table 2.1.

TEST STRUCTURE	COLUMNS IN TEST STRUCTURE					
	Type	Number	Axis of Bending	Section	Length	Base Joint
1	A.1 A.2	2 2	Weak Weak	4x4 WF 4x4 WF	84" 84"	Simple butt Trapezoidal Straps
2	A.2	4	Weak	4x4 WF	84"	Trapezoidal Straps
3	A.2	4	Strong	4x4 WF	84"	Trapezoidal Straps
4	A.3	4	Weak	4x4 WF	84"	Parabolic Straps
5	A.4	4	Weak	4x4 M	84"	Parabolic Straps
6	B.1 Dummy	2 2	Weak ---	4x4 WF ----	64 1/2"	Parabolic Straps
7	B.2 Dummy	2 2	Weak ----	4x4 WF* ----	64 1/2"	Parabolic Straps

* Reduced section

Table 2.1 Types of Columns in Each Test Structure.

2.2 Vibration Generators

The dynamic forces were applied to the test structure by one of the two vibration generators bolted to the top of the steel platform, Figs. 2.1 and 2.2. It was never necessary to use the second machine since, for these tests, a single machine provided sufficient power. The vibration generators (4) were developed at the California Institute of Technology under the supervision of the Earthquake Engineering Research Institute for the Office of Architecture and Construction, State of California. The machines operate on the eccentric-mass principle and each consists essentially of two counter-rotating baskets mounted on a common vertical shaft. They are driven by 1-1/2 HP DC motors and can develop a rectilinear sinusoidal force up to a maximum amplitude of 5,000 lb and maximum frequency of 10 cps.

The machines were developed to test full-scale structures. In such tests heavy lead plates are inserted in the baskets, but these weights were too heavy for use in these tests in which the maximum desired force amplitude was less than 100 lb. Instead, small 18 gage steel plates (3 1/4 x 4 7/16 in weighing .145 lb) were used as the unit of eccentric-mass, and the baskets had to be carefully counter-balanced (by a static balance procedure) in order to produce force amplitudes of sufficiently small magnitude.

The speed of rotation of the motor driving the baskets is controlled by an Electronic Amplidyne housed in a control unit. The machines can operate in the frequency range 0.5 to 10 cps, but more accurate results can be obtained if it is possible to keep the range of operation from 2 to 7 cps.

2.3 Transducers

The responses of the test structures were measured in terms of the acceleration and displacement of the platform and strains at various locations on the columns. The platform acceleration was measured by a Statham ± 5 g accelerometer, and displacement by a ± 3.0 in Sanborn DC-DC differential transformer. Both standard SR-4 strain gages, and SR-4 strain gages of the post-yield type attached at locations where strains greater than yield strain were expected, were used to detect strains in the columns.

2.4 Recording Equipment

The signals from the accelerometer and strain gages were fed to a Honeywell carrier amplifier system and then to an ultra-violet recorder (Visicorder). The output of the displacement transducer was fed directly to the Visicorder.

The frequency of the exciting forces was measured by a digital counter which recorded a signal from a tachometer driven by the DC motor. The frequency of this signal was 300 times the frequency of the exciting force.

2.5 Calibration

The accelerometer, displacement meter, and strain gage bridges were calibrated individually. The accelerometer was calibrated by rotating it through 180° to cause a change of 2 g in the measured acceleration. The displacement meter was calibrated by moving the core through known distances, and the strain-gage bridges were calibrated by switching a known resistance in parallel with one of the gages.

The digital counter was checked against the frequency of the AC power supply, and on a few occasions a check was made to verify that the measured acceleration agreed with the product of the displacement and frequency squared.

CHAPTER 3

EXPERIMENTAL RESULTS

3.1 Test Structure No. 1

Test structure no. 1 was assembled with two columns of type A.1 and two columns of type A.2, see Table 2.1. Column type A.2 was similar to type A.1, except for the addition of trapezoidal straps at the joint between the column section and the base plate. The columns were oriented in the structure so they would undergo bending about their weak axes in the dynamic tests. The purpose of the tests was the collection of data to plot frequency response curves.

A number of frequency responses for different levels of exciting force amplitude have been plotted for structure no. 1. The exciting force amplitude was varied by changing the number of steel plates acting as eccentric mass in the rotating baskets. The resonant frequency was determined in an initial exploratory test. In subsequent tests of differing force levels, the vibration generator was started and the frequency of excitation increased to within 1 or 2% of the resonant frequency. The exciting frequency was increased in small steps until resonance was achieved, and then increased further until it was 1 or 2% greater than the resonant frequency. This range of frequencies was sufficient to obtain the resonance curve of the vibration mode under investigation.

At each frequency step the vibration was given time to become steady-state, and the platform's acceleration and displacement, as well as strains at various locations on the columns were recorded. At the same time the frequency of excitation, as measured by the digital counter, was observed and written on the recording chart alongside the appropriate traces. The procedure was continued until sufficient data to define a complete resonance curve were obtained.

A number of frequency response curves for test structure no. 1 are shown in Figs. 3.1 and 3.2. In these figures, the displacement amplitude of the platform (measured by means of the differential transformer) has been plotted as a function of the frequency. The curve's resonant frequencies, those corresponding to maximum response, can be read directly from the figures. The resonant frequencies depend slightly on vibration amplitude, decreasing from 2.435 cps at a displacement amplitude of 0.2 in to 2.424 cps at a displacement amplitude of 1.6 in. The exciting force amplitude at resonance and the damping capacity of each curve are indicated in the figures.

The exciting force amplitude, P, may be calculated from

$$P = 2m\,\omega^2\,r \tag{3.1}$$

in which m is the mass of the steel plates inserted in one basket of the vibration generator, r the eccentricity of the center of gravity of the steel plates, and ω the circular frequency of the excitation. Thus, the resonance curves result from a force whose amplitude increases with the square of the exciting force frequency. The curves could have been normalized to a constant force amplitude by dividing each displacement by the square of the corresponding frequency of excitation, but this was considered unnecessary since the force changed only by about 2% over the frequency range of the resonance curves. The resonant force amplitude shown for each resonance curve in Figs. 3.1 and 3.2 was obtained by substituting the resonant circular frequency for ω in the above formula. It ranged from 1 to 11 lb.

The damping capacity of the structure was evaluated from the resonance curves in terms of a damping factor ζ defined by

$$\zeta = \frac{\Delta f}{2f} \tag{3.2}$$

in which Δf is the difference in frequency of the two points on the resonance curve with amplitude $1/\sqrt{2}$ times the resonant amplitude and f is the resonant frequency. The damping factors evaluated from the resonance curves are also shown in Figs. 3.1 and 3.2. The damping factor ranged from 0.16% to 0.28%.

The resonant displacement amplitudes of the resonance curves have been plotted against their corresponding exciting force amplitudes in Fig. 3.3. (The results from all recorded frequency responses are shown in Fig. 3.3, even though only a few of these curves are shown in Figs. 3.1 and 3.2.) The resonant displacement amplitude (x) of a structure is related to the exciting force amplitude (P) by

$$x = \frac{1}{2K\zeta} P \tag{3.3}$$

in which K is the equivalent spring stiffness and ζ the damping factor. Since x has a linear relationship with P in Fig. 2.3, and K is essentially constant because the resonant frequency of the system is essentially independent of amplitude, Eq. 3.3 shows that ζ must also be essentially independent of amplitude.

The dynamic tests were terminated on structure no. 1 when fatigue cracks developed in the welds at the base joints of the two type A.1 columns.

3.2 Test Structure No. 2

In test structure no. 1 fatigue cracks had developed in the welds at the base of both type A.1 columns. However, cracks did not occur in either column of type A.2, even though these columns had been subjected to the same stress history as the columns of type A.1. Therefore, a second structure, test structure no. 2 was assembled with all four columns of type A.2. Again, the columns were placed in the structure to undergo bending about their weak axes. The tests were similar to those conducted on test structure no. 1.

Some of the frequency response curves obtained for test structure no. 2 are shown in Fig. 3.4. The resonant frequency of the structure was 2.440 cps while vibrating at the larger amplitudes of vibration, and slightly greater while vibrating at the smaller amplitudes of vibration. The resonant force amplitude and the damping capacity evaluated for each resonance curve are indicated on Fig. 3.4. The maximum resonant force amplitude was 18.1 lb and the damping factor ranged from 0.18 to 0.27%.

The resonant displacement amplitudes of all the resonance curves recorded are plotted against their corresponding resonant force in Fig. 3.5. The resulting curve shown in Fig. 3.5 reveals that at small amplitudes of vibration the relationship between the resonant displacement amplitude and the resonant force amplitude is linear (as was the case for test structure no. 1). However, at displacement amplitudes approaching the yield displacement of the structure, the slope of the curve decreases abruptly and approaches zero. Because the resonant frequency of the structure did not change appreciably at the higher amplitudes of vibration, the stiffness of the structure must have remained essentially constant. Thus, since the slope

of these curves is inversely proportional to the stiffness and damping factor of the structure, the damping factor must have increased rapidly when the vibration amplitudes were in the region of the yield displacement.

The dynamic tests were again terminated by the formation of fatigue cracks. In this structure the cracks occurred in the welds at the top of the trapezoidal straps and in the flanges of one of the columns at the top of the straps.

3.3 Test Structure No. 3

After the dynamic tests on test structure no. 2 had been completed, two columns of type A.2 that had been fabricated previously remained unused. These two columns, together with two uncracked columns from test structure no. 2, were used to assemble test structure no. 3. The columns were placed in the structure so they would undergo bending about their strong axes during the dynamic tests.

The frequency response curves obtained from test structure no. 3 are shown in Fig. 3.6. The resonant frequency decreased from 4.380 cps at a displacement amplitude of 0.4 in to 4.360 cps at a displacement amplitude of 1.2 in. The maximum resonant force amplitude was 44.5 lb and the damping factor ranged from 0.16 to 0.22%.

Resonant displacement amplitudes are plotted as a function of resonant force amplitude in Fig. 3.7; the resulting curve is linear. However, fatigue cracks developed at relatively small vibration amplitudes in one of the columns that had been used previously in test structure no. 2.

Hence, the vibration amplitudes did not reach the yield displacement of the structure in this test.

3.4 Test Structure No. 4

A new type of column, type A.3, was used to assemble test structure no. 4. In columns of type A.3, the shape of the straps at the base of the columns were parabolic instead of trapezoidal as in type A.2, see Fig. 2.5. This change was made in an attempt to reduce the stress concentrations and to increase further the fatigue strength of the joint at the base of the columns.

Some of the frequency response curves that were observed for test structure no. 4 are shown in Figs. 3.8 and 3.9. The resonant frequency decreased from 2.455 cps at a displacement amplitude of 0.5 in to 2.440 cps at a displacement amplitude of 1.9 in. The damping factor evaluated from the resonance curves increased from 0.15% at the smallest displacement amplitude to 0.42% at the largest displacement amplitude.

In Fig. 3.10 the resonant displacement amplitudes are plotted against resonant force amplitude for all the resonance curves that were observed. An exciting force of amplitude 14 lb at resonance produced a displacement amplitude of 1.55 in, but an exciting force of amplitude 38 lb at resonance produced only a displacement amplitude of 1.90 in. The slope of the curve in Fig. 3.10 is inversely proportional to the stiffness and the damping factor of the structure. The resonant frequency at the largest displacement amplitudes was 0.6% smaller than the resonant frequency at the smallest displacement amplitudes, which implies that the stiffness of the structure decreased only 1.2%. Thus, the reduction in

the slope of the curve in Fig. 3.10 near the yield displacement is attributable mainly to an increase in the damping factor of the structure.

After frequency response curve no. 14 (see Fig. 3.10) had been completed, the eccentric-mass in the baskets of the vibration generator was reduced to the value used in run no. 9. Then the frequency response of the structure was observed for a second time with this particular value of eccentric-mass. The resonant displacement amplitude in the second frequency response, no. 15 in Fig. 3.10, was considerably smaller than it had been for run no. 9. A similar effect was observed for frequency response curve no. 16 which had the same amount of eccentric-mass as frequency response curves no. 5 and 6 (see Fig. 3.10). Thus, the damping capacity in frequency response curves no. 15 and 16 was considerably greater than it has been previously in curves no. 9 and 5 (or 6), respectively. After this test it was assumed (erroneously) that invisible cracks had formed in the welds at the base joints and had increased the damping factor. In tests conducted on structure no. 7 and described later, the same effect was observed more fully. The results from those tests show that for a given amplitude the damping factor of a structure increases after a number of cycles in which the displacement amplitude is greater than the yield amplitude.

After frequency response curve no. 16 had been observed, the eccentric-mass in the baskets of the vibration generator was increased again to a value greater than had been used in frequency response no. 14. However, cracks appeared in the welds at the bases of the columns before the frequency response curve with this eccentric-mass could be completed.

The energy input per cycle at resonance has been calculated for each resonance curve and is plotted as a function of resonant amplitude on a log-log scale in Fig. 3.11. The energy dissipated per cycle by a structure undergoing sinusoidal forced vibration may be calculated from

$$\Delta W = \pi P x \sin \alpha \tag{3.4}$$

in which P and x are the exciting force and displacement amplitudes, respectively, and α is the phase angle by which the displacement lags the excitation. If P and x are measured at resonance, then $\alpha = 90^\circ$ and $\sin \alpha = 1$. For displacement amplitudes less than the yield displacement, the slope of the curve is 2.0 indicating that the damping factor is independent of amplitude. At an amplitude approximately equal to the yield displacement, the slope of the curve increases showing that the damping factor is a function of amplitude when the vibration amplitude is greater than the yield displacement.

The damping factor of the structure, evaluated in two ways, is shown explicitly as a function of amplitude in Fig. 3.12. In the bandwidth method the damping factor has been evaluated from the resonance curves as described in Section 3.1. In the other method the damping factor has been evaluated from the energy ratio

$$\zeta = \frac{\Delta W}{4\pi W} \tag{3.5}$$

in which ΔW is the energy dissipated per cycle by the structure, and W is the energy stored in the steady state vibration. For a linear viscously damped system the values of ζ evaluated by these methods are equal.

The energy stored in the vibration (W) is equal to the kinetic energy of the structure at zero displacement, $1/2\ \omega^2 M x^2$. The circular frequency (ω) and the displacement amplitude (x) may be measured directly. The generalized mass (M) may be determined by adding a known mass to the structure and measuring the consequent shift of the resonant frequency; that is,

$$M = \frac{-\Delta M}{2}\ \frac{f}{\Delta f} \tag{3.6}$$

in which ΔM is the mass added, Δf is the reduction in resonant frequency, and f is the resonant frequency before the mass is added. Resonance curves observed before and after adding a mass weighing 150 lb are shown for structure no. 4 in Fig. 3.13. The generalized mass of structure no. 4 was found to weigh 3650 lb. (The weight of the platform and vibration generators determined conventionally was approximately 3600 lb).

Both the bandwidth and energy-ratio methods yielded nearly the same damping factors, see Fig. 3.12. The damping factor remained essentially constant for displacement amplitudes up to approximately the yield displacement. At displacement amplitudes greater than the yield displacement the damping factor increased rapidly with displacement amplitude.

The increase of damping capacity at a displacement amplitude approximately equal to the yield displacement had been intimated previously by the sudden change of slope in the plot of resonant displacement amplitude vs. resonant force amplitude, Fig. 3.10. In fact, a close relationship exists between plots of x vs. P and ζ vs. x when ζ is evaluated from the energy ratio because,

$$\zeta = \frac{\Delta W}{4\pi W} = \frac{\pi P x}{4\pi \frac{1}{2} k x^2} = \frac{P}{2Kx} \tag{3.7}$$

and hence $$x = \frac{1}{2\zeta k} P \tag{3.8}$$

as indicated previously.

Free decay tests were conducted on the structure at various times. In these tests the structure was excited at resonance, then the vibration generator was stopped quickly, and the resulting free vibration recorded. The displacement amplitudes of the free vibration have been plotted against the number of elapsed cycles on a semi-log scale in Fig. 3.14. The slope of this curve is proportional to the damping factor, which has been evaluated at a number of points on the curve using the expression,

$$\zeta = \frac{1}{2\pi n} \log_e \frac{x_o}{x_n} \tag{3.9}$$

in which x_o is the initial displacement amplitude and x_n is the displacement amplitude after n cycles have elapsed. At small amplitudes of vibration the damping factor evaluated from the logarithmic decay curves is about 0.1%. The logarithmic decay curve also indicates that at large vibration amplitudes the damping factor is a function of amplitude. Of course this method could not yield any information about the damping factor at amplitudes causing plastic strains since only one or two cycles of free vibration would occur at such large amplitudes.

3.5 Test Structure No. 5

During a period when 4 x 4 WF 13 lb steel sections were not readily available, four columns were fabricated from 4 x 4 M 10 lb steel sections.

These columns, type A.4, were identical to columns of type A.3, except for the difference in sections. Test structure no. 5 was assembled with four columns of type A.4, see Table 2.1.

Dynamic tests similar to those conducted on the previous structures were performed on test structure no. 5. The results have been plotted in Figs. 3.15 through 3.19. Again, the tests were terminated when fatigue cracks developed in the welds at the base of the columns.

The resonant frequency of test structure no. 5 ranged from 2.307 to 2.323 cps depending on the amplitude of vibration, as shown in Fig. 3.15. The resonant frequency was somewhat lower for test structure no. 5 than for test structure no. 4 due to the smaller moment of inertia of the 4 x 4 M 10 lb sections.

The damping factor of structure no. 5 at displacement amplitudes less than the yield amplitude was about 0.2%. For displacement amplitudes greater than the yield displacement the damping factor increased with vibration amplitude reaching a maximum of 0.5% at the largest amplitude of vibration, see Figs. 3.16 through 3.19.

Some of the results from the initial tests on structure no. 5 were erratic because a few of the bolts attaching the columns to the attachment plate, see Fig. 2.6, were slack. These bolts were tightened after frequency response curve no. 6 was obtained; results thereafter were more consistent, as shown in Fig. 3.16.

3.6 Test Structure No. 6

The dynamic tests on structures no. 1 through 5 were terminated when fatigue cracks formed in or close to welds at the base joint of one or

more columns. An improved design of the joint may have increased marginally the ratio of maximum displacement amplitude to yield displacement (ductility factor) attainable by dynamic test procedures. However, the real cause of the cracks in the welds was the accumulation of stress cycles during the dynamic tests. Thus, significantly larger ductility factors could only be attained if the number of stress cycles in the test procedure could be reduced substantially. This conclusion led to the initiation of a research project conducted under a National Science Foundation Grant (NSF GK 1319) to the University of California, Berkeley.

In the NSF project, individual columns similar to those used in the assembly of the dynamic test structures were subjected to reversed bending tests. These tests were similar to the cyclic loading tests conducted under American Iron and Steel Institute Project 120, (9); in fact, the same rig (10) was employed to execute the tests under the NSF contract.

The test rig required the length of the specimens to be 5'-6". Thus, the types of columns used to assemble test structures no. 1 through 5 were too long to be tested in the rig. Therefore, a new type of column, B.1, was designed. It was identical to type A.3, except that the length of 4 x 4 WF 13 lb section was shortened so the overall length of column was 5' $4\frac{1}{2}$", see Fig. 2.8(a). The remaining $1\frac{1}{2}$" was obtained by attaching a pillow block bearing to the top of the column; the reversed loads were applied through the bearing.

In order to derive the maximum benefit from these reversed bending tests, it was necessary that parallel dynamic tests be conducted on a structure assembled from columns of type B.1. Test structure no. 6 was assembled with two columns of type B.1, using two dummy columns as described in Section

2.1 and shown in Fig. 2.7. The results of the dynamic tests conducted on test structure no. 6 are shown in Figs. 3.20 through 3.25. The graphs are similar to those plotted for test structures no. 4 and 5. Again the tests were terminated by the formation of fatigue cracks.

The resonant frequency of test structure no. 6 decreased from 2.507 cps at small displacement amplitudes to 2.475 cps at a displacement amplitude of 1.42 in, as shown in the resonance curves of Figs. 3.20 and 3.21. The damping factors evaluated from the resonance curves ranged from .15% at the lower displacement amplitudes to 1.23% at the largest resonant displacement amplitude. The damping factor is plotted against displacement amplitude in Fig. 3.24. The agreement between the bandwidth method and the energy-ratio method in evaluating the damping factors is seen to be excellent. Similar values of damping capacity were obtained from the logarithmic plots of free vibration tests shown in Fig. 3.25.

3.7 Test Structure No. 7

In test structures no. 1 through 6, the highest dynamic stresses occurred either in the welds at the base joints of columns, or in regions close to those welds. In order to avoid these joint failures, columns with reduced sections were then designed so that the highest stresses would occur in material some distance from a weld. These columns, type B.2, have been described already in Section 2.1, and shown in Figs. 2.6 and 2.8(b). Test structure no. 7 was assembled by replacing the two active columns of test structure no. 6 by two columns of type B.2, but retaining the two dummy columns of that structure.

Some frequency response curves observed for test structure no. 7 are shown in Figs. 3.26 through 3.29. The resonant displacement amplitudes of all frequency response curves are plotted against their corresponding exciting force amplitude in Fig. 3.30. More frequency response curves were observed for this structure than for any previous structure because anomalous response behavior was observed in certain cases. When a frequency response run was repeated with a given eccentric-mass, the resonant displacement amplitude could be significantly less in the repeated run than it had been for the original run. This effect had been observed earlier in structure no. 4.

After frequency response curve no. 9 had been observed (Fig. 3.26) the amount of eccentric-mass in the baskets of the vibration generator was increased for frequency response curve no. 10. However, the resonant displacement amplitude of frequency response no. 10 was less than that for frequency response curve no. 9, see Fig. 3.30. Another frequency response curve, no. 11, was observed for the same amount of eccentric-mass as for curve no. 10; but the resonant displacement amplitude decreased further. The amount of eccentric-mass in the baskets was reduced again and frequency response no. 12 observed. Then frequency response curves no. 13 through 24 were observed. The resulting resonant displacement amplitudes are plotted against their corresponding exciting force amplitudes in Fig. 3.30.

After frequency response no. 24 had been observed, the amount of eccentric-mass in the baskets was reduced for curve 25 to the value it had been for runs no. 7 and 12. The resonant displacement amplitude of resonance curve 25 was less than for resonance curve no. 12, see Fig. 3.30. Then frequency response curves no. 26 through 31 were observed.

After frequency response curve no. 31 had been observed, the amount of eccentric-mass for curve no. 32 was reduced to the value that it had been for curve no. 25. The resonant displacement amplitude of curve no. 32 was only slightly less than the resonant displacement amplitude of curve 25. Similarly, the resonant displacement amplitude of curve no. 33 was only slightly less than the resonant displacement amplitude of curve no. 27, see Fig. 3.30. After frequency response no. 33 had been observed, the amount of eccentric-mass was increased above the level it had been for curves no. 24 and 31, but cracks formed in the welds at the base of the columns before the frequency response run could be completed.

The resonant frequency of test structure no. 7 decreased from 2.200 cps at small amplitudes of vibration to 2.155 cps at a displacement amplitude of 0.95 in, as shown in Figs. 3.26 through 3.29. The damping factors evaluated from the resonance curves ranged from .15% to 1.25%.

The energy dissipated per cycle at resonance and the damping factors evaluated by the bandwidth and energy-ratio methods are plotted against resonant displacement amplitude in Figs. 3.31 and 3.32. Each figure, like Fig. 3.30, consists of a set of three curves. The first curve in Fig. 3.32 indicates the damping factor was .15%, essentially independent of amplitude. The second set indicates the damping factor was 0.2% at small vibration amplitudes and increased gradually to 1.1% at a displacement amplitude of 1.2 in. The third set indicates the damping gradually increased from 0.25% to 1.2%.

These curves show that undergoing a number of vibration cycles at amplitudes close to the yield displacement increases the damping capacity of the structure. This effect has been reported previously by Lazan (5)

and (6) from work in which small specimens were tested in a rotating-bending machine. The experimental results from the model structure are compared in more detail with the results of Lazan's work as well as with Hanson's (3) in Chapter 4.

Finally, two logarithmic decay curves for structure no. 7 are shown in Fig. 3.33.

CHAPTER 4

DISCUSSION OF EXPERIMENTAL RESULTS

4.1 Dynamic Test Results and Comparison with Results from Lazan's Tests

The dynamic tests conducted on structures no. 1 through 6 did not display any stress history effects. In the absence of such effects, the damping factor of a structure was found to be independent of vibration amplitude up to a reasonably well defined amplitude slightly smaller than the calculated yield displacement. This amplitude is assumed to be equivalent to what Lazan calls the cyclic stress sensitivity limit, (5) and (6). At amplitudes of vibration greater than the equivalent cyclic stress sensitivity limit, the damping factor of the test structures was found to be approximately a linear function of amplitude up to the maximum amplitudes achieved before fatigue cracks developed.

The damping factor of structures no. 1 through 6 ranged from 0.15 to 0.28% for vibration amplitudes smaller than the cyclic stress sensitivity limit. The factors are indicative of the total energy dissipated by material and external damping. Since the energy dissipated per cycle is proportional to the square of the displacement amplitude, the factors are directly comparable to those determined for full-scale structures. However, the damping factors of 'clean' multi-story steel buildings lie in the range 1-2%. Thus, even if the energy dissipated by external sources in the model test structures were negligible, material damping alone could not explain the relatively large damping factors exhibited by steel buildings. Therefore, a large fraction of the damping factors that have been obtained for multi-story steel buildings must be caused by the dissipation of energy in joints, floor slabs, etc., and the transmission of energy into the ground.

At amplitudes of vibration greater than the equivalent cyclic stress sensitivity limit, the damping factors of the model steel structures are approximately linear functions of amplitude. The most accurate results were obtained for test structure no. 6, and for that structure the damping factor increased linearly from 0.15% to 1.2% as the displacement amplitude increased from 1.1 in to 1.4 in. In test structure no. 5 the damping increased from 0.19% to 0.50% as the displacement amplitude increased from 1.6 in to 1.8 in. The damping factors of test structure no. 4 were similar to those of no. 5. The stress sensitivity limit was not exceeded in the case of structures no. 1 and 3, and although it was exceeded by a small amount in the test of structure no. 2, no accurate measurements were made in this range.

The increased damping factors at vibration amplitudes greater than the stress sensitivity limit is caused by a plastic strain mechanism. The energy dissipated by the plastic strain mechanism is not proportional to the square of the vibration amplitude; the exponent was 9.1 for test structure no. 6 and approximately 8 for test structure no. 7. Thus, the damping factors recorded at vibration amplitudes greater than the stress sensitivity limit are not directly comparable to those that might be expected in a multi-story steel building if the vibration amplitude were large enough to cause yielding in some members.

In order to predict the damping factors of a multi-story steel building vibrating at large amplitudes, a general method similar to that proposed by Lazan (5) would have to be employed. Lazan's method consists of assuming that the energy (D) dissipated by unit volume of a material (for the present purposes, steel) is related to the stress amplitude (σ)

by

$$D = J\sigma^n \tag{4.1}$$

in which J and n are constants. These constants may be determined from tests such as those conducted on the model steel structure. After the constants have been determined, the total energy that would be dissipated by plastic strain mechanisms in a structure vibrating at large amplitudes could be calculated by an integration procedure.

Stress history effects were observed in the tests conducted on structure no. 7, as shown in Fig. 3.32, and some effort has been made to explain the effects. In the initial tests on structure no. 7, the damping factor was constant (0.15%) up to an amplitude of 1.0 in, which appeared to be the cyclic stress sensitivity limit. However, vibration at this limit changed the damping properties of the structure. In subsequent tests the damping factors at vibration amplitudes smaller than the initial cyclic stress sensitivity limit were greater than the values found in the initial tests, and the cyclic stress sensitivity limit became less distinct. These tests with vibration amplitudes smaller than the initial cyclic stress limit could be repeated with nearly identical results until the vibration amplitude exceeded the previous highest amplitude. Then similar stress history effects were observed again. The cyclic stress sensitivity limit became even less distinct, and the damping capacity became a function of amplitude even for small amplitudes of vibration.

In the initial set of tests on structure no. 7 the cyclic stress sensitivity limit appeared to be about 1.0 in. At this vibration amplitude the measured elastic strain amplitude at the extreme fibre of the reduced

section was 1750 μ in/in, as shown in Fig. 4.1, indicating that the stress amplitude at that point was 50 ksi. In the final set of tests, see Fig. 3.32, the stress sensitivity limit appears to have been reduced to about one-half the initial value. The above values may be compared to those obtained by Lazan for small specimens tested in a rotating-bending machine. He found the stress sensitivity limit of mild steel specimens to be 0.8 times the fatigue strength of the specimens at 20×10^6 cycles, i.e., approximately 29 ksi. Although Lazan preferred to relate the cyclic stress sensitivity limit to fatigue strength, this is not a very suitable parameter for model or full-scale steel structures.

4.2 Correlation Between Dynamic Tests and Reversed Loading Tests of Individual Columns

The maximum vibration amplitudes obtainable in the dynamic tests were always limited by the formation of fatigue cracks in the welds at the base joint of the columns, or in metal close to these welds. Since the number of vibration cycles accumulated in the dynamic tests was instrumental in the formation of the cracks, it was essential to reduce the number of stress cycles on the columns to obtain reasonable ductility factors. The maximum ductility factors in the dynamic tests were not much greater than unity. But since Hanson (3) and (5) had found hysteresis loops obtained by dynamic and static methods to be similar, it appeared feasible to extend the results by a series of reversed loading tests on individual columns. The reversed loading tests were conducted under NSF Grant GK-1319 to the University of California, Berkeley.

The rig employed to subject the columns to reversed loading tests has been described previously by Bertero and Popov (10). The

specimen installed in the rig (a column of either type B.1 or B.2) was supported as a cantilever. Vertical alternating loads were applied to the free end of the cantilever by means of a hydraulic jack. The force applied to the specimen was measured by a load-cell interposed between the jack's piston and the cantilever. The force transmitted by the load-cell, the displacement of the free end of the cantilever, and strains at various locations in the specimen were recorded by the same oscillograph system that was used in the dynamic tests.

The load applied to the free end of the cantilever was cycled two or three times at constant displacement amplitude until a stable hysteresis loop was established. The force, displacement and strains were recorded over the next two cycles; the constant displacement amplitude was then increased and the process repeated. The initial displacement amplitudes were smaller than the yield displacement of the specimen, and they were increased in a sequence of steps up to a ductility factor (ratio of displacement amplitude to yield amplitude) between 3 and 4. The force applied to the beam was plotted against displacement over each cycle to obtain hysteresis loops for the specimen. Typical hysteresis loops obtained for a column of type B.1 are shown in Fig. 4.2.

The energy dissipated per cycle by the structure equals the area within the hysteresis loop, which was measured by means of a planimeter. The energy dissipated per cycle by the individual columns of type B.1 and B.2 was doubled for direct comparison with the appropriate test structure, and it has been plotted as a function of the displacement amplitude of the cycle in Fig. 4.3. The energy dissipated per cycle by the test structure (measured in the dynamic tests) has also been included in Fig. 4.3.

Over the displacement amplitude range common to both, the two methods give the same quantity of energy dissipated per cycle.

The hysteresis loops for the columns represent the force-deformation relationship of the structure, assuming rate of loading effects are negligible. On this assumption, the damping capacity of the structure may be evaluated from the hysteresis loops of the columns. To evaluate the damping capacity, the energy ratio method (see Section 3.4) may be used. The energy dissipated per cycle (ΔW) is the energy represented by the area within the hysteresis loop, and W is a quantity of energy associated with the hysteresis loops that makes ζ dimensionless. However, there are four basic ways to define W which lead to four definitions of ζ. The four definitions of W are illustrated with reference to the Ramberg-Osgood type force-deformation relationship shown in Fig. 4.4. They are: $W_1 = A+B+C+D+E$, $W_2 = D+E$, $W_3 = C+D+E$, and $W_4 = E$, where the letters A through E designate the areas of spaces in which the letters are immediately enclosed by either solid or dashed lines. If the definition of damping corresponding to W_1, W_2, W_3 and W_4 are ζ_1, ζ_2, ζ_3 and ζ_4, then the definition of damping capacity ζ_1, has been used by Hudson (11), the definition ζ_2 by Rosenblueth and Herrera (12) as well as Berg (13), and definition ζ_3 by Jacobsen (14) and Hudson (11). These definitions of damping factors have been discussed by Jennings (15) and Rea (16).

The damping capacities implicit in the hysteresis loops of columns of types B.1 and B.2 have been evaluated according to definitions ζ_1, ζ_2, ζ_3 and ζ_4. (For each hysteresis loop, the areas ΔW and W_3 were measured by planimeter and the areas W_1 and W_2 calculated.) The damping

capacities determined from the dynamic tests and reversed bending tests are compared on a semi-log scale in Figs. 4.5 and 4.6 for columns of types B.1 and B.2, respectively. For test structure no. 6, the curve obtained from the dynamic tests is continuous with the curves obtained from the reversed loading tests, indicating a correlation between the two test methods. However, correlation is not so apparent in the case of test structure no. 7.

The reversed loading tests were conducted at ever increasing amplitudes and therefore stress history effects did not influence the results significantly. Thus, for test structure no. 7, it might be expected that the reversed loading tests would correlate with the first set of dynamic test results, Fig. 4.6, rather than the second and third set in which stress history effects were significant. Unfortunately, there are insufficient data points to determine if the correlation suggested in Fig. 4.6 (dashed line) is valid. But it does appear that the second and third sets of dynamic test results do not correlate with the reversed loading tests.

The reversed loading tests show that at ductility factors greater than two, the numerical value assigned to the damping factor of the model steel structure would depend largely on the definition of damping factor.

4.3 Comparison of Test Results with Results from Hanson's Tests

The results described in this report cannot be compared directly with the results obtained by Hanson (3) and (7), due to the completely different types of columns employed in the test structures. (Details of Hanson's columns are given in Fig. 1.1.) The amplitude ranges of the tests differed also. In the dynamic tests described in this report, the vibration

amplitudes ranged between zero and the yield amplitude. In both the dynamic and static (reversed loading) tests conducted by Hanson, the amplitudes ranged between ductility factors of 1 and 2. However, if the dynamic results from the tests described in this report are combined with the results of the reversed loading tests on individual columns described in the previous section, then some qualitative comparisons with Hanson's results may be made.

First, the damping capacities of Hanson's test structures and the test structures used for the work described in this report increased rapidly at vibration amplitudes approximately equal to the yield amplitudes of the structures. This is illustrated in Fig. 4.7 where the average damping factors obtained for a number of structures (with columns of type S) tested by Hanson are compared with the damping factors obtained for test structure no. 6. Of course, quantitative agreement between the different tests cannot be expected because the columns in the structures were not geometrically similar, the behavior of the structures was nonlinear, and the structures were subjected to different stress histories.

Second, in both sets of tests, the results indicated that the energies dissipated per cycle in dynamic tests and reversed loading tests are nearly equal. The agreement between the energy dissipated per cycle in the dynamic tests and in reversed loading tests of individual columns over the common amplitude range has been described in the previous section. Hanson found close similarity between dynamic and static hysteresis loops (7) and observed that stress history effects appeared more important than frequency effects. This latter observation is corroborated by the present studies, see Fig. 4.6.

CHAPTER 5

SUMMARY AND CONCLUSIONS

The damping capacities of seven model steel structures, each consisting of a heavy steel platform supported on four columns, have been determined from forced vibration tests. The vibration amplitudes of the structures ranged from small displacements up to amplitudes slightly greater than yield displacement. At vibration amplitudes smaller than the stress sensitivity limit, which in the absence of stress history effects is slightly smaller than the yield displacement, the damping factors of the structures were independent of amplitude and ranged from .15 to .25%. At vibration amplitudes greater than the stress sensitivity limit, the damping factors were dependent on vibration amplitudes; for example, in the case of test structure no. 6, the damping increased from 0.15 to 1.2% as the displacement amplitude increased from 1.1 to 1.4 in.

Stress history effects were observed in the results from the tests on structure no. 7. In the initial tests on this structure, the damping factor was constant (0.15%) up to a vibration amplitude of 1.0 in which appeared to be the stress sensitivity limit. However, after vibration at this limit, the damping properties of the structure changed. In subsequent tests the damping factors at vibration amplitudes smaller than the initial stress sensitivity limit were greater than the values found in the initial tests. The cyclic stress sensitivity limit became less distinct. When the vibration amplitudes exceeded the previous highest amplitude this phenomenon was repeated. Finally, the damping factors

became a function of amplitude even for small vibration amplitudes.

The vibration cycles accumulated by the structures during the dynamic tests eventually caused fatigue cracks in the columns. The cracks formed in the welds at the base joints of the columns, and the tests were terminated as soon as the cracks were observed. The cracking limited the maximum vibration amplitudes in the dynamic tests to ductility factors only slightly greater than unity. The number of stress cycles appeared to be instrumental in causing the cracks, and thus significantly larger ductility factors could be attained only by reducing the number of stress cycles in the test procedure. This conclusion led to the initiation of a complementary project in which individual columns of the steel structures were subjected to reversed loading tests in the range of ductility factors 1 to 4. It was concluded that the results from these tests could be used to predict the damping capacity of the model steel structures if they were to vibrate at amplitudes in this range. However, the numerical value assigned to the damping factor was found to depend greatly on the definition of damping factor (8).

Finally, the combined results of the dynamic and reversed loading tests are compared with the results obtained by Lazan (5) from tests on small steel specimens, and with the results obtained by Hanson (3) on steel structures similar to the ones tested in this work. In both cases, qualitative agreement is shown.

APPENDIX 1

REFERENCES

1. Nielsen, N. N., "Vibration Tests of a Nine-Story Steel Frame Building", Proc. ASCE, J. Engineering Mechanics Division, Vol. 92, No. EM 1, 1966.

2. Rea, D., J. G. Bouwkamp and R. W. Clough, "The Dynamic Behavior of Steel Frame and Truss Buildings", Structures and Materials Research Report No. 66-24, University of California, Berkeley, 1966.

3. Hanson, R. D., "Post-Elastic Response of Mild Steel Structures", Ph.D. Thesis, California Institute of Technology, Pasadena, Calif., 1965.

4. Hudson, D. E., "Synchronized Vibration Generators for Dynamic Tests of Full-Scale Structures", Earthquake Engineering Laboratory Report, California Institute of Technology, November, 1962.

5. Lazan, B. J., "Energy Dissipation Mechanisms in Structures, With Particular Reference to Material Damping", Section One of "Structural Damping", (Ed. J. E. Ruzicka), Pergamon Press, 1959.

6. Lazan, B. J., "Damping of Materials and Members in Structural Mechanics", Pergamon Press, 1968.

7. Hanson, R. D., "Comparison of Static and Dynamic Hysteresis Curves", Proc. ASCE, J. Engineering Mechanics Division, Vol. 92, No. EM 5, 1966.

8. Rea, D., R. W. Clough, J. G. Bouwkamp and U. Vogel, "Damping Capacity of a Model Steel Structure", Proceedings, Fourth World Conference on Earthquake Engineering, Santiago, Chile, 1969.

9. Popov, E. P. and R. B. Pinkney, "Behavior of Steel Building Connections Subjected to Repeated Inelastic Strain Reversal", Structures and Materials Research Report No. SESM 67-31, University of California, Berkeley, December 1967.

10. Bertero, V. V., and E. P. Popov, "Effect of Large Alternating Strains of Steel Beams", Proc. ASCE, J. Structural Division, Vol. 91, St 1, 1965.

11. Hudson, D. E., "Equivalent Viscous Friction for Hysteretic Systems With Earthquake-like Excitations", Proceedings, Third World Conference on Earthquake Engineering, New Zealand, 1965.

APPENDIX 1

REFERENCES
(Continued)

12. Rosenbleuth, E. and I. Herrera, "On a Kind of Hysteretic Damping", Proc. ASCE, J. Engineering Mechanics Division, Vol. 90, No. EM 2, 1964.

13. Berg, G. V., "A Study of the Earthquake Response of Inelastic Systems", Proceedings, 34th Annual Convention of the Structural Engineers Association of California, October 1965.

14. Jacobsen, L. S., "Damping in Composite Structures", Proceedings, 2nd World Conference on Earthquake Engineering, Japan, 1960.

15. Jennings, P. C., "Equivalent Viscous Damping for Yielding Structures", Proceedings ASCE, J. Engineering Mechanics Division, Vol. 94, No. EM 1, February 1968.

16. Rea, D., Discussion of "Equivalent Viscous Damping for Yielding Structures", by P. C. Jennings, Proceedings ASCE, J. Engineering Mechanics Division, Vol. 94 No. AM 6, December 1968.

APPENDIX 2

FIGURES

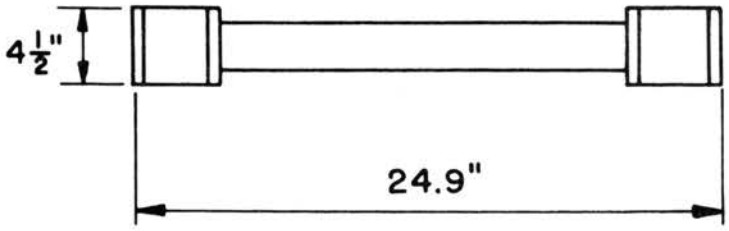

a) COLUMN

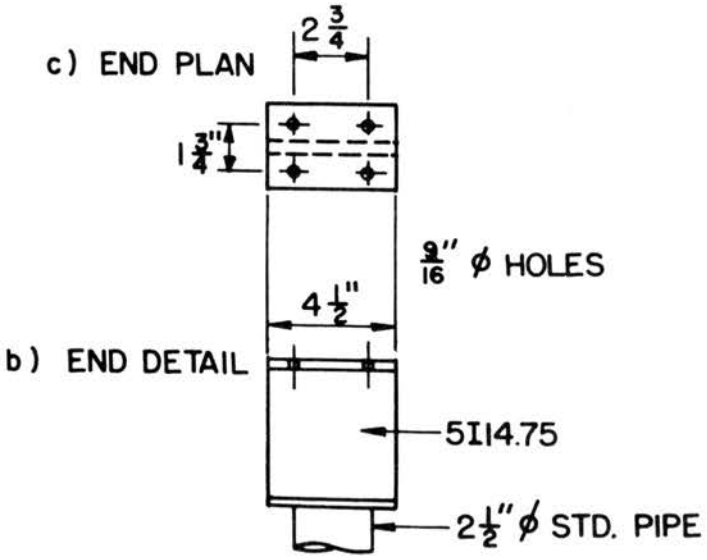

FIG. I.I DETAILS OF HANSON'S COLUMNS, TYPE S

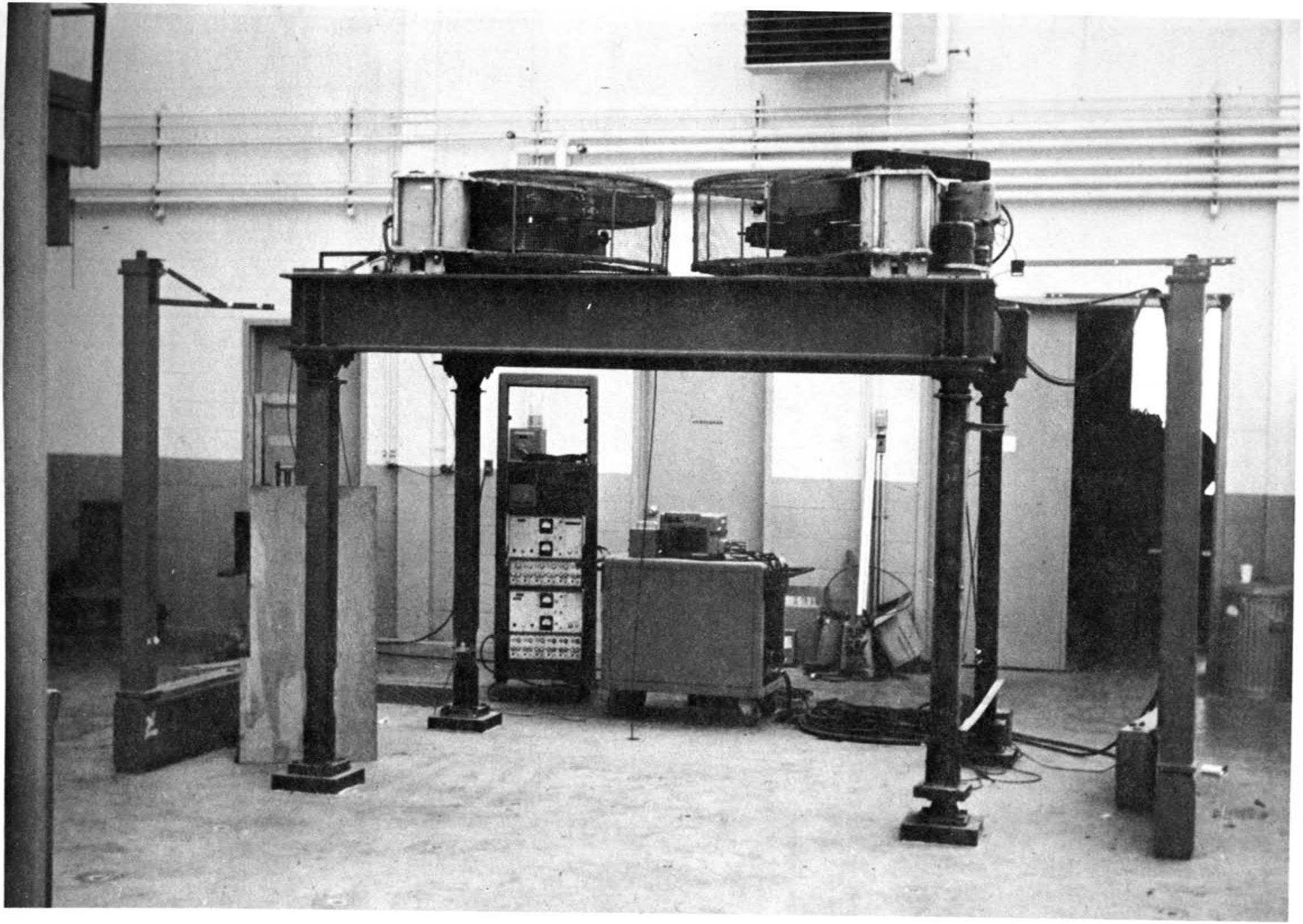

FIG. 2.1 MODEL STEEL STRUCTURE: SIDE VIEW

FIG. 2.2 MODEL STEEL STRUCTURE: VIEW FROM ABOVE

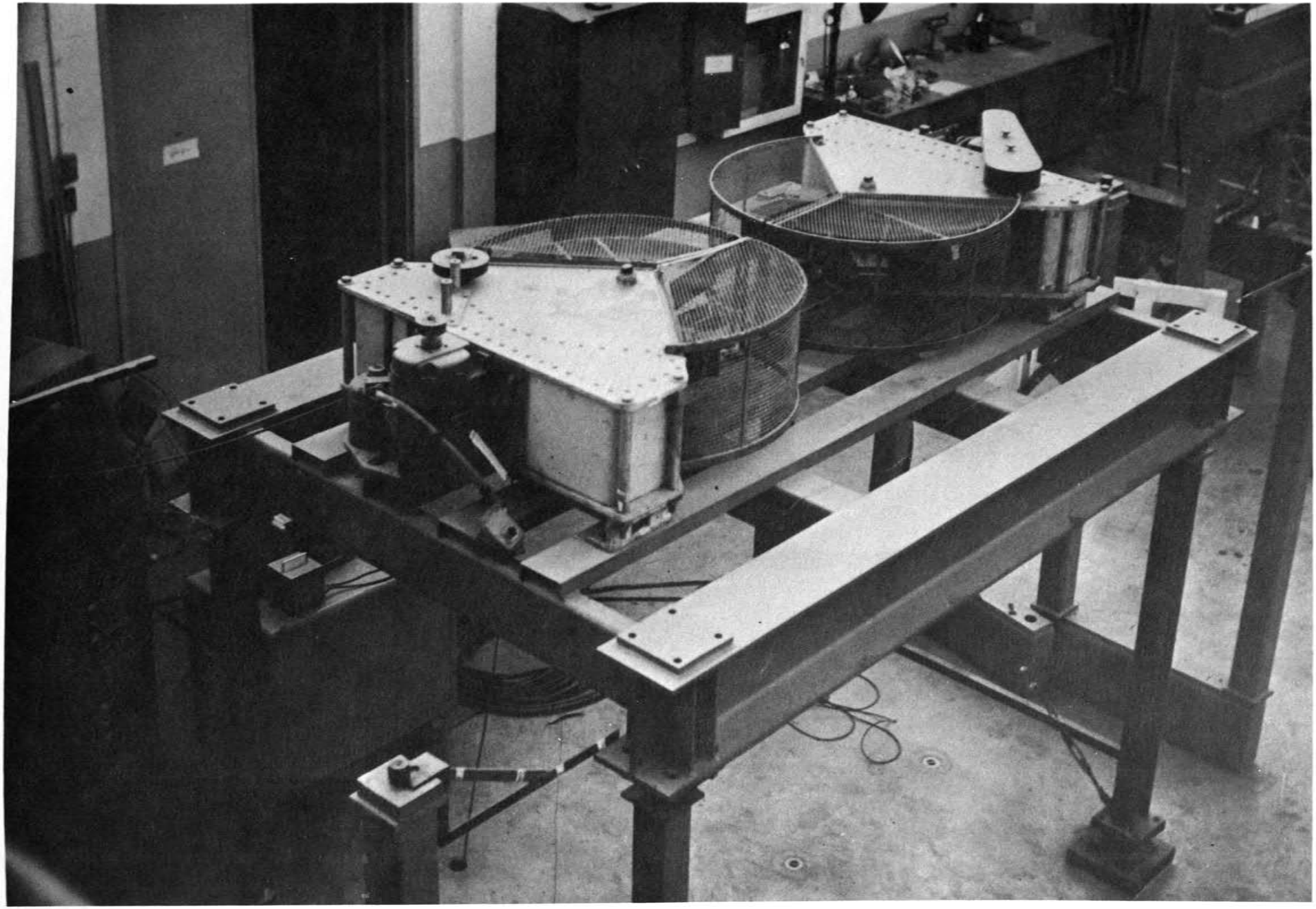

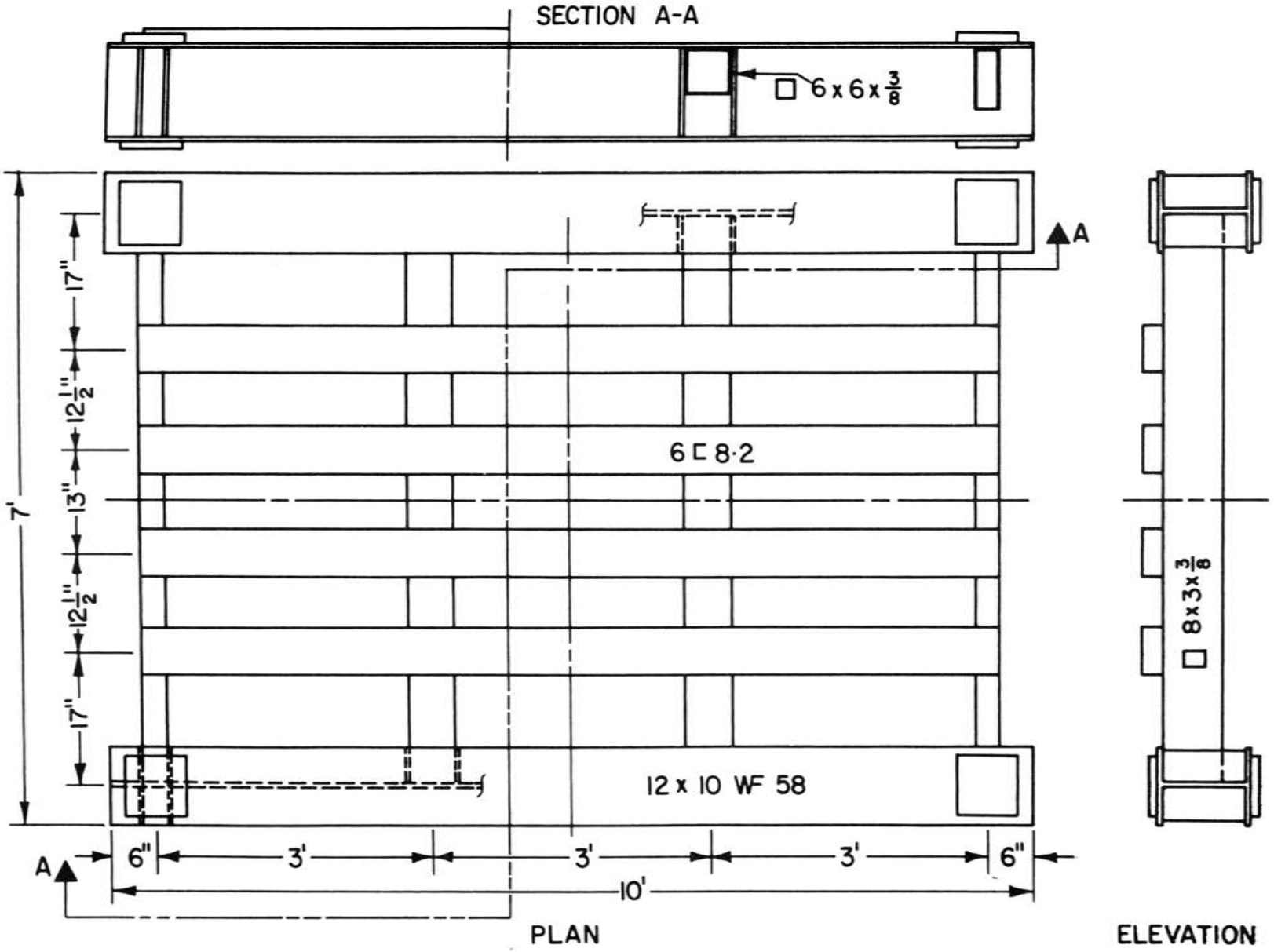

FIG. 2.3 STEEL PLATFORM

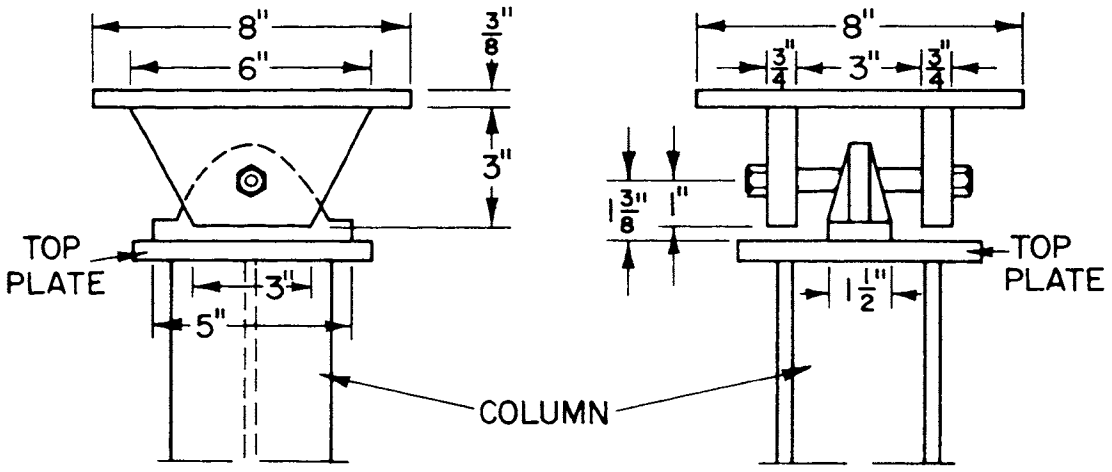

a) PINNED CONNECTION

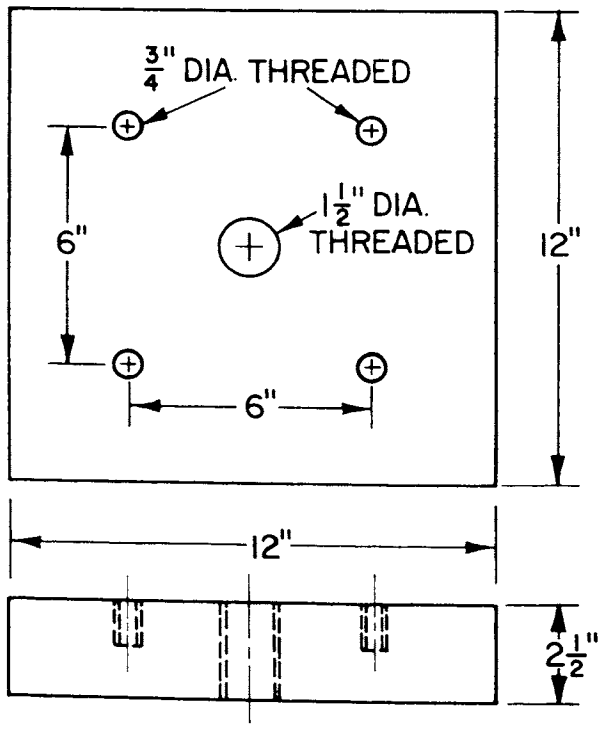

b) ATTACHMENT PLATE FOR COLUMN BASE PLATE

FIG. 2.4 PINNED CONNECTION AND ATTACHMENT PLATE

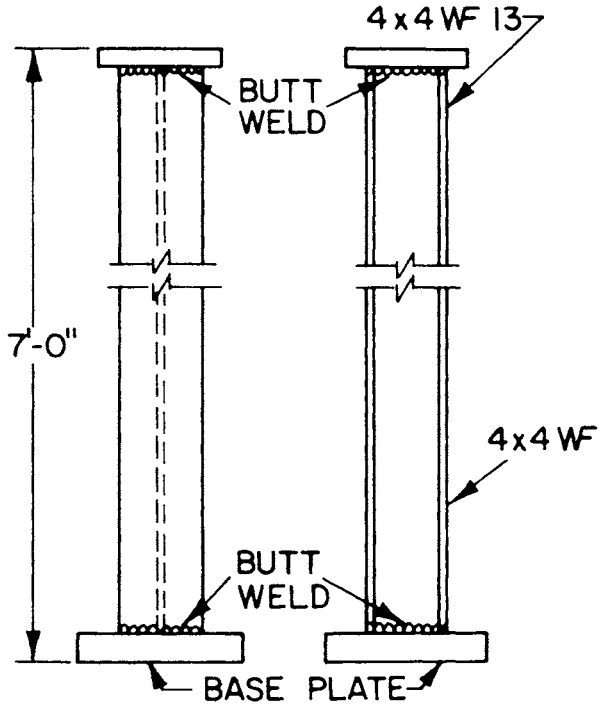

a) BASIC COLUMN AND COLUMN TYPE A1

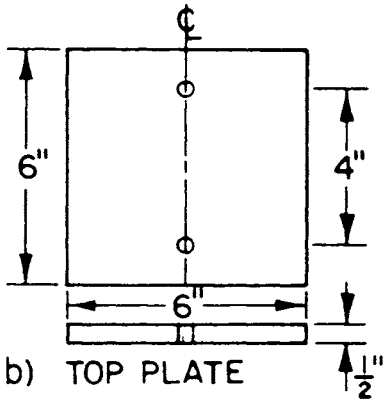

b) TOP PLATE

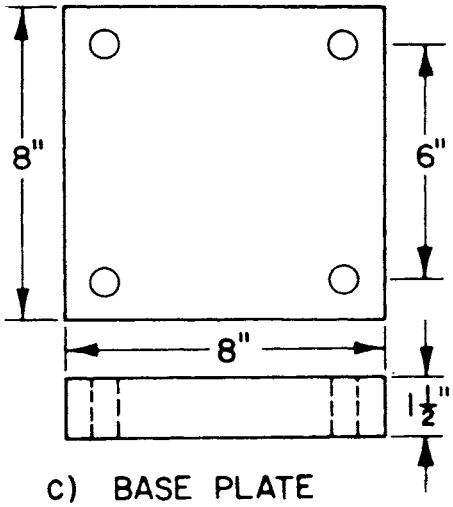

c) BASE PLATE

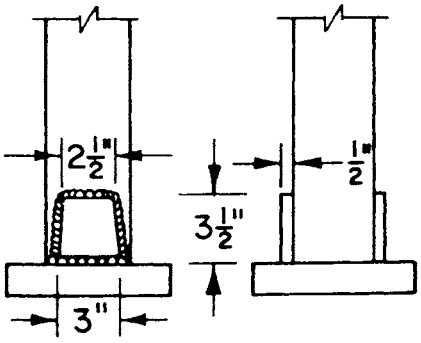

d) BASE PLATE WITH TRAPEZOIDAL STRAPS COLUMN TYPES A2

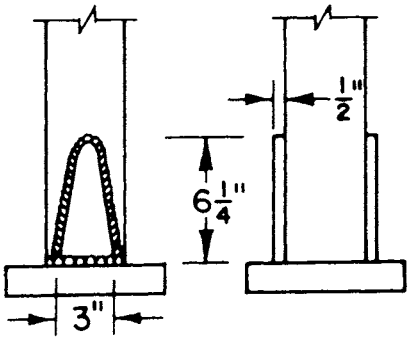

e) BASE PLATE WITH PARABOLIC STRAPS COLUMN TYPES A3, A4, B1, B2

FIG. 2.5 DETAILS OF COLUMNS FOR TEST STRUCTURES

FIG. 2.6 CLOSE-UP OF REDUCED SECTION OF COLUMN TYPE B.2

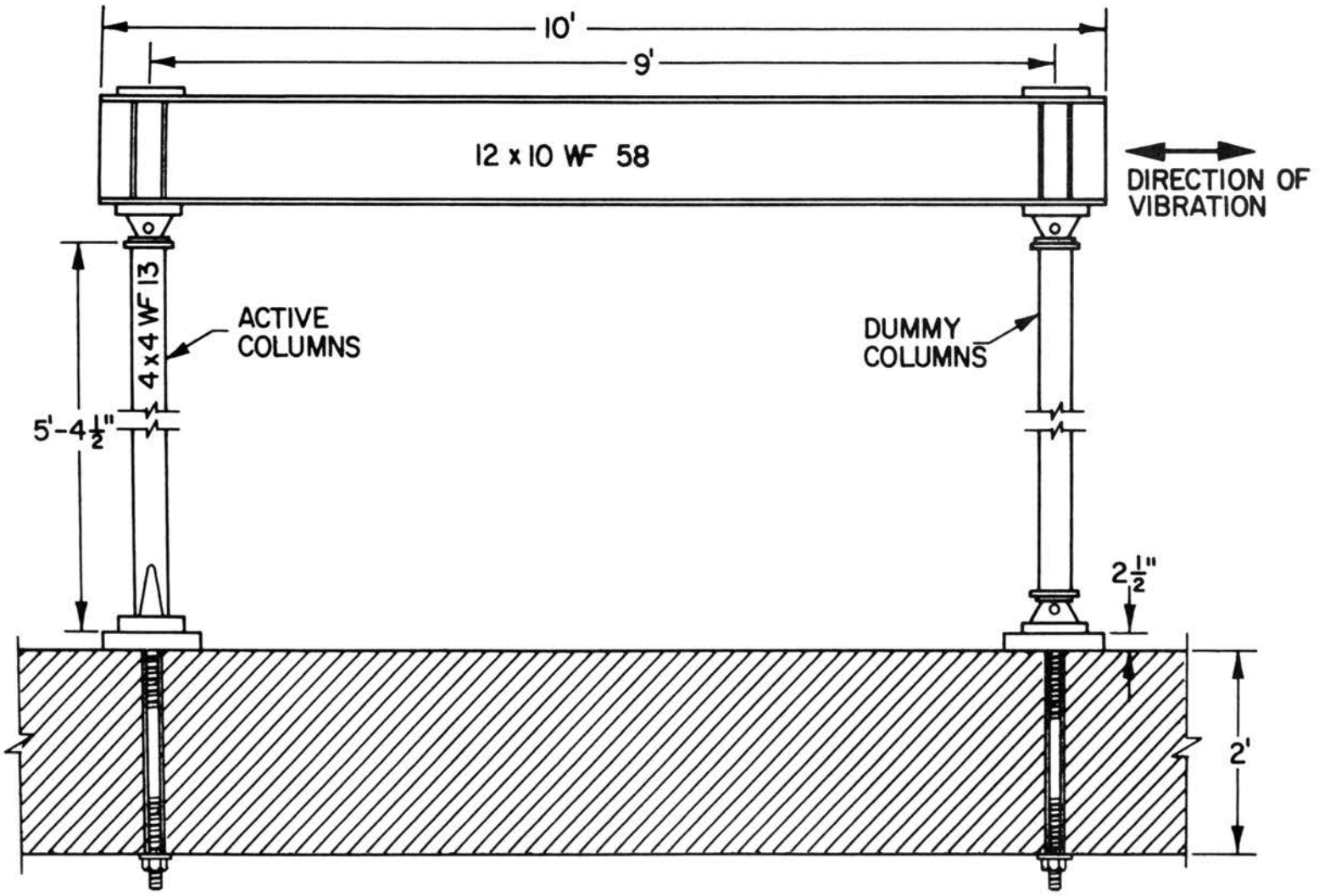

FIG. 2.7 ELEVATION VIEW OF MODEL TEST STRUCTURE NO. 6

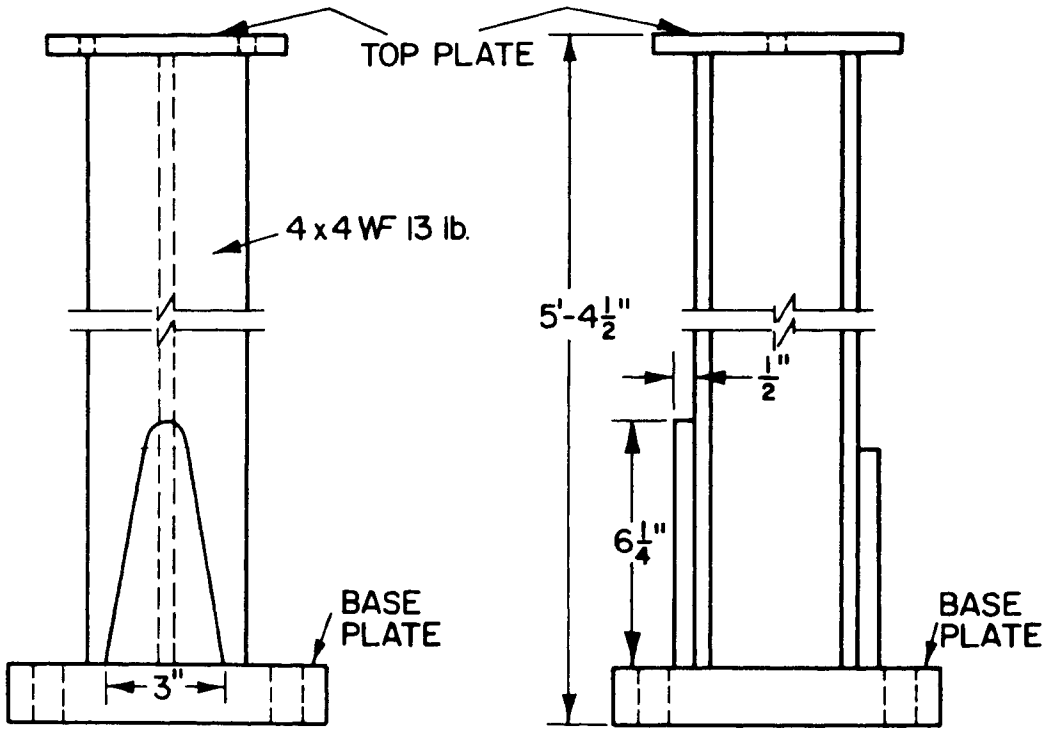

a) COLUMN TYPE B1

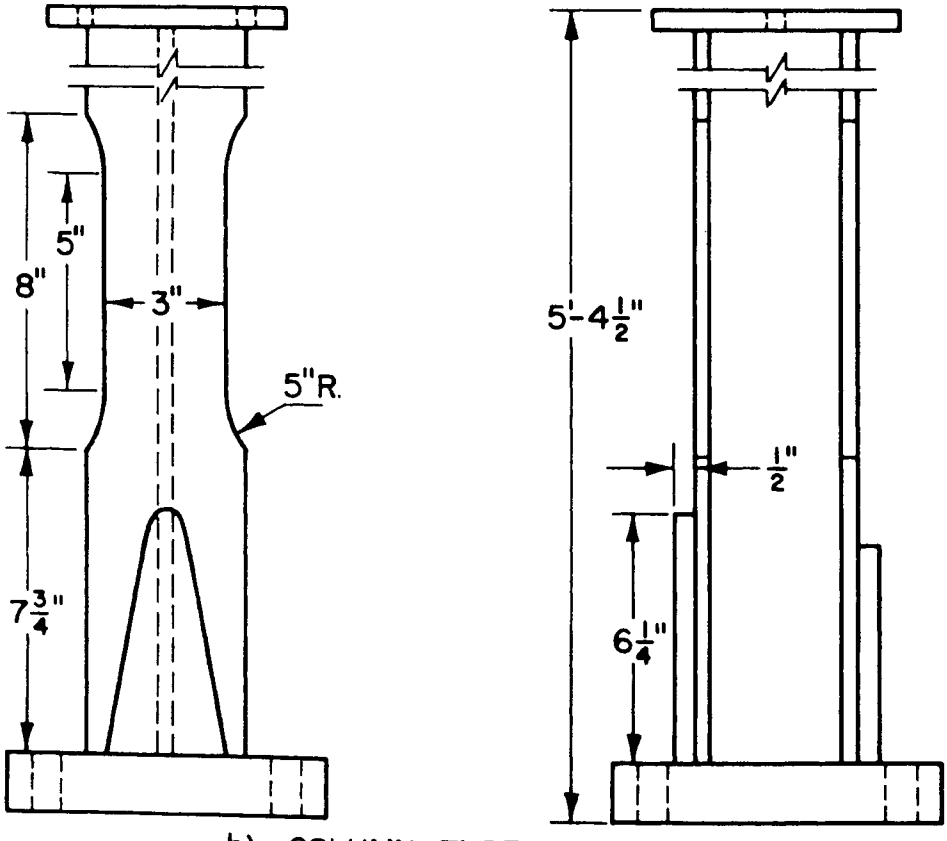

b) COLUMN TYPE B2

FIG. 2.8 DETAILS OF COLUMNS FOR TEST STRUCTURES NO. 6 AND 7

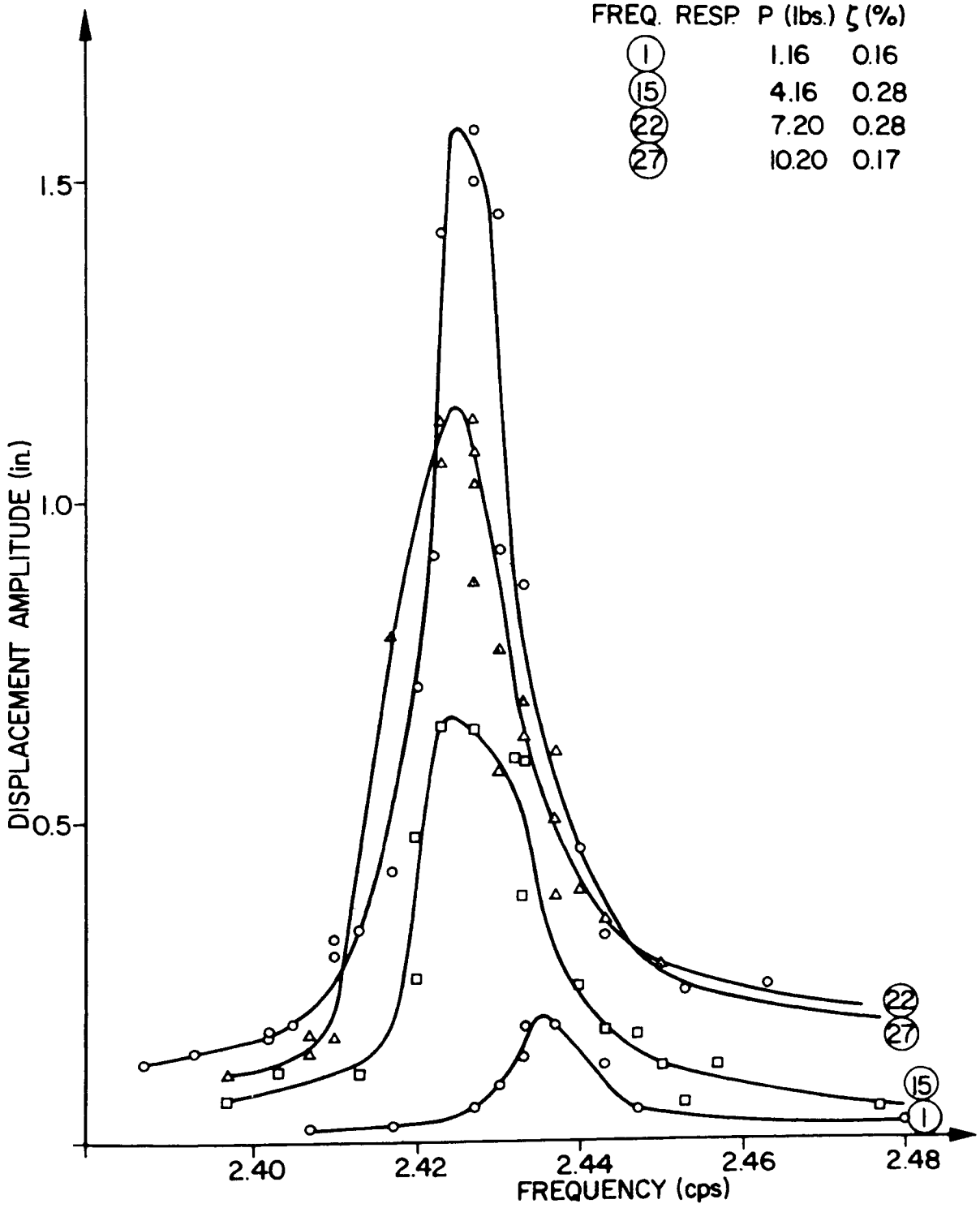

FIG. 3.1 FREQUENCY RESPONSES: TEST STRUCTURE NO. 1

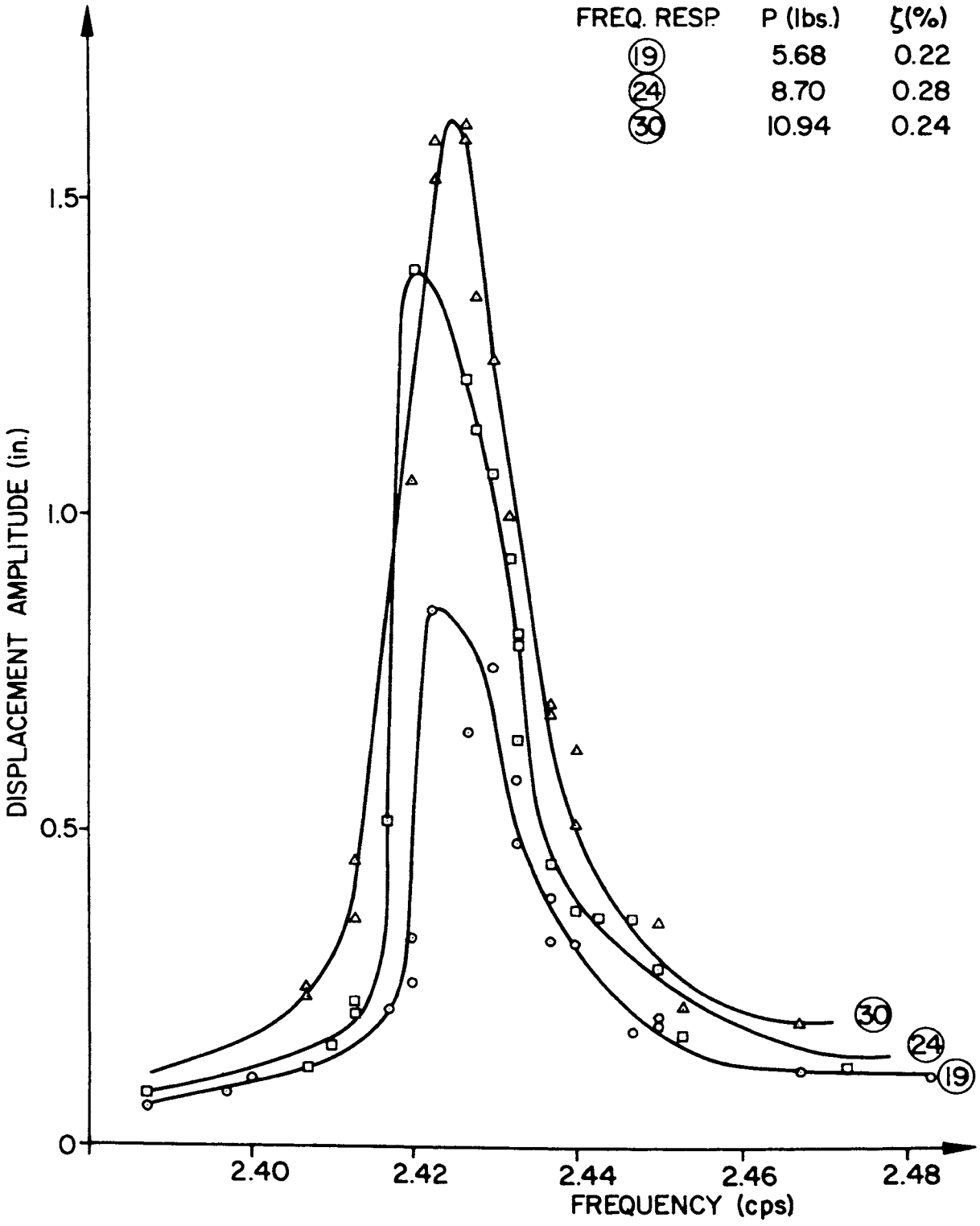

FIG. 3.2 FREQUENCY RESPONSES: TEST STRUCTURE NO. 1

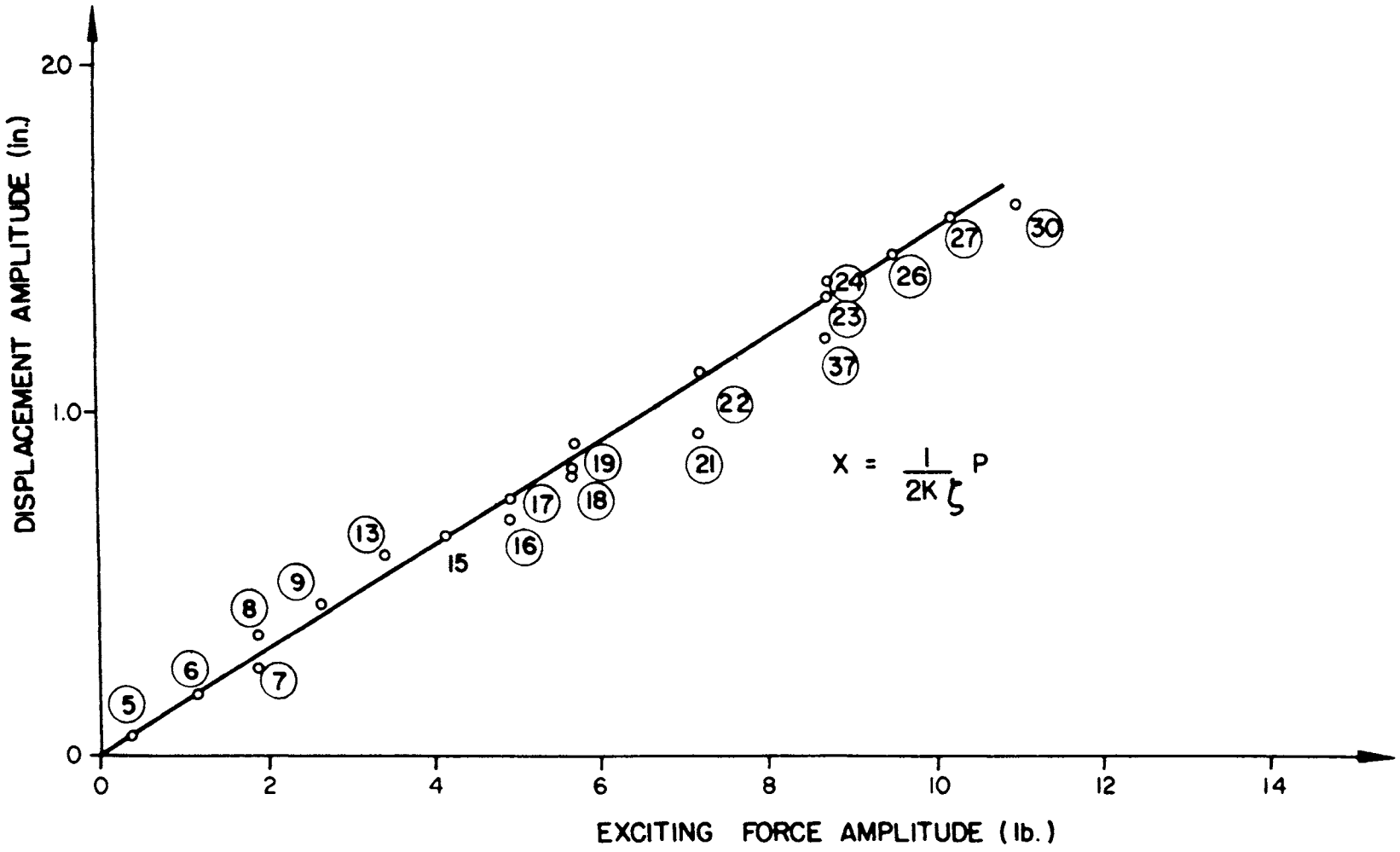

FIG. 3.3 RESONANT AMPLITUDE vs. EXCITING FORCE: TEST STRUCTURE NO. 1

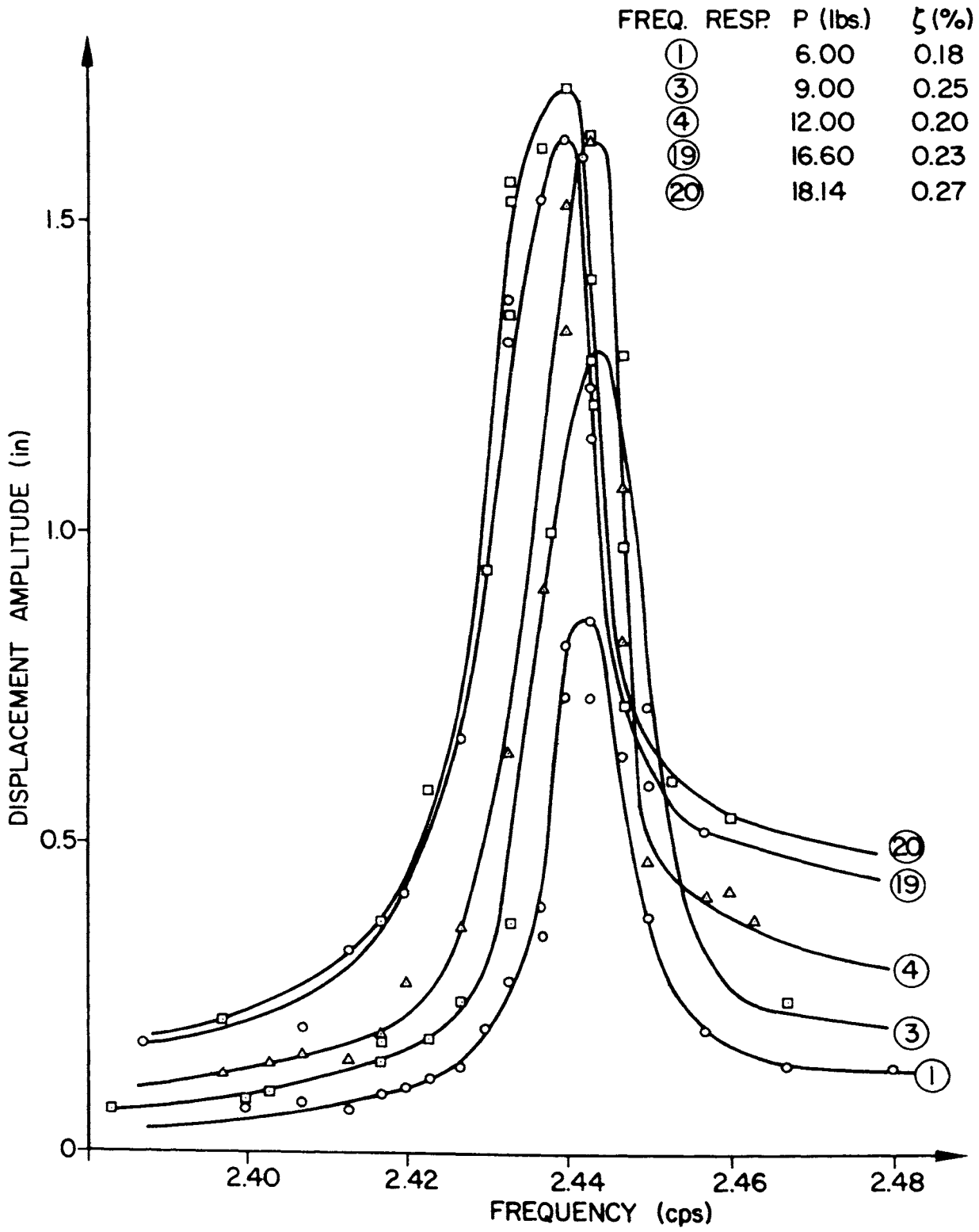

FIG. 3.4 FREQUENCY RESPONSES: TEST STRUCTURE NO. 2

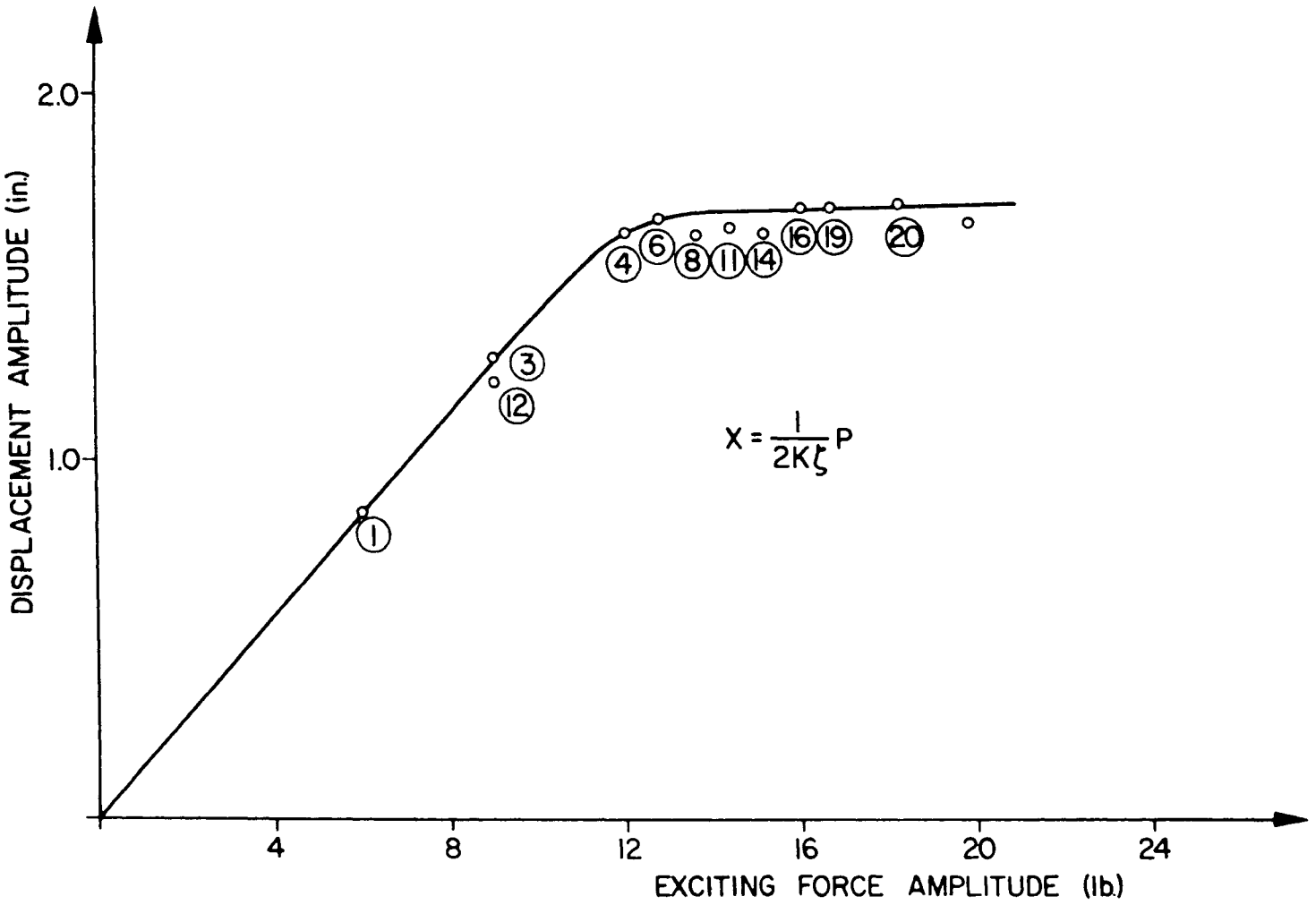

FIG. 3.5 RESONANT AMPLITUDE vs. EXCITING FORCE: TEST STUCTURE NO. 2

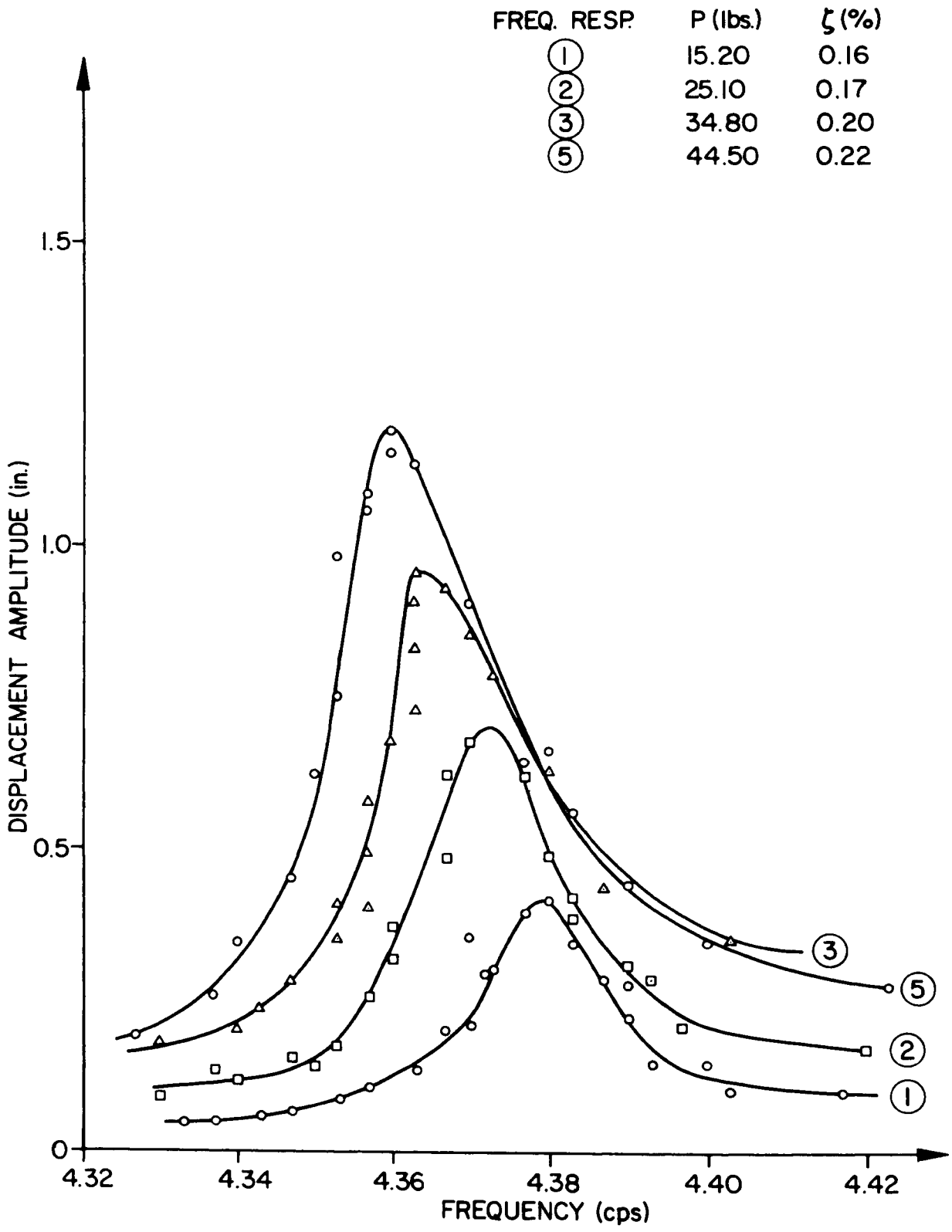

FIG. 3.6 FREQUENCY RESPONSES: TEST STRUCTURE NO. 3

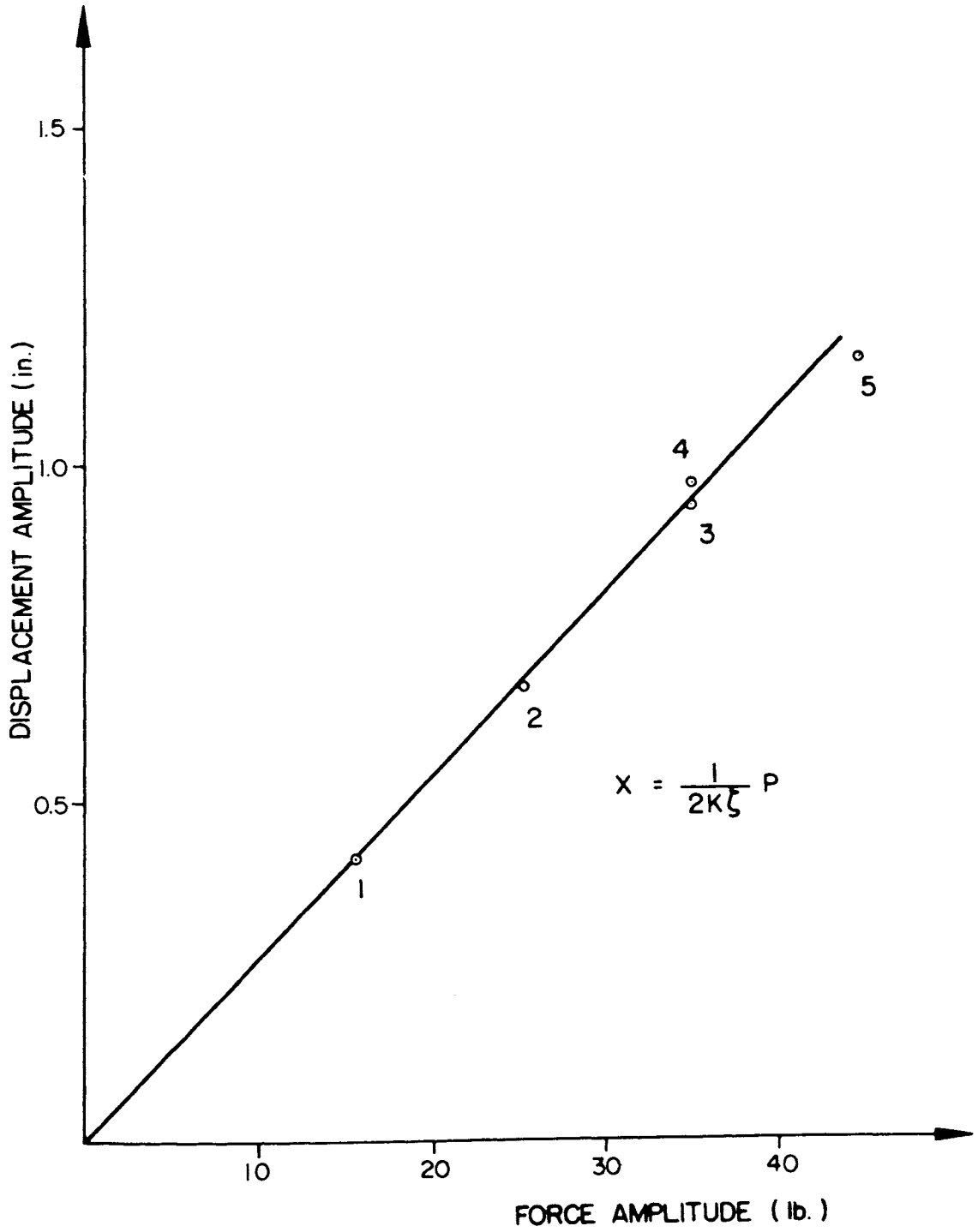

FIG. 3.7 RESONANT AMPLITUDE vs. EXCITING FORCE : TEST STRUCTURE NO. 3

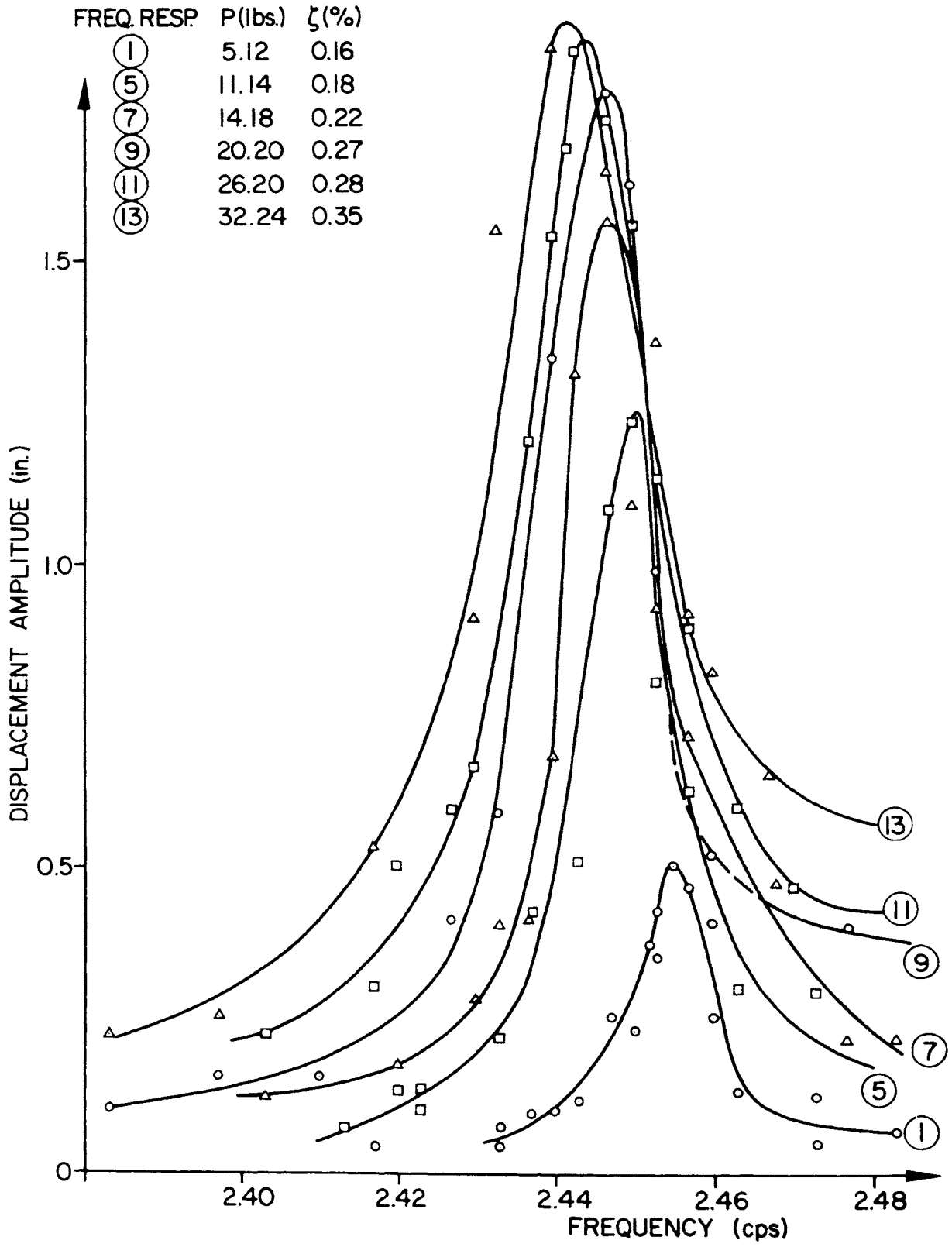

FIG. 3.8 FREQUENCY RESPONSES: TEST STRUCTURE NO. 4

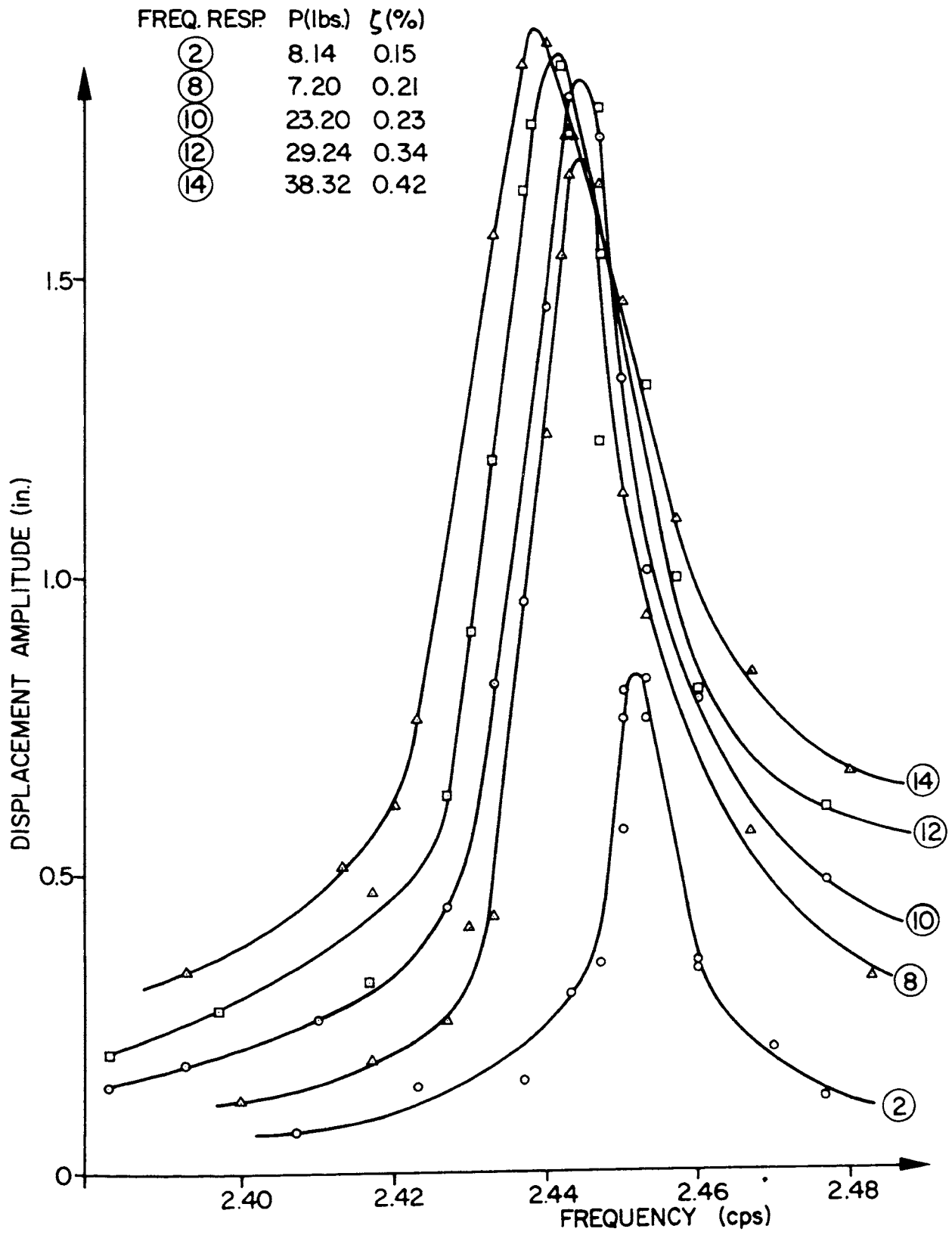

FIG. 3.9 FREQUENCY RESPONSES: TEST STRUCTURE NO. 4

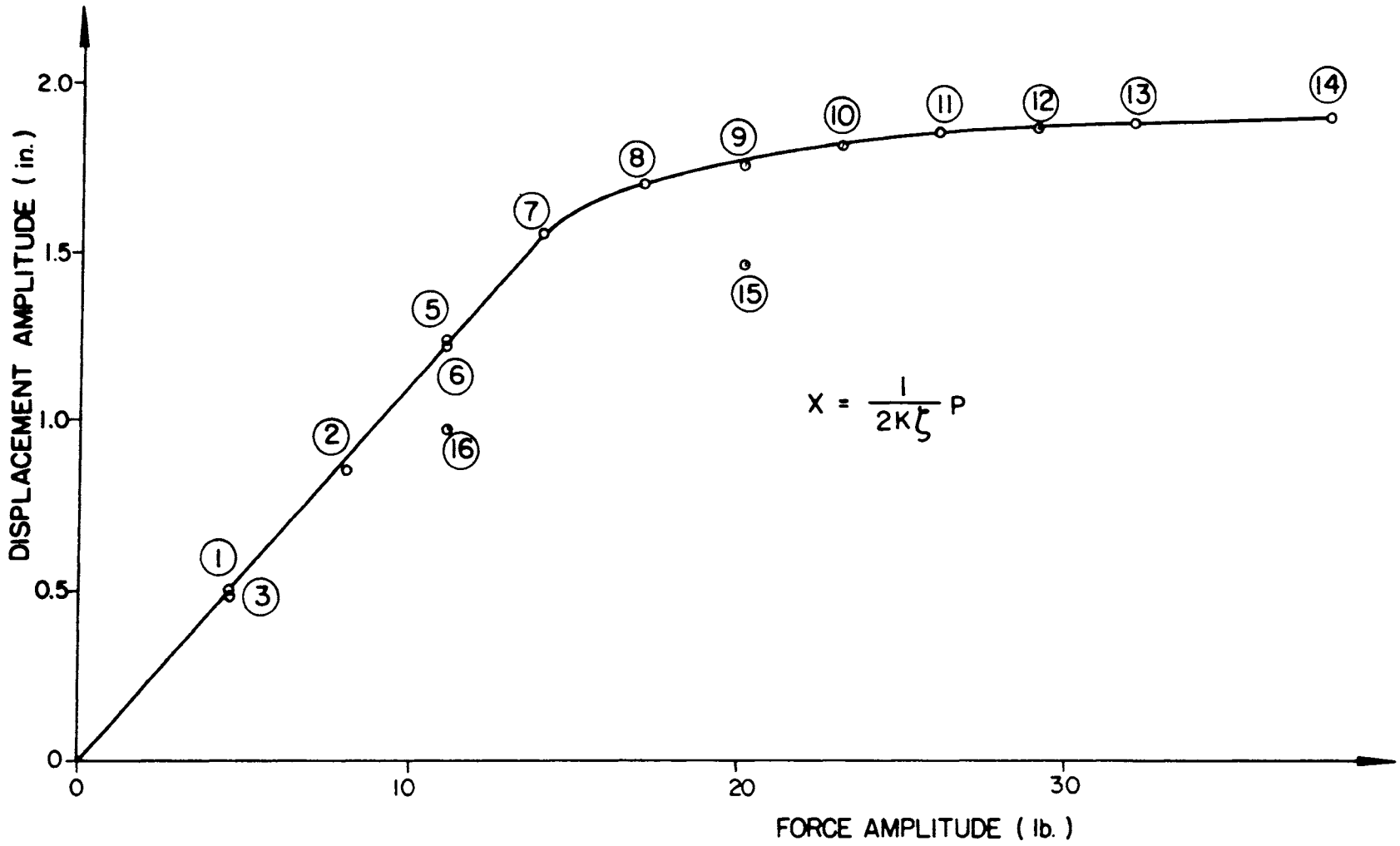

FIG. 3.10 RESONANT AMPLITUDE vs. EXCITING FORCE: TEST STRUCTURE NO. 4

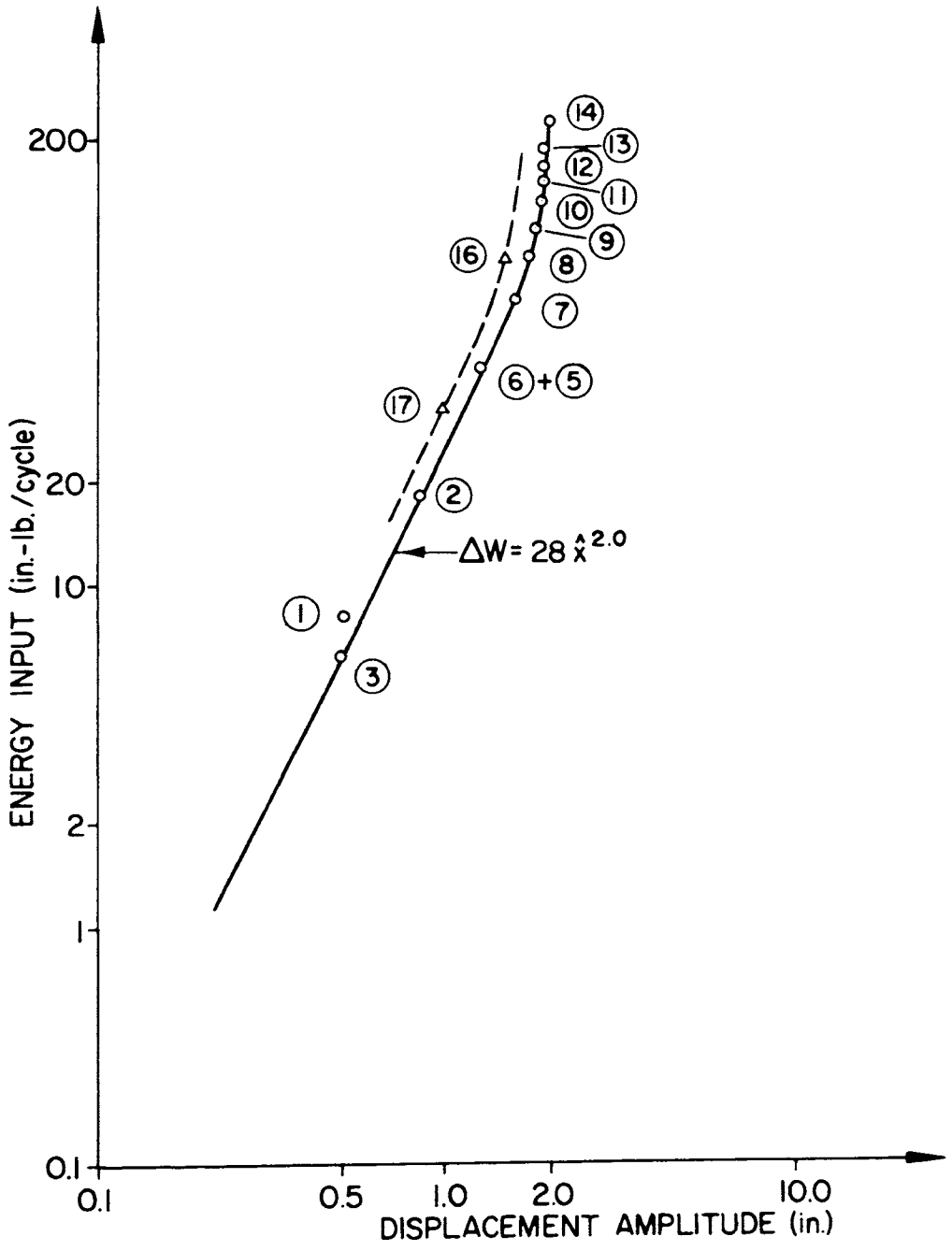

FIG. 3.11 ENERGY DISSIPATED PER CYCLE: TEST STRUCTURE NO. 4

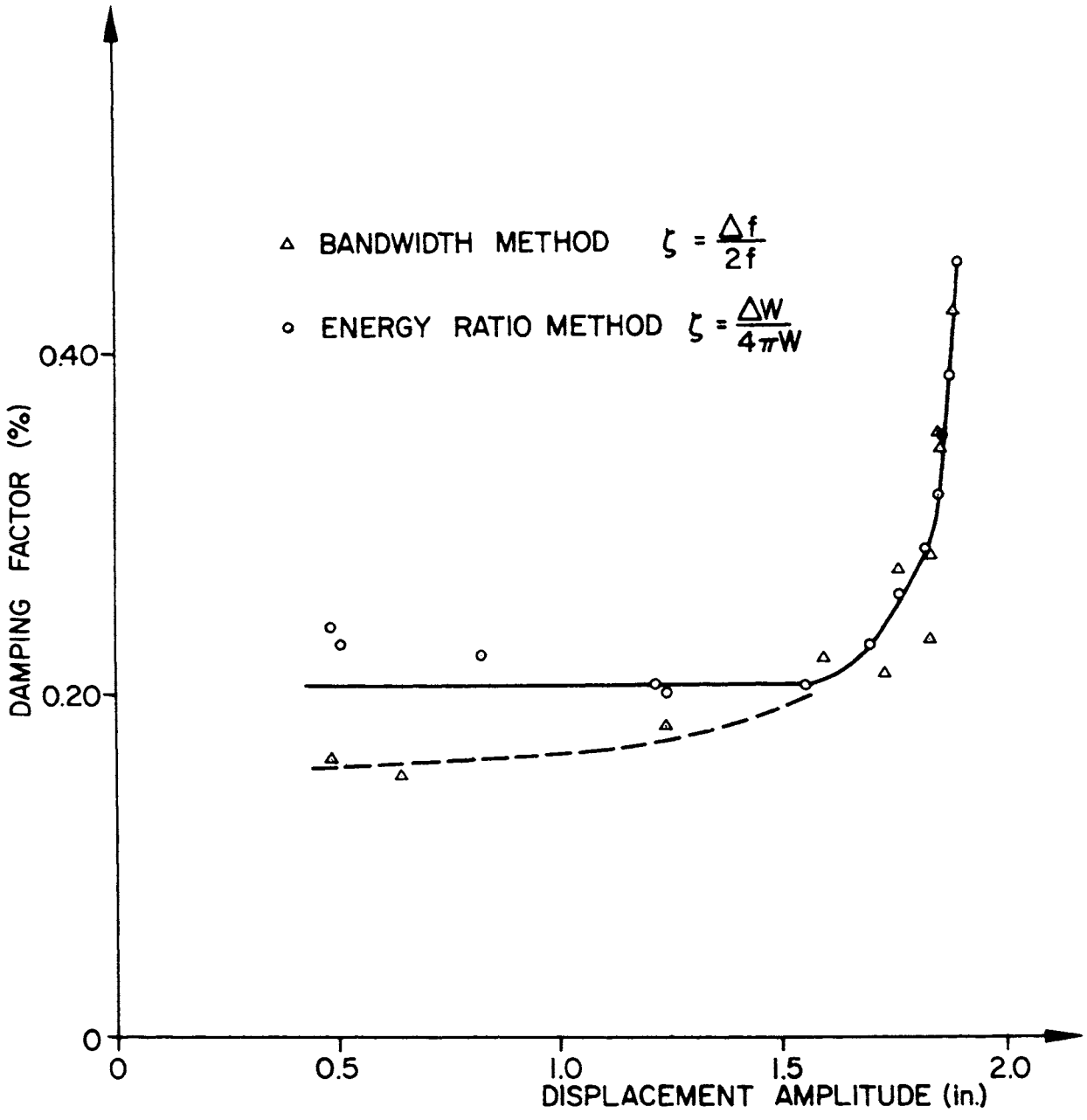

FIG. 3.12 DAMPING FACTORS FOR TEST STRUCTURE NO. 4

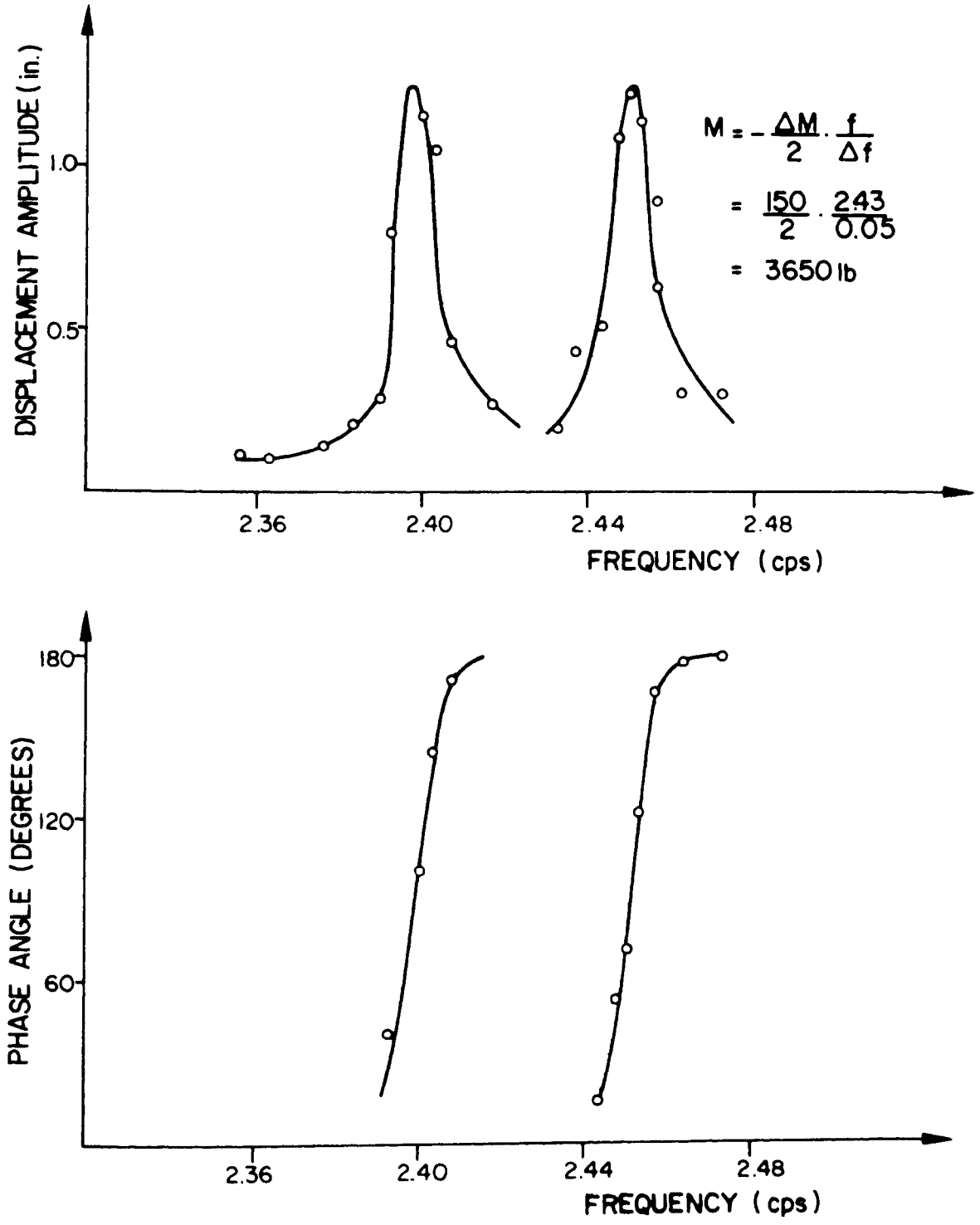

FIG. 3.13 DETERMINATION OF GENERALIZED MASS OF TEST STRUCTURE NO. 4

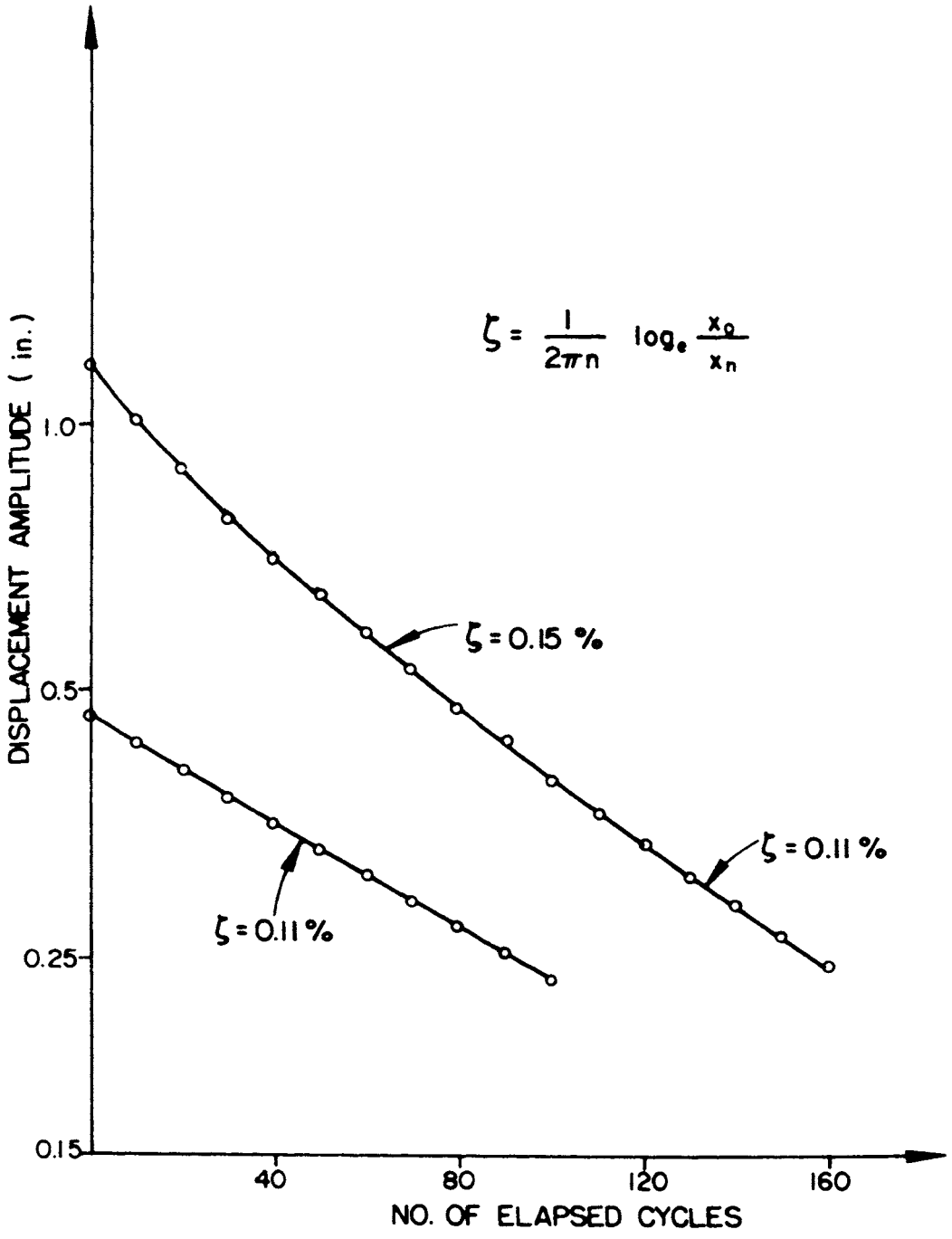

FIG. 3.14 LOGARITHMIC DECAY CURVE: TEST STRUCTURE NO. 4

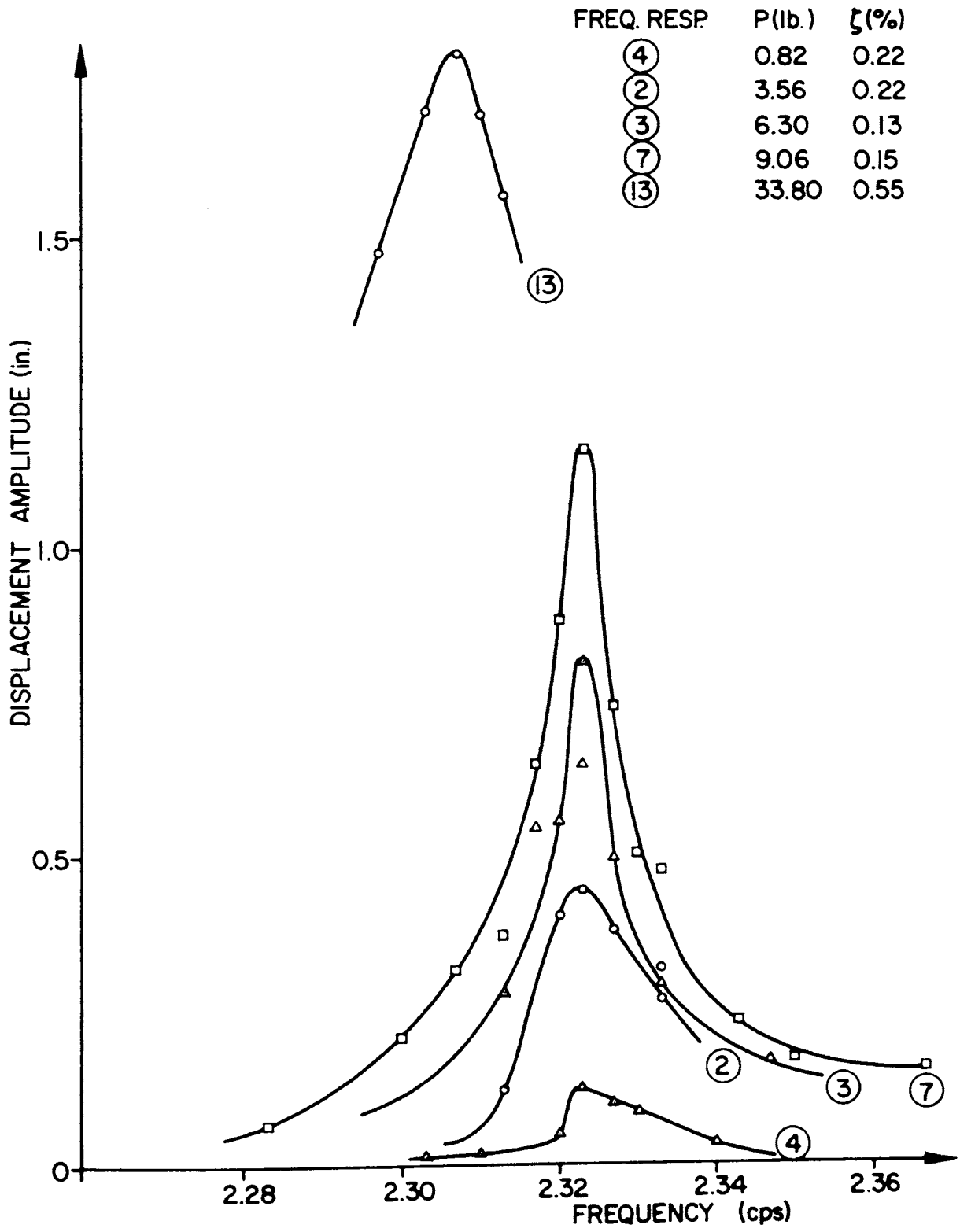

FIG. 3.15 FREQUENCY RESPONSES: TEST STRUCTURE NO. 5

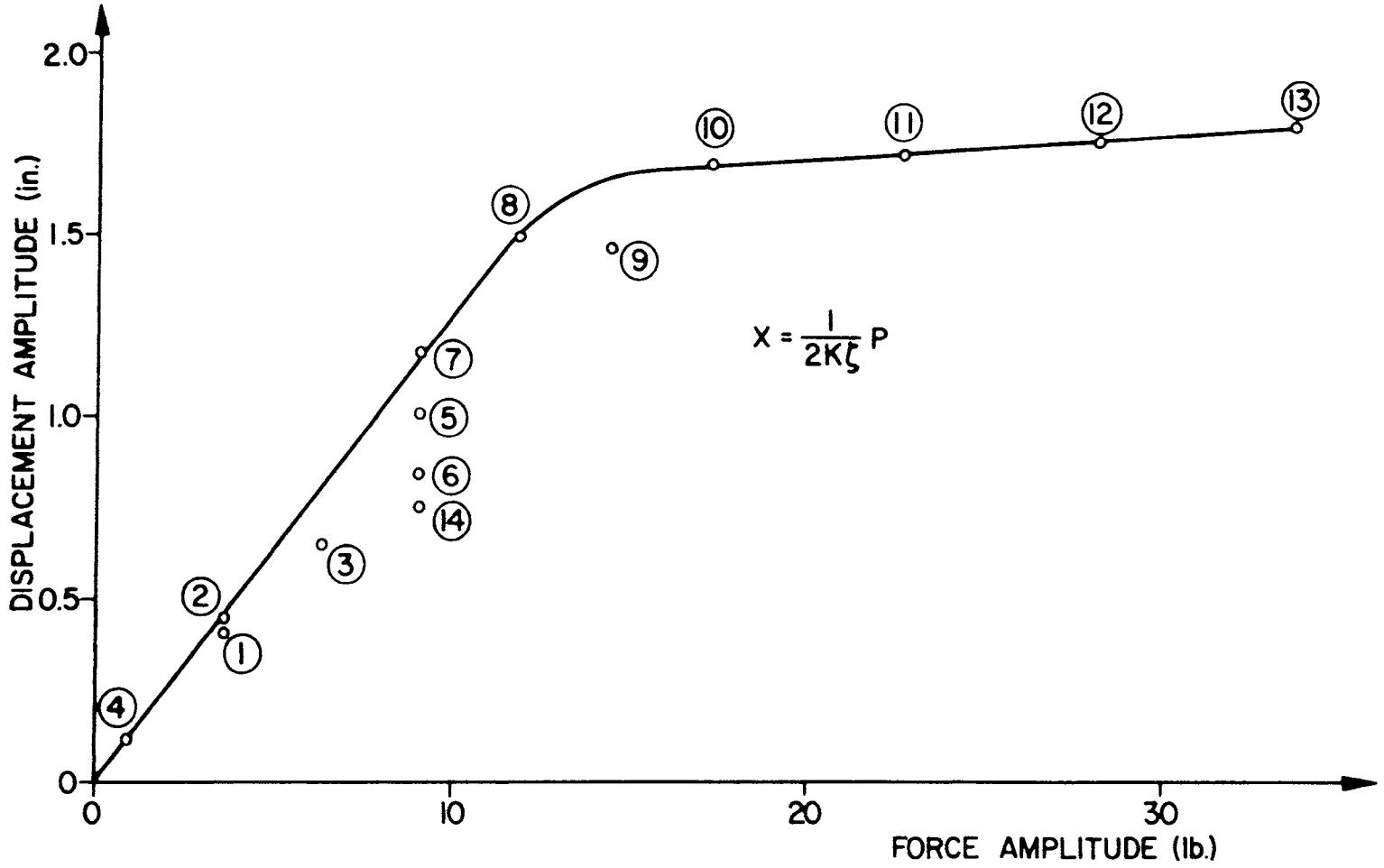

FIG. 3.16 RESONANT AMPLITUDE vs. EXCITING FORCE: TEST STRUCTURE NO. 5

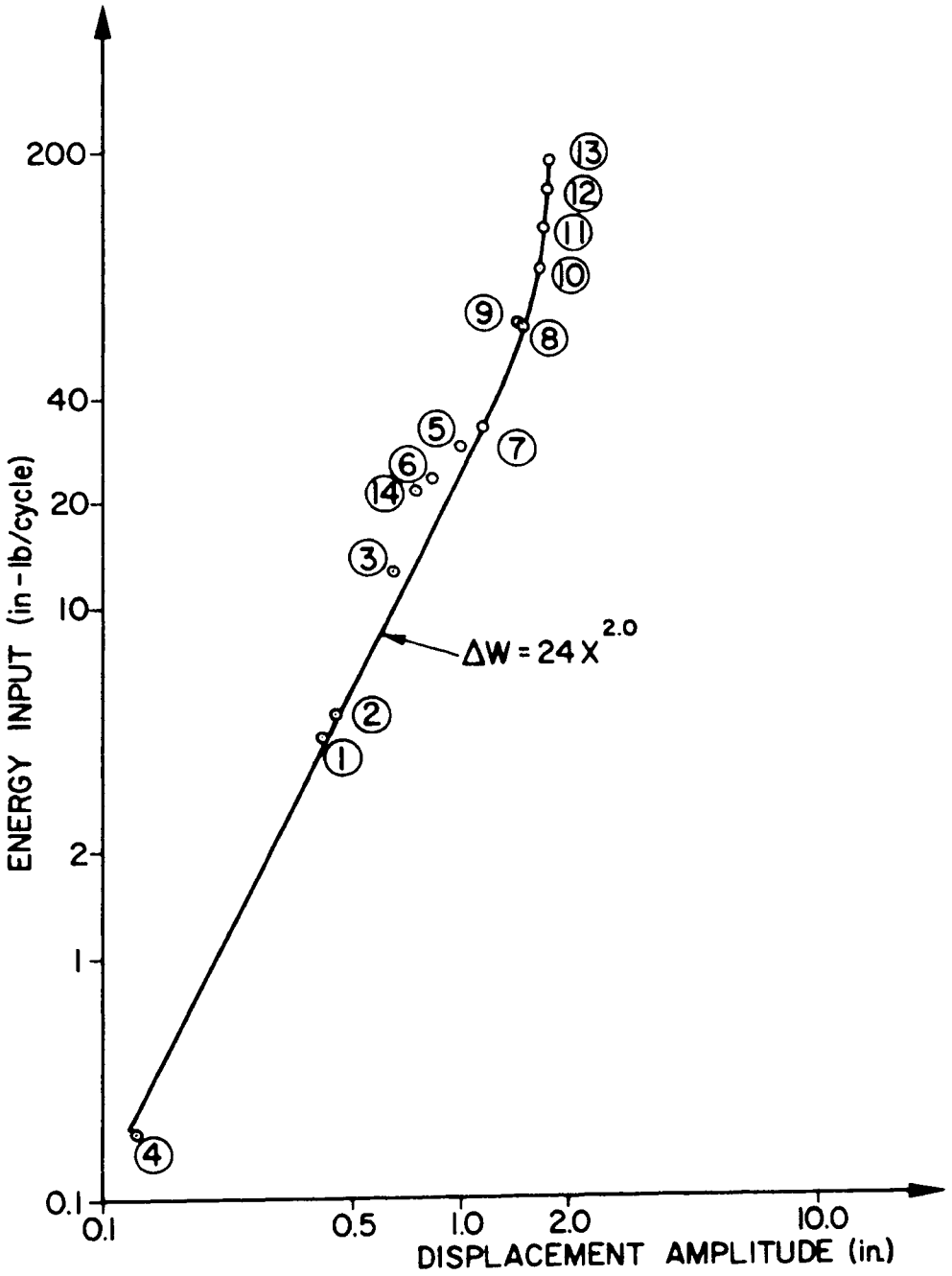

FIG. 3.17 ENERGY DISSIPATED PER CYCLE: TEST STRUCTURE NO. 5

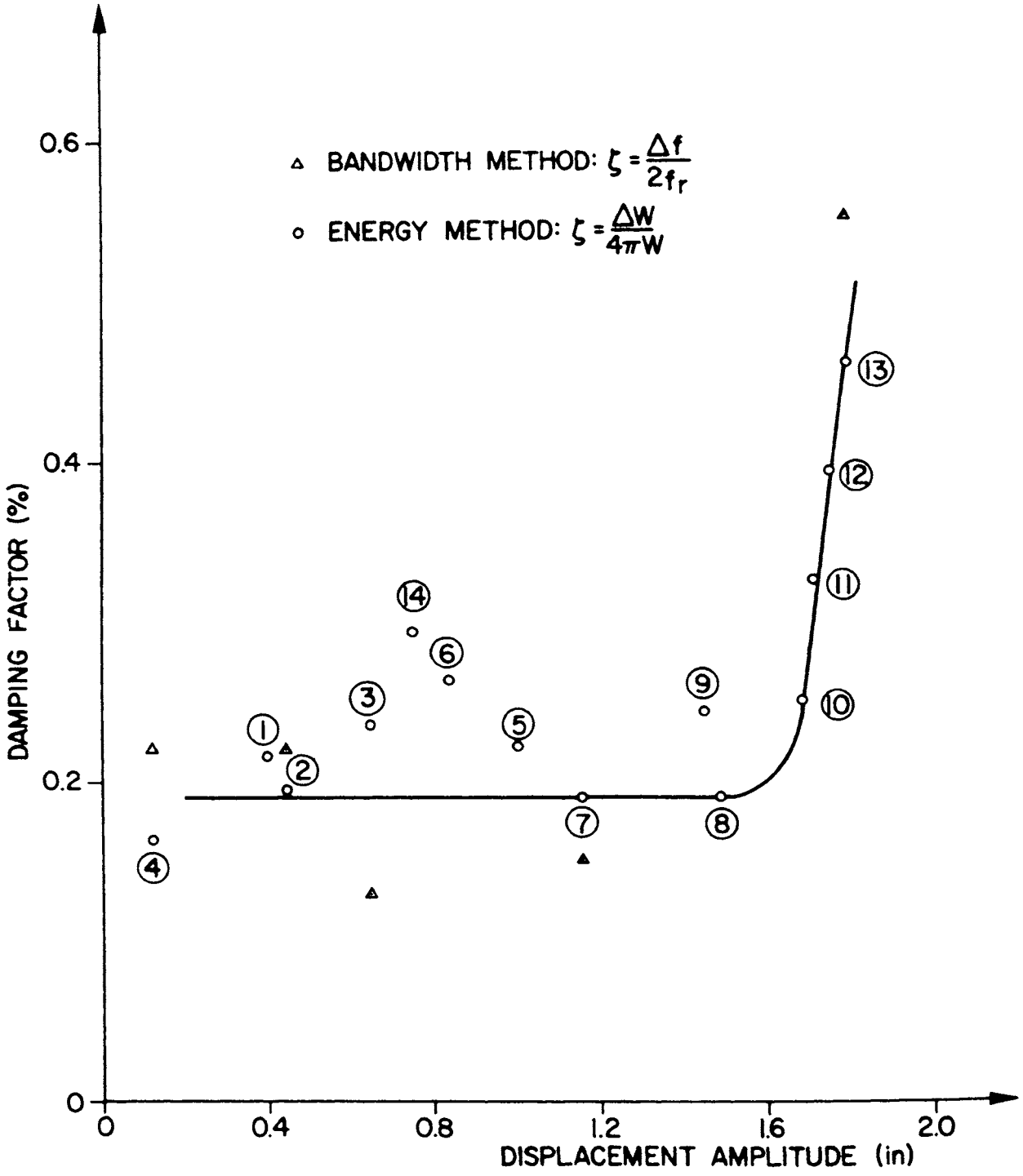

FIG. 3.18 DAMPING FACTORS FOR TEST STRUCTURE NO. 5

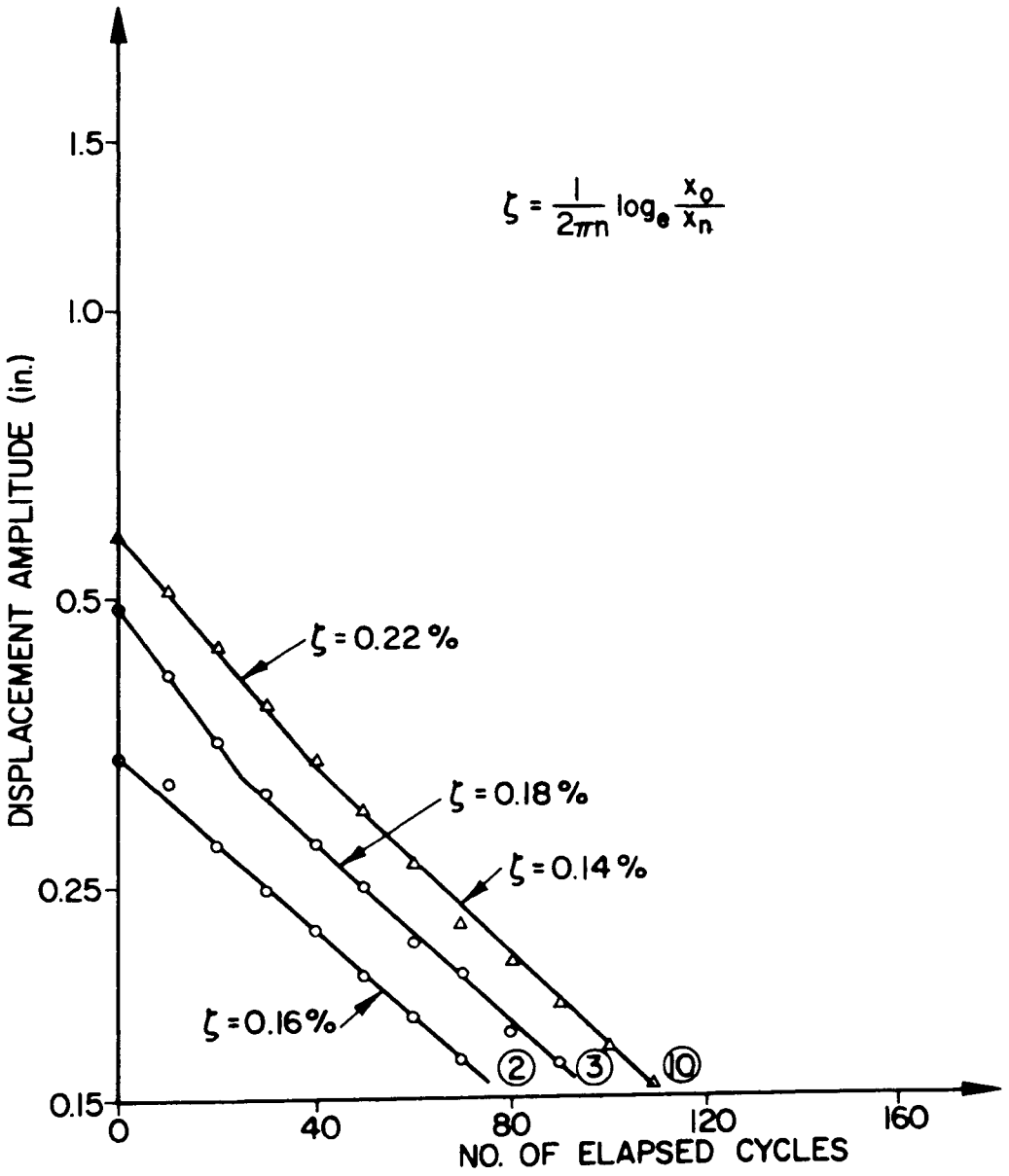

FIG. 3.19 LOGARITHMIC DECAY CURVES: TEST STRUCTURE NO. 5

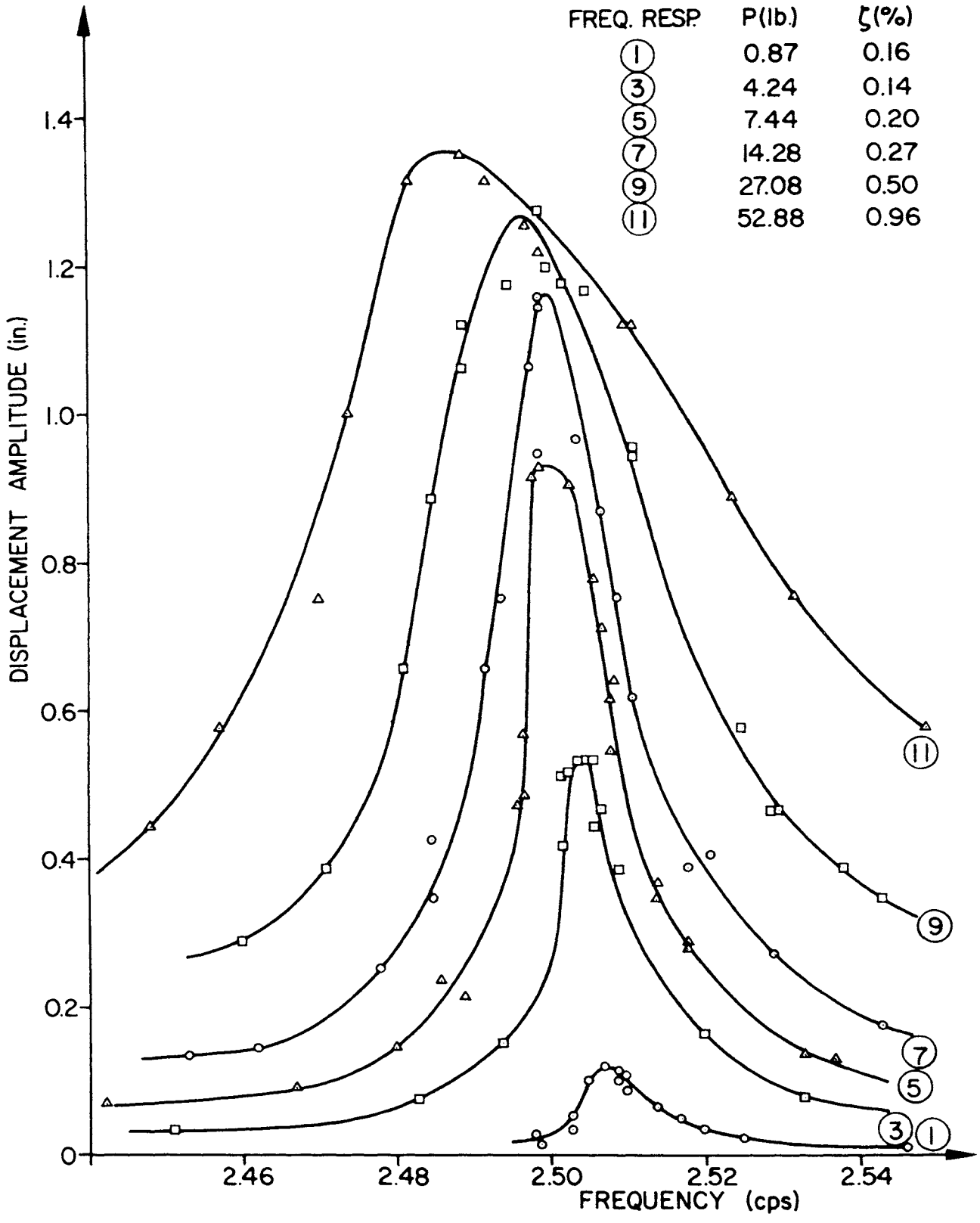

FIG. 3.20 FREQUENCY RESPONSES: TEST STRUCTURE NO. 6

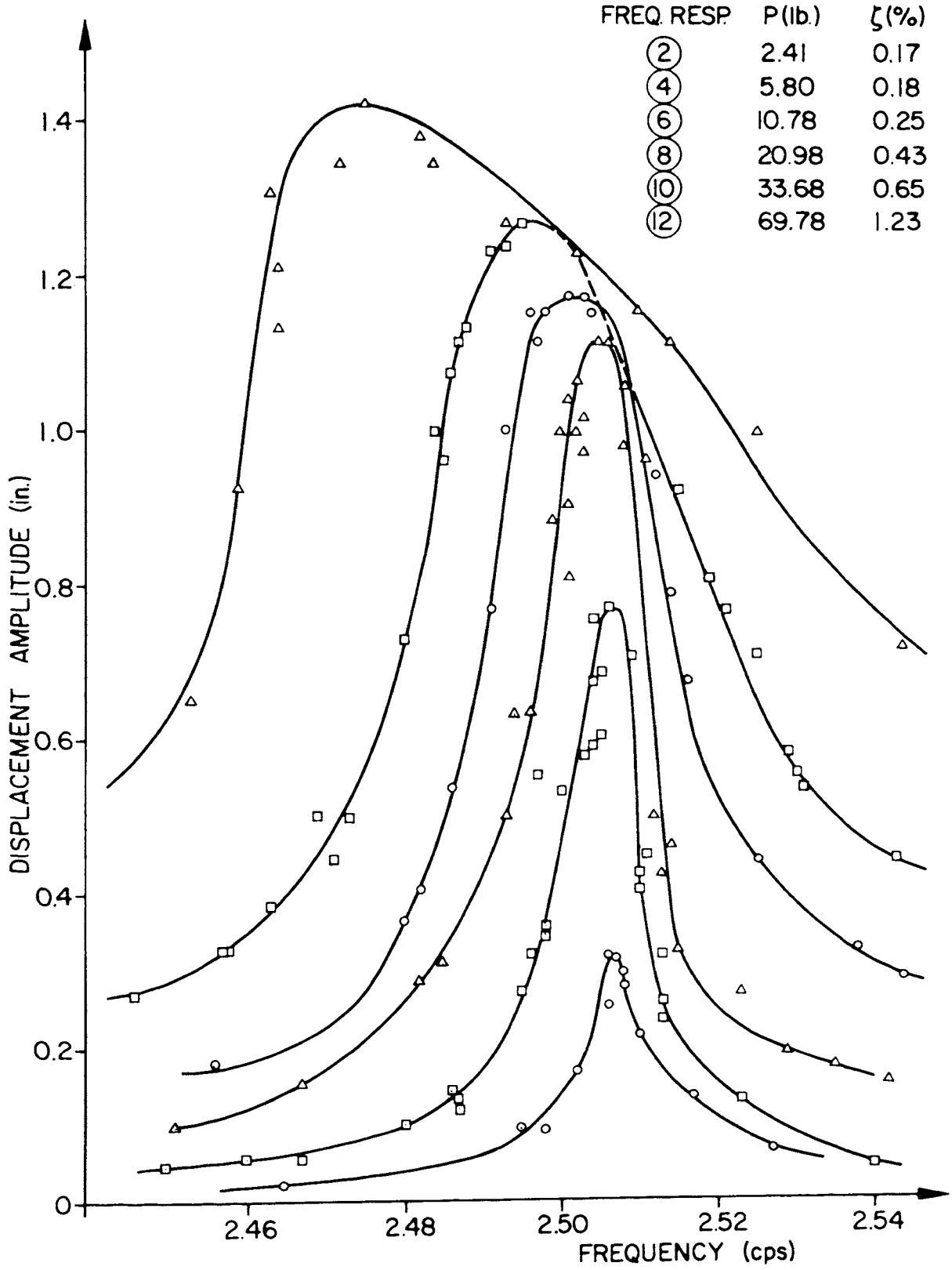

FIG. 3.21 FREQUENCY RESPONSES: TEST STRUCTURE NO. 6

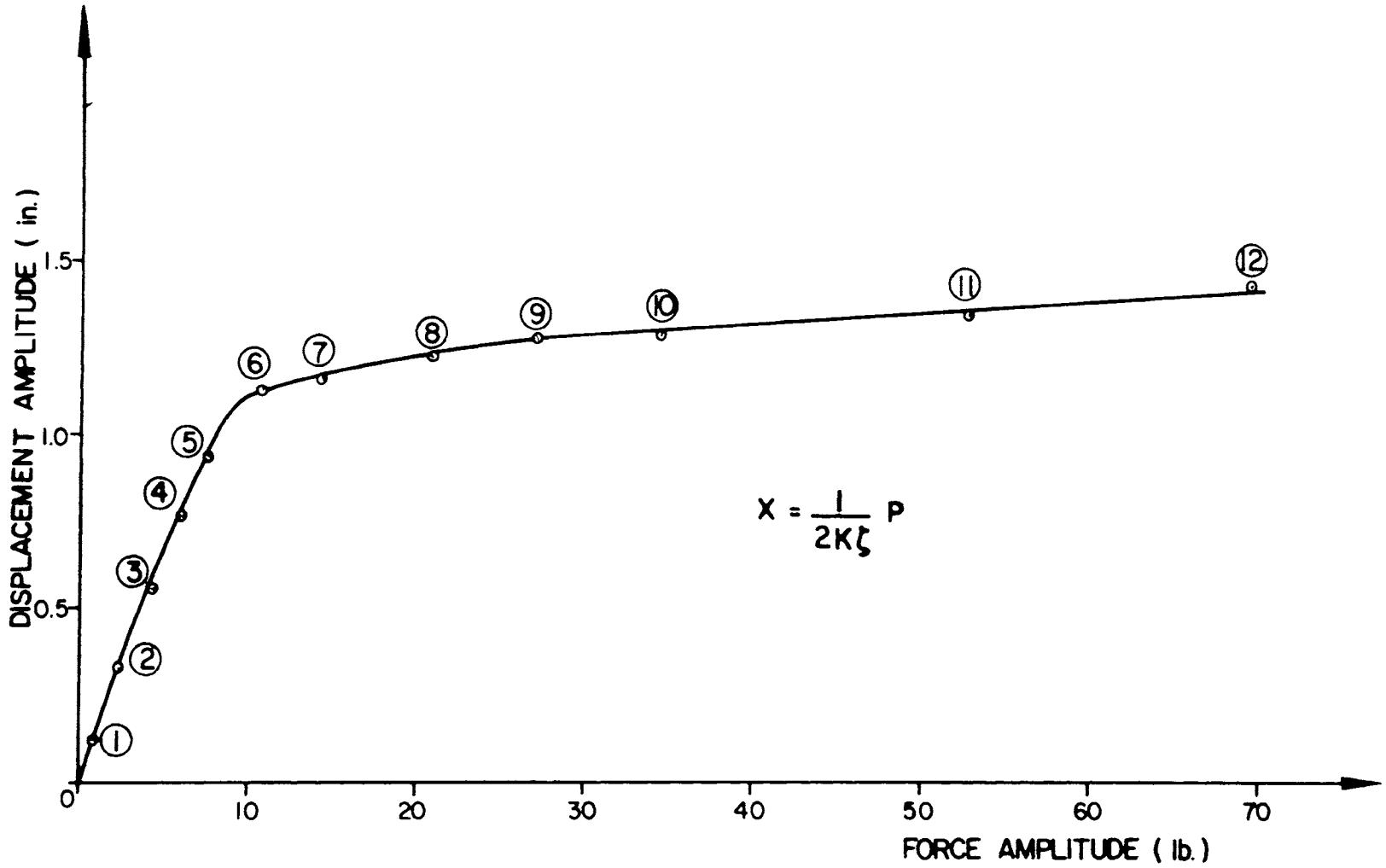

FIG. 3.22 RESONANT AMPLITUDE vs. EXCITING FORCE: TEST STRUCTURE NO.6

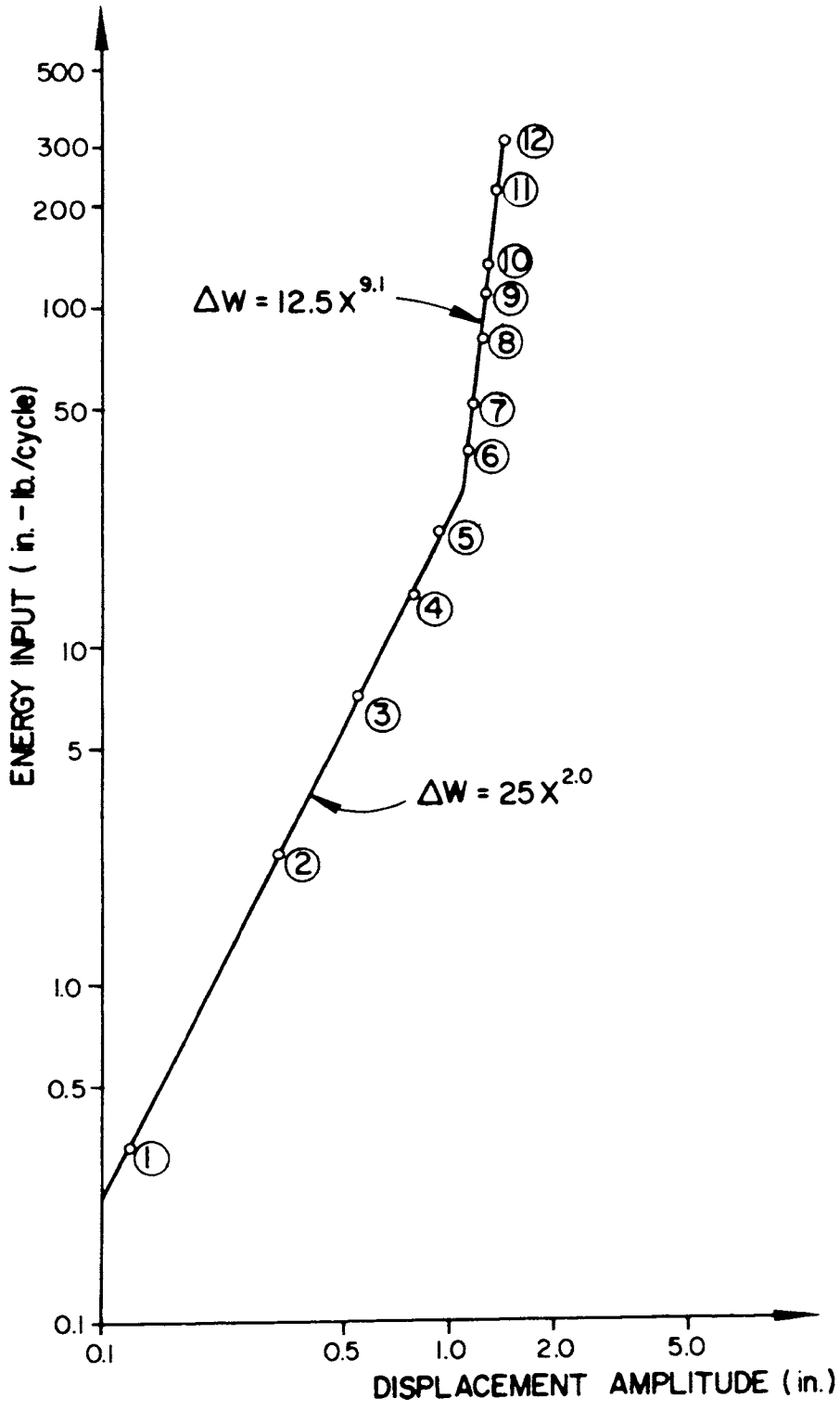

FIG. 3.23 ENERGY DISSIPATED PER CYCLE : TEST STRUCTURE NO. 6

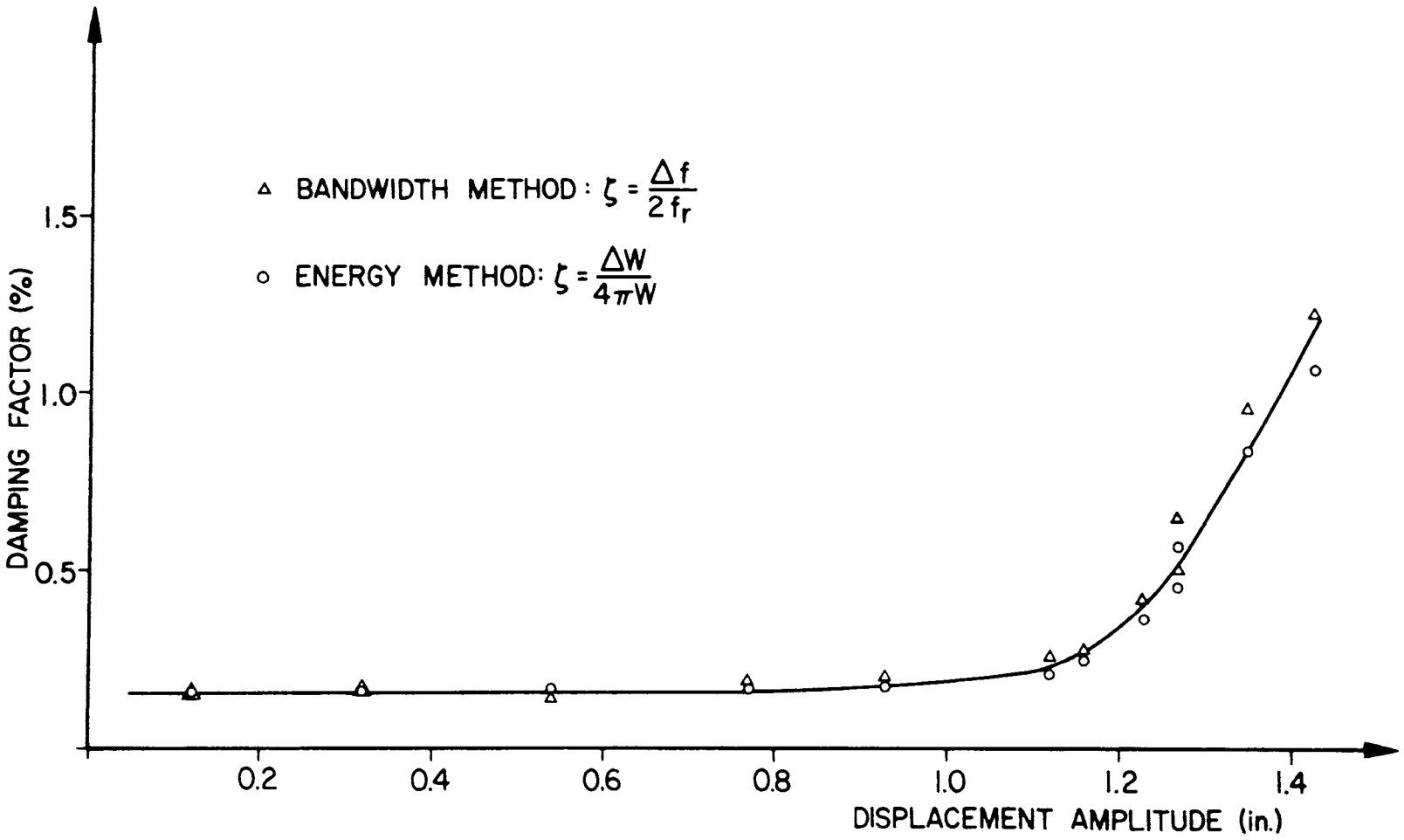

FIG. 3.24 DAMPING FACTORS FOR TEST STRUCTURE NO. 6

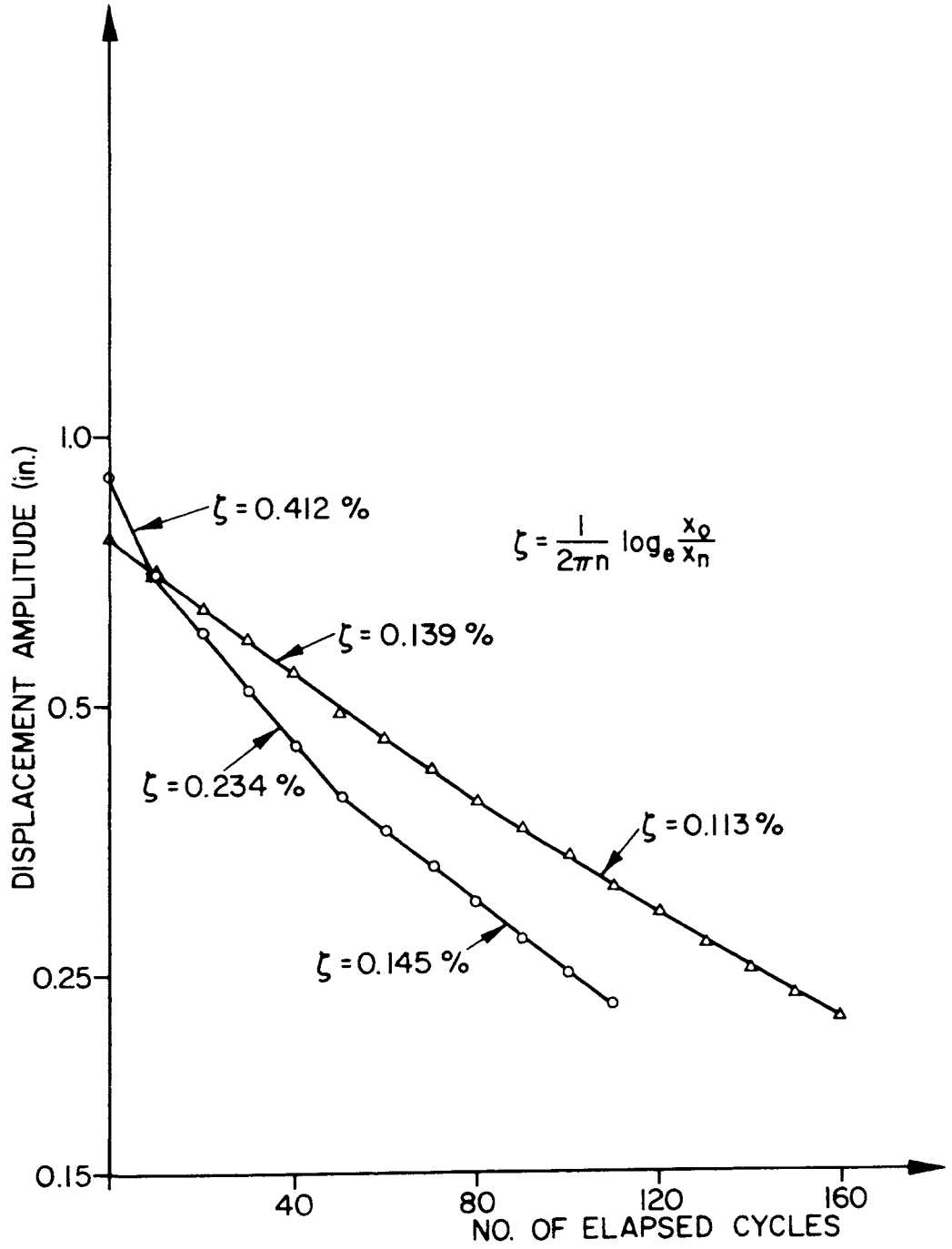

FIG. 3.25 LOGARITHMIC DECAY CURVES: TEST STRUCTURE NO. 6

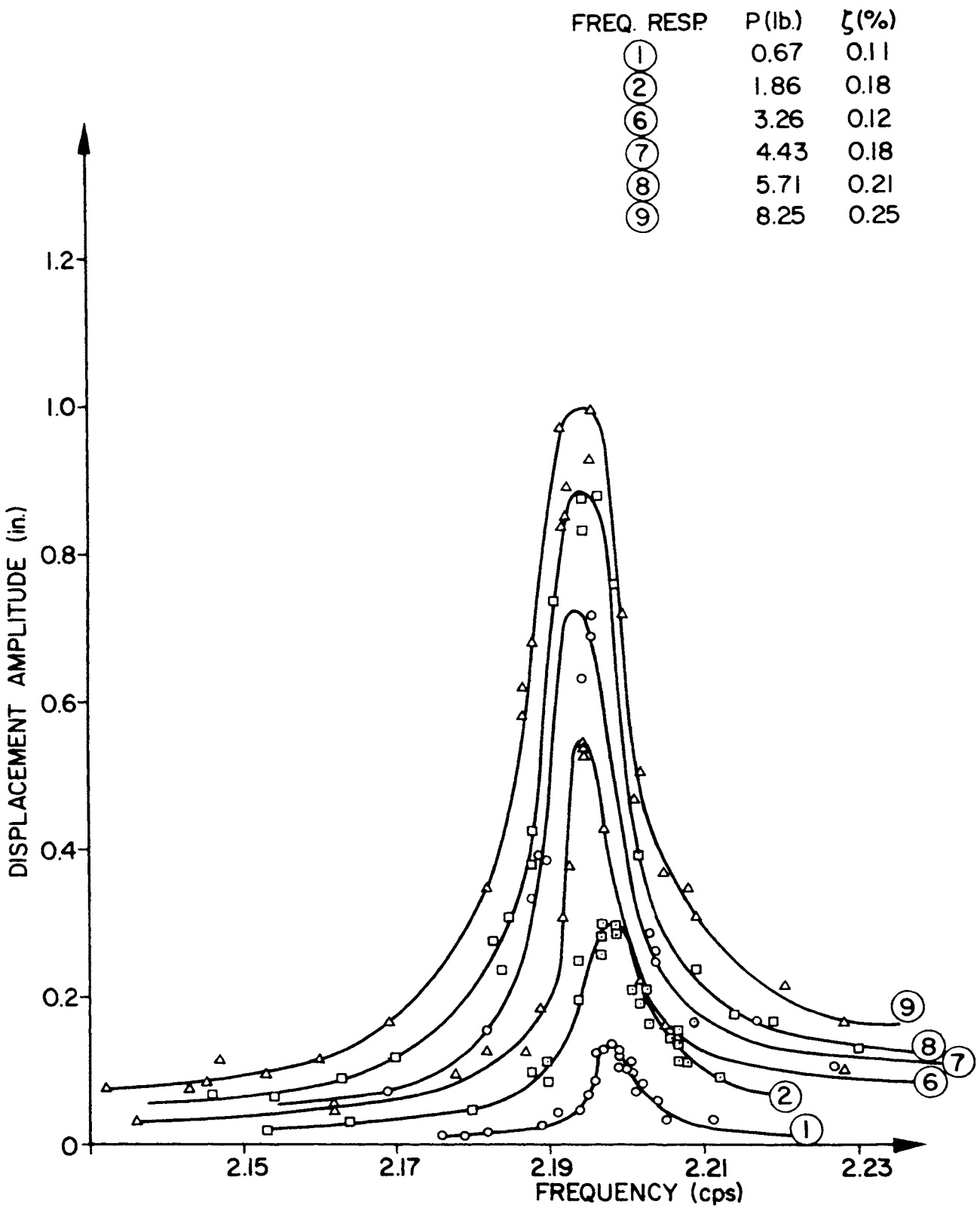

FIG. 3.26 FREQUENCY RESPONSES: TEST STRUCTURE NO. 7

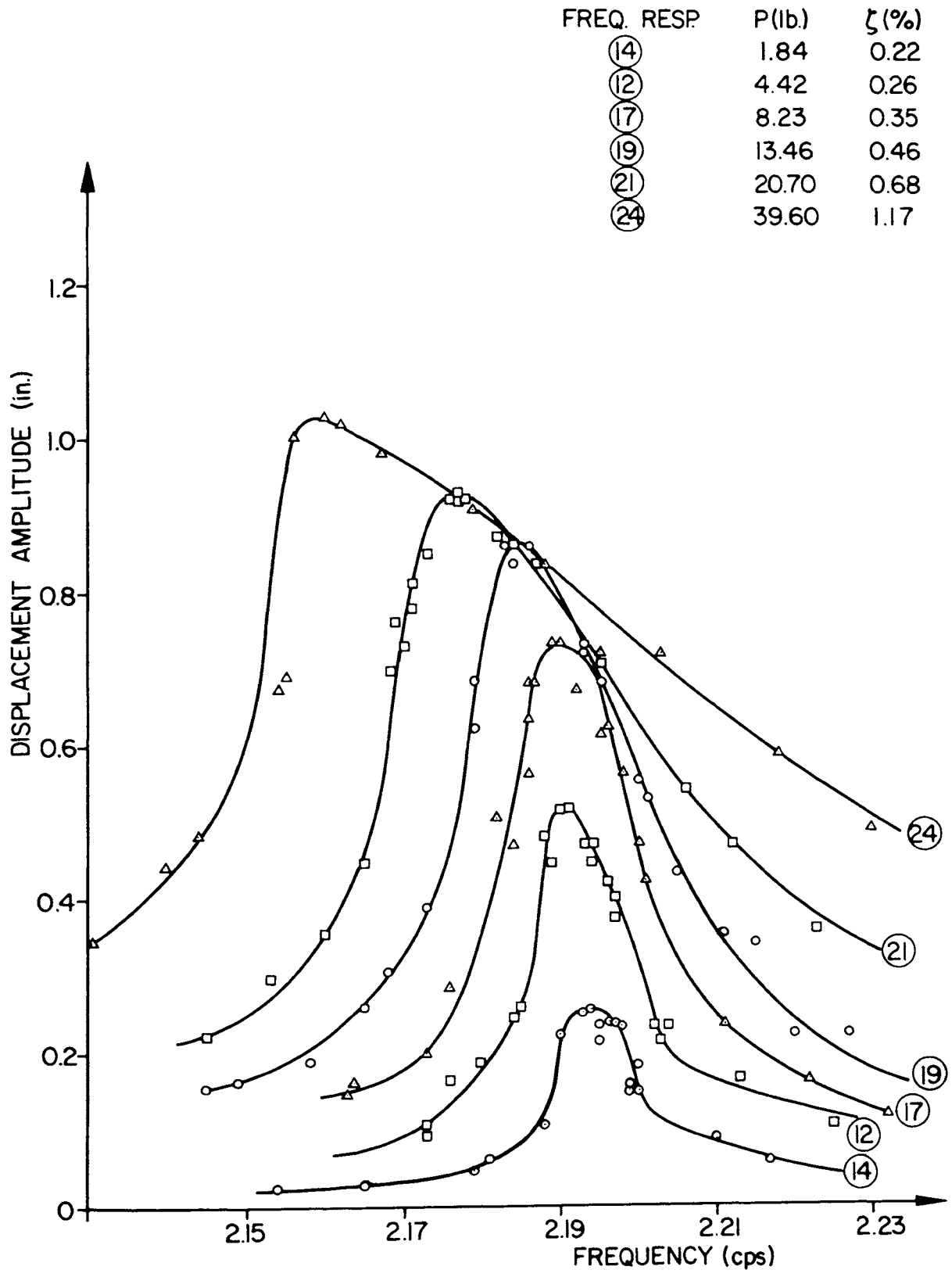

FIG. 3.27 FREQUENCY RESPONSES: TEST STRUCTURE NO. 7

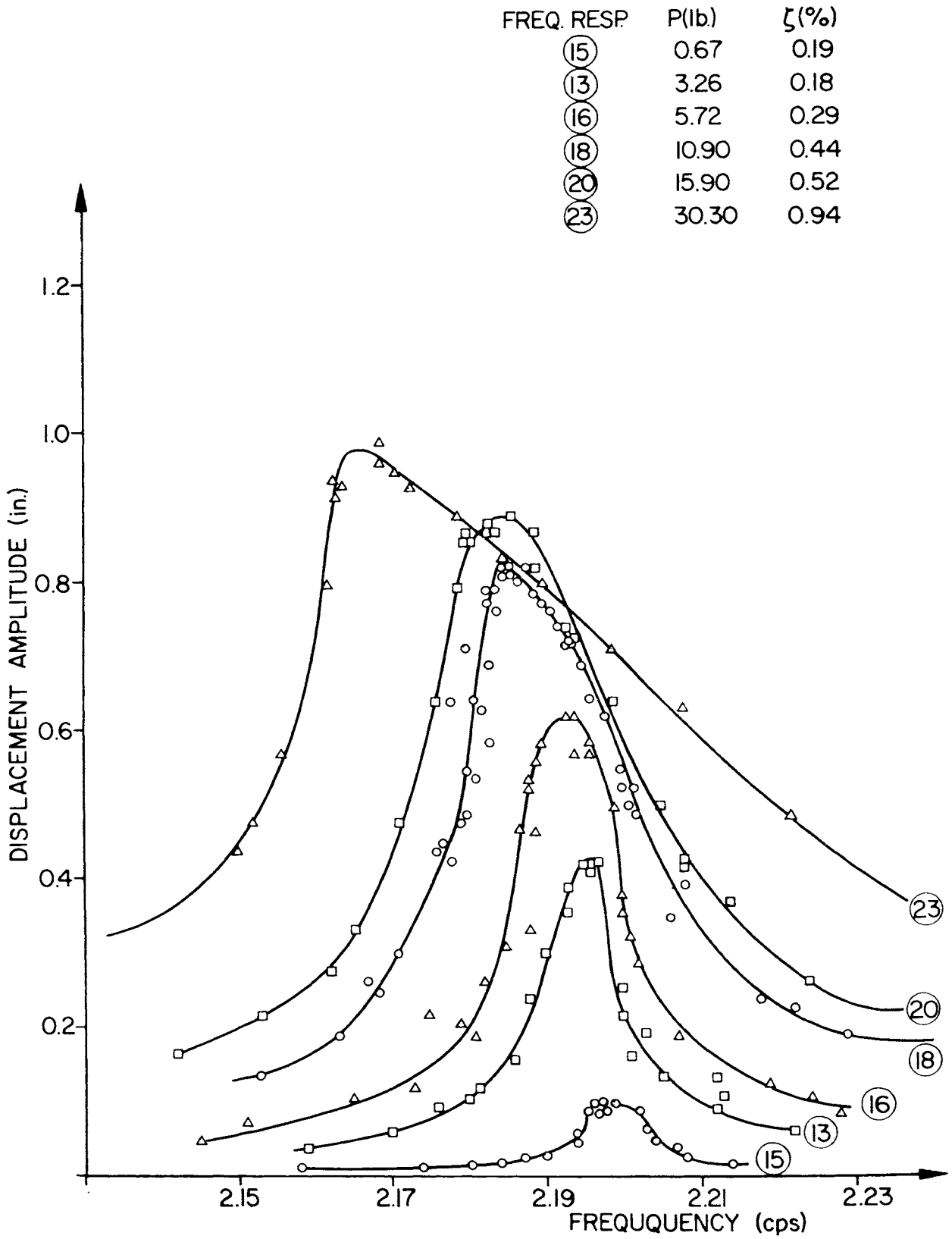

FIG. 3.28 FREQUENCY RESPONSES: TEST STRUCTURE NO. 7

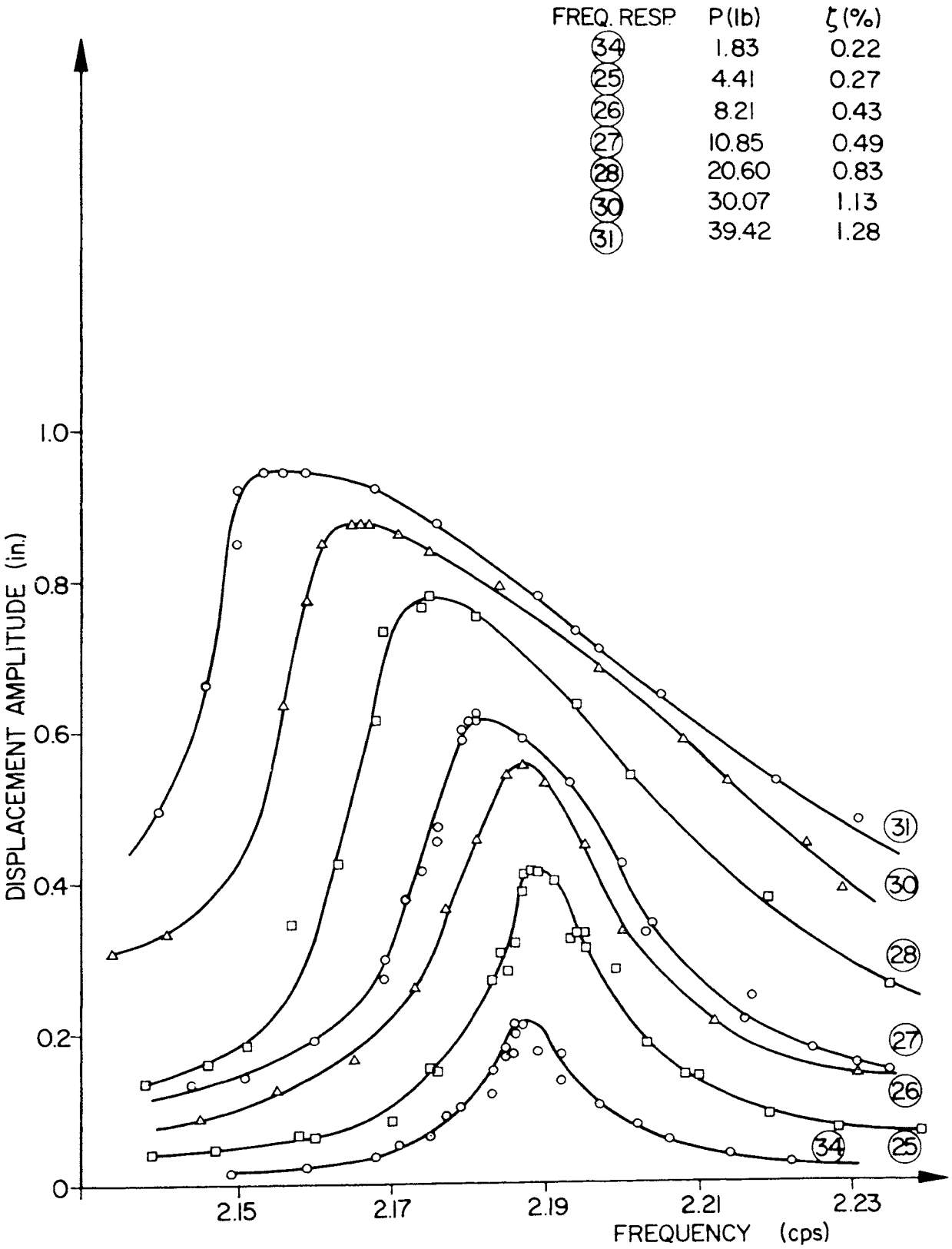

FIG. 3.29 FREQUENCY RESPONSES: TEST STRUCTURE NO. 7

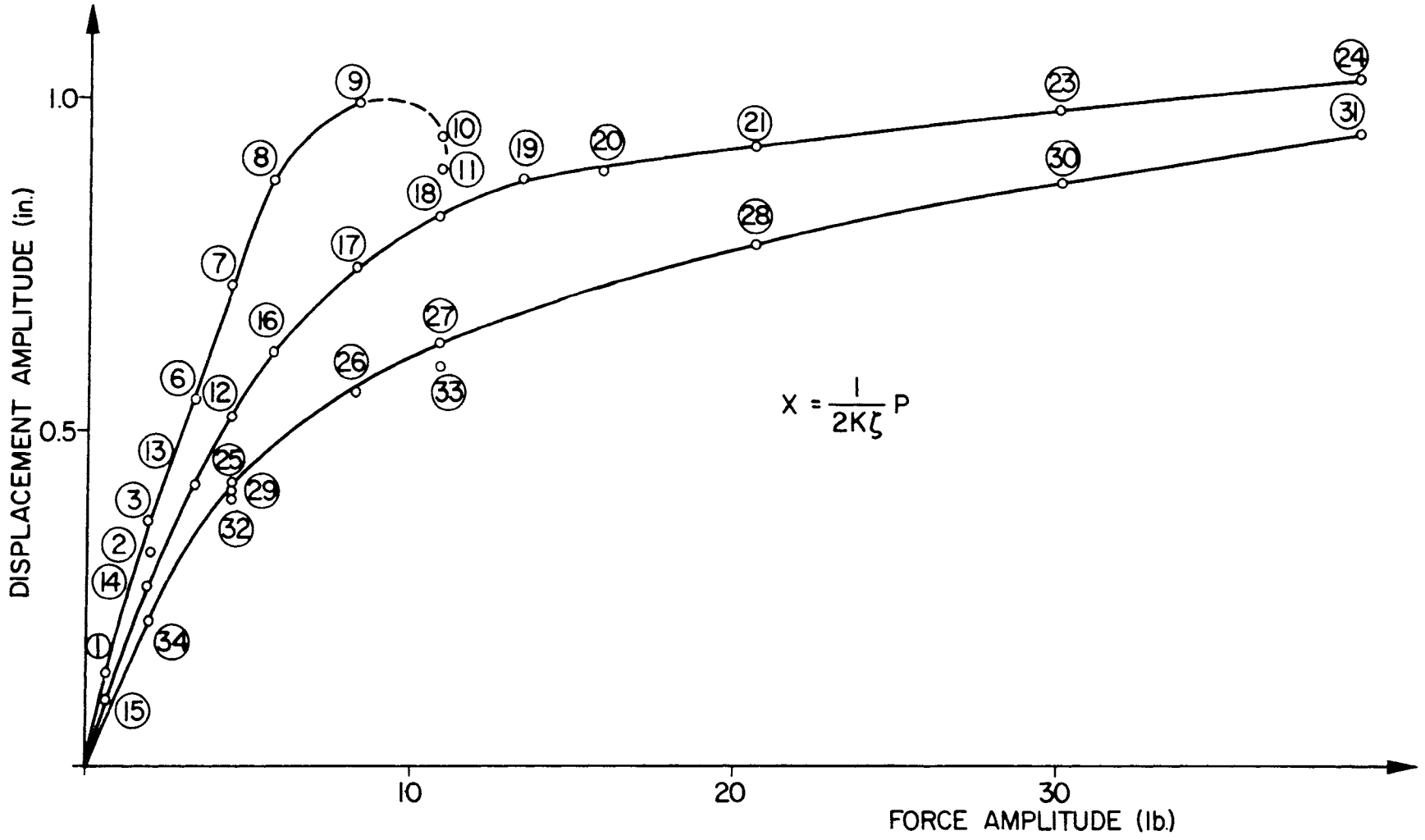

FIG. 3.30 RESONANT AMPLITUDE vs. EXCITING FORCE: TEST STRUCTURE NO. 7

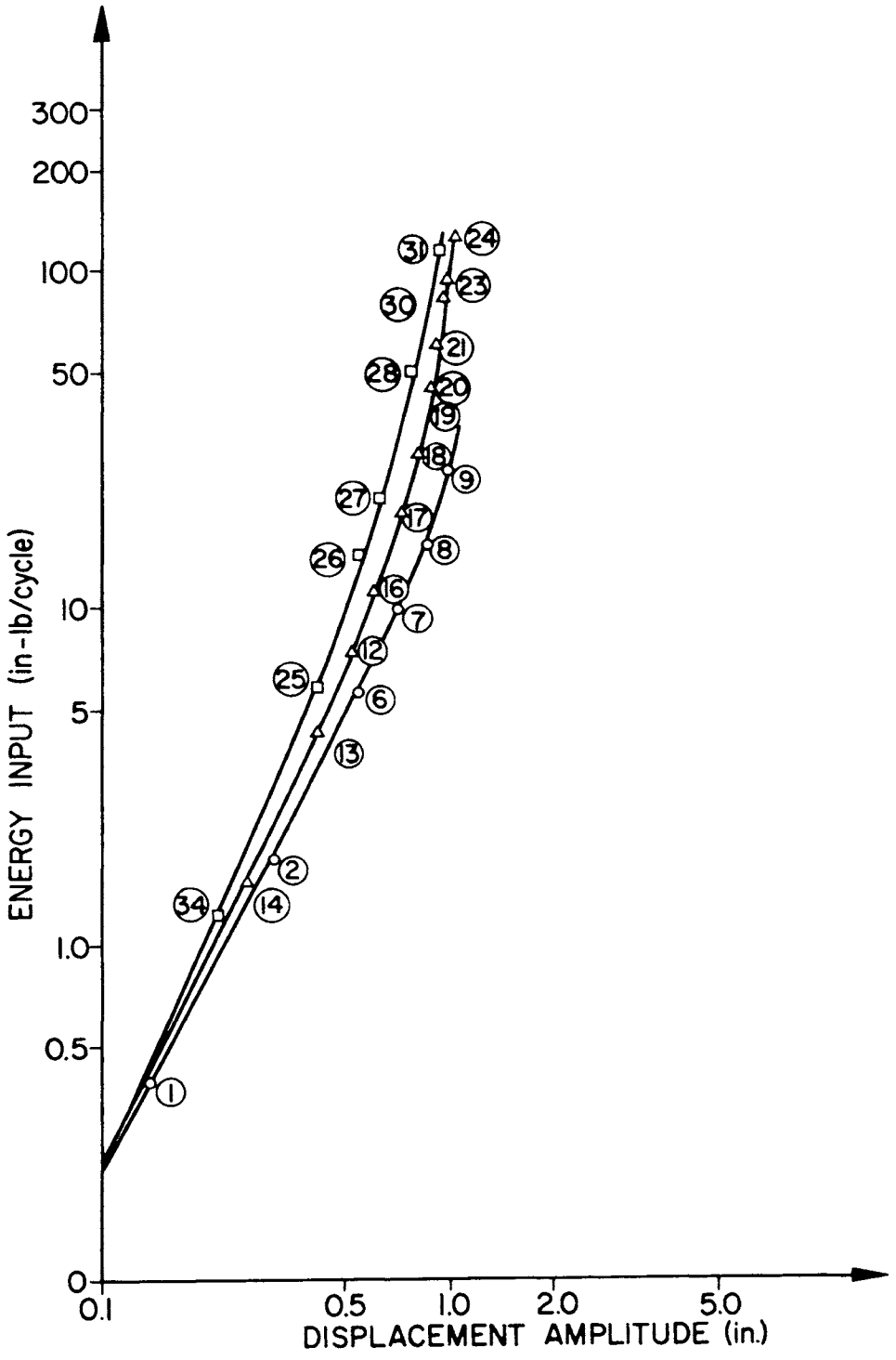

FIG. 3.31 ENERGY DISSIPATED PER CYCLE: TEST STRUCTURE NO. 7

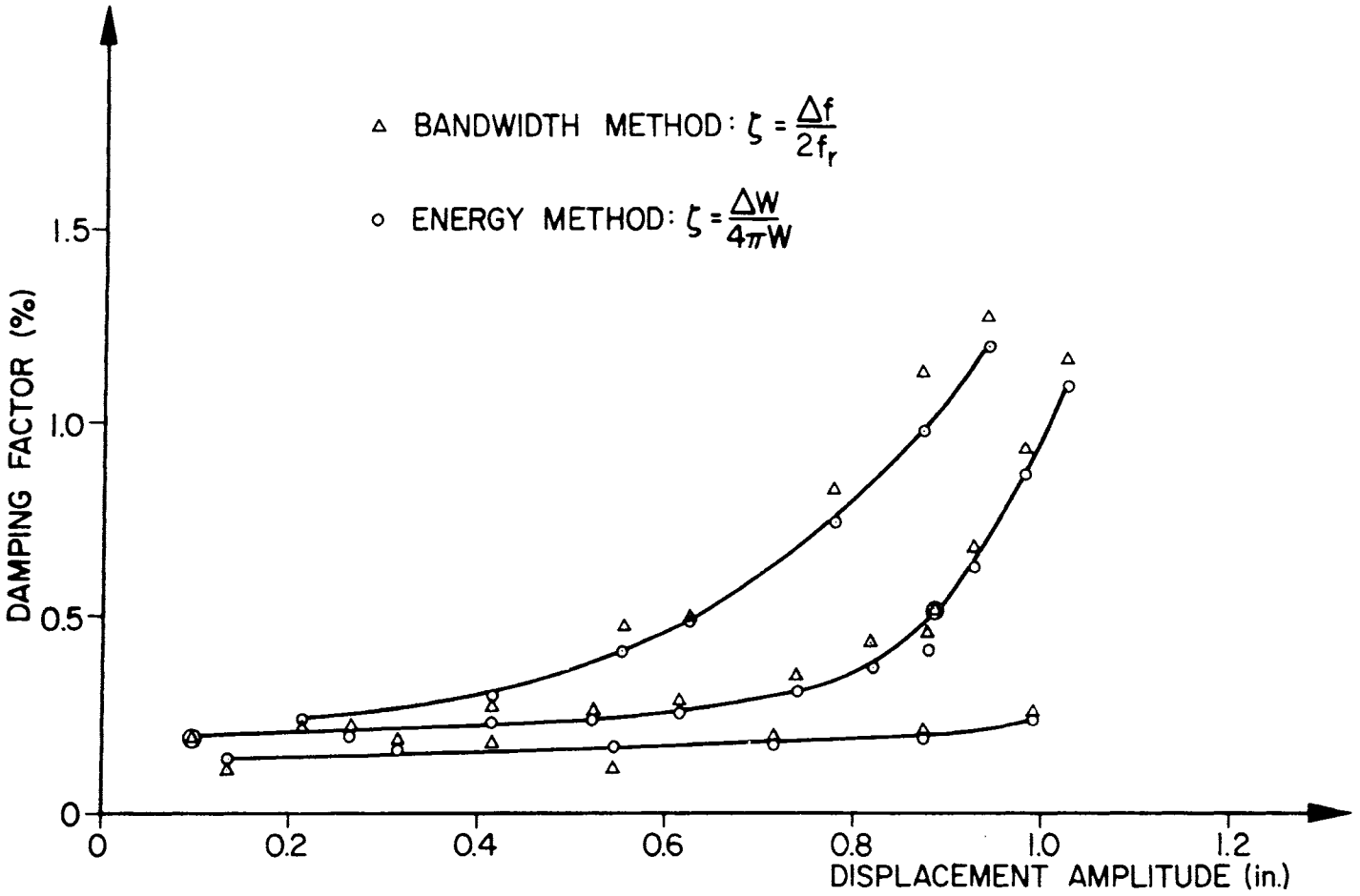

FIG. 3.32 DAMPING FACTORS FOR TEST STRUCTURE NO. 7

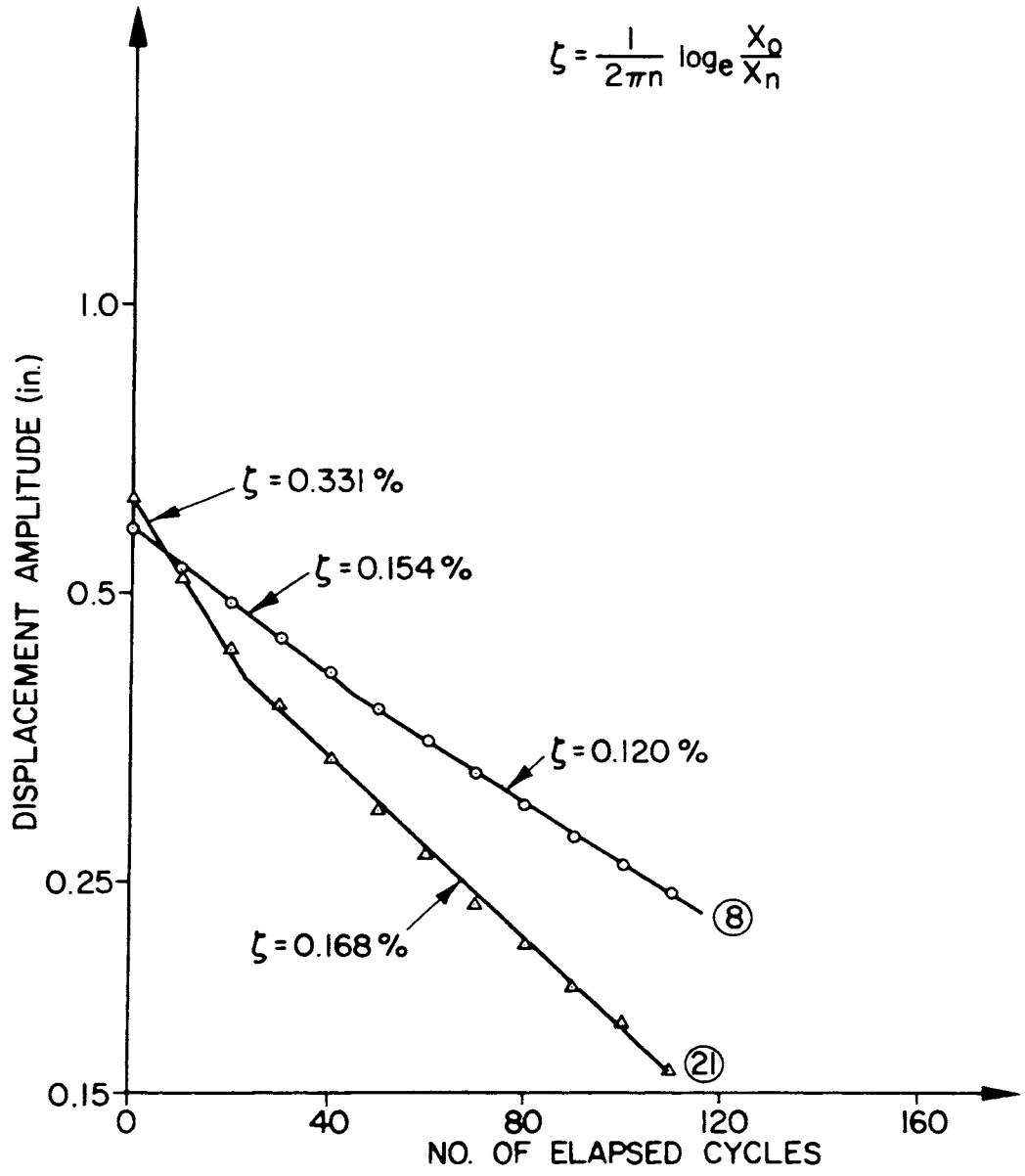

FIG. 3.33 LOGARITHMIC DECAY CURVES: TEST STRUCTURE NO. 7

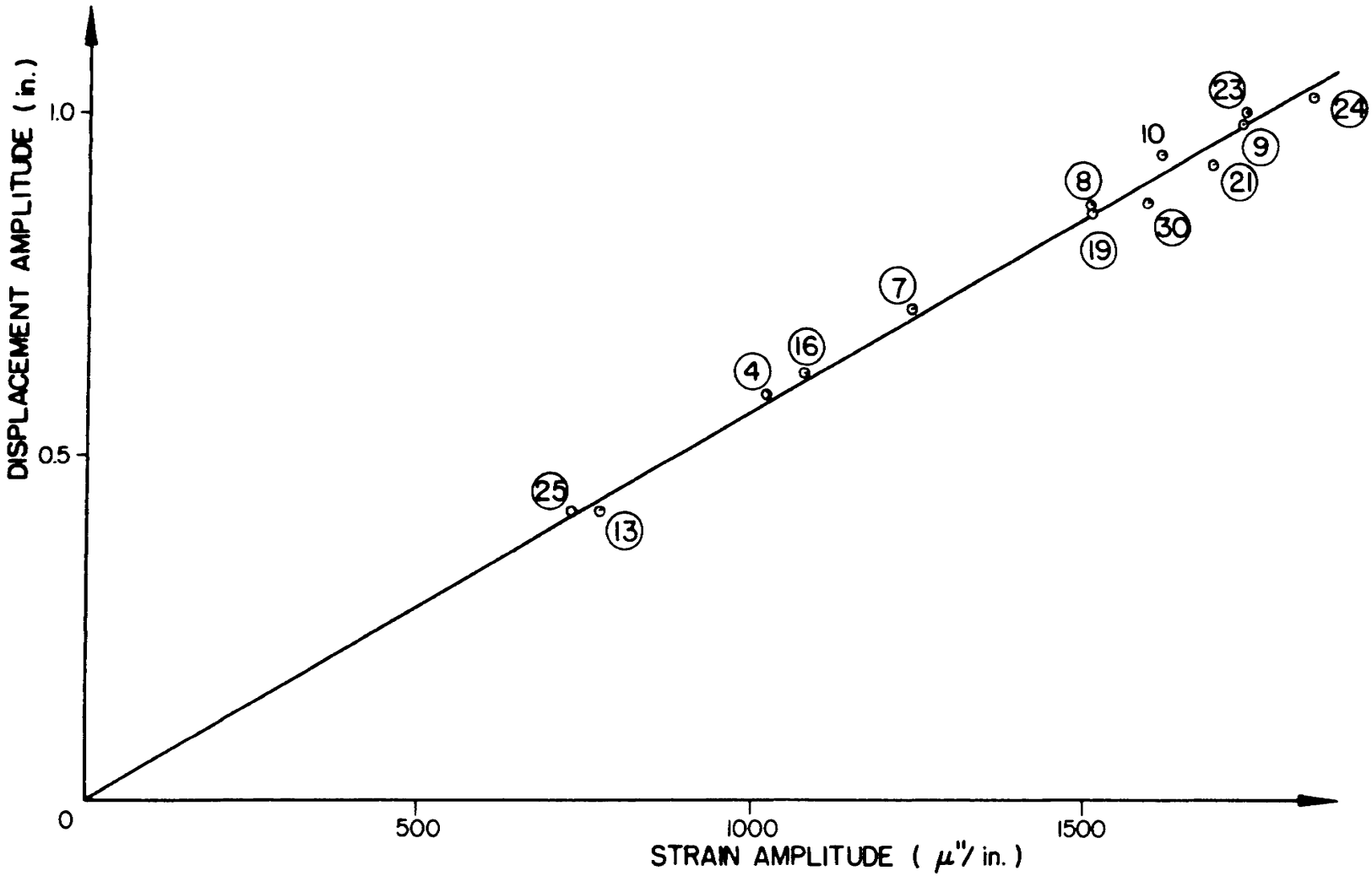

FIG. 4.1 DISPLACEMENT vs. STRAIN AT REDUCED SECTION: TEST STRUCTURE NO.7

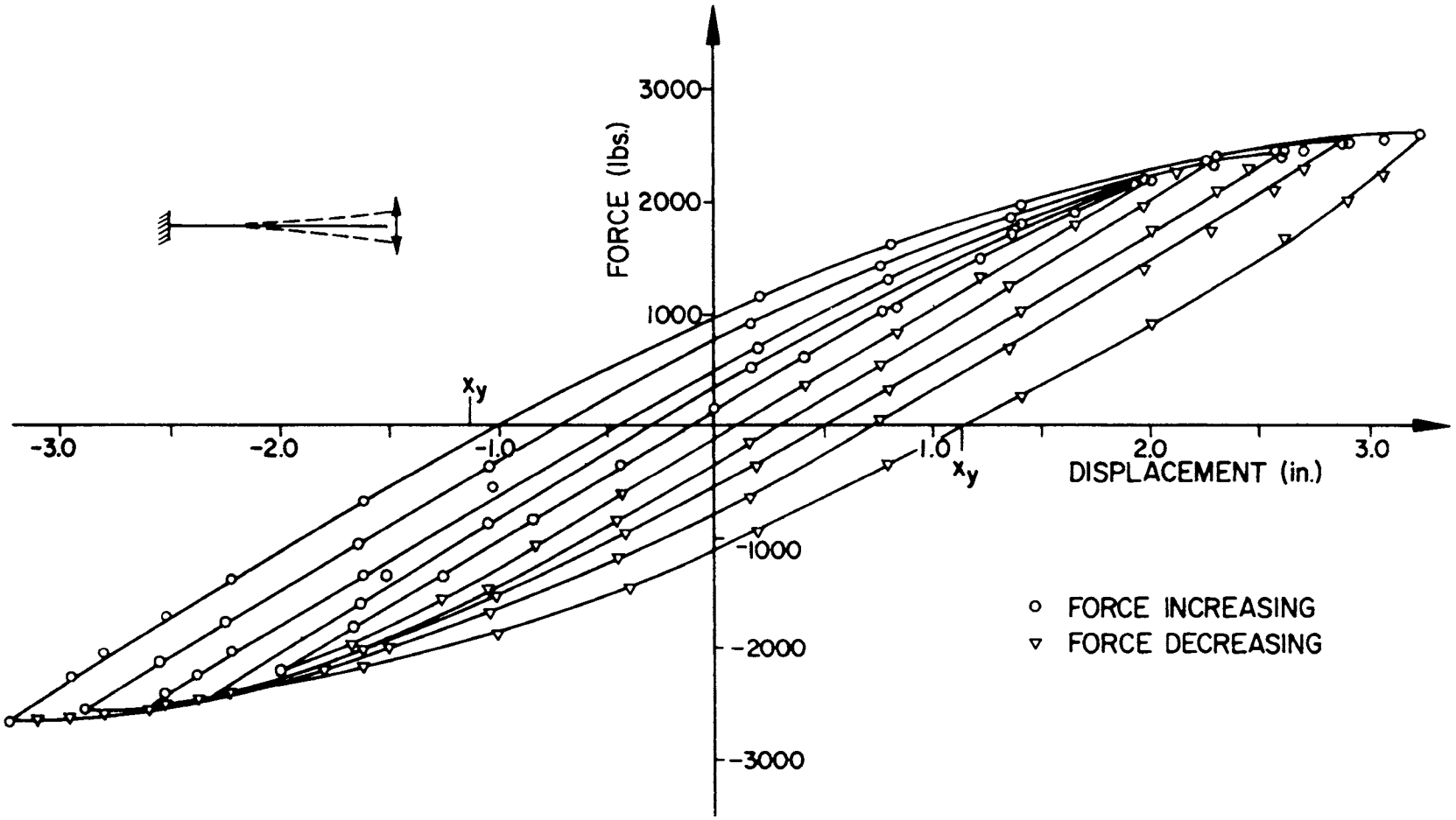

FIG. 4.2 EXPERIMENTAL HYSTERESIS LOOPS FOR COLUMN TYPE B1

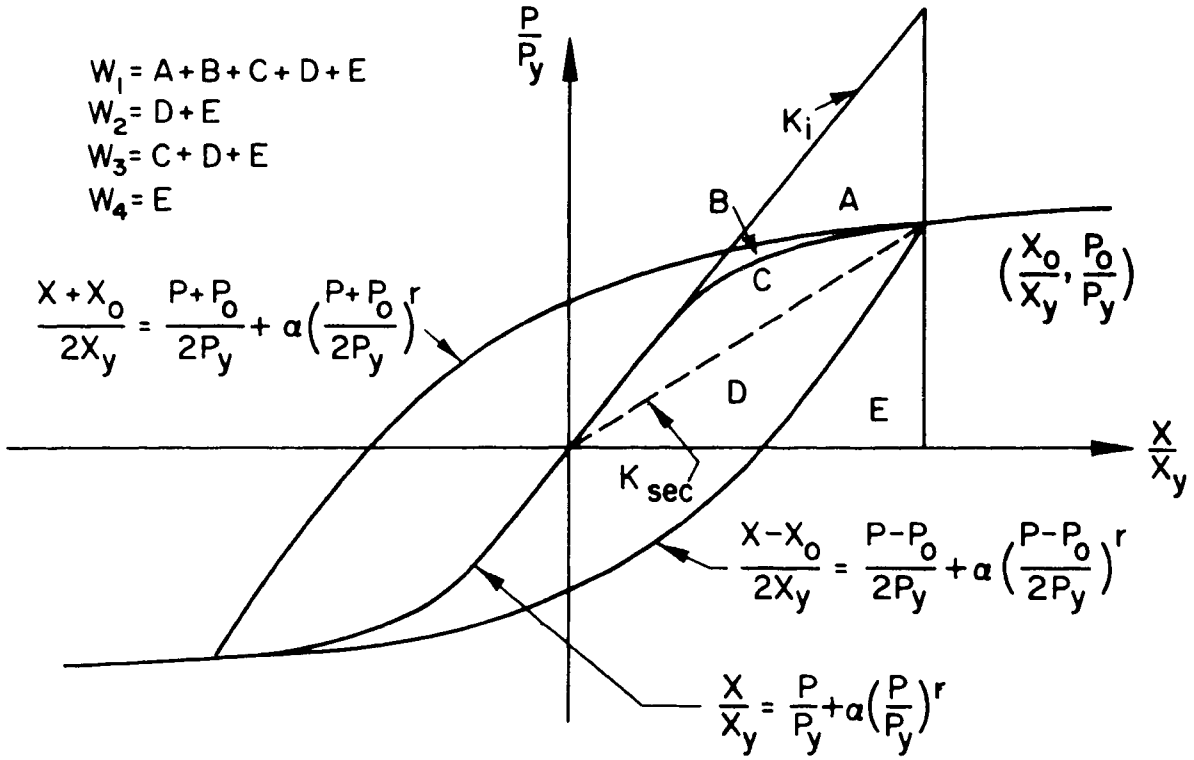

$$\zeta_n = \frac{\Delta W}{4\pi W_n}$$

$$\zeta_1 = \frac{2}{\pi}\left(\frac{r-1}{r+1}\right)\frac{X_y}{X_o}\frac{P_o}{P_y}\left(1-\frac{X_y}{X_o}\frac{P_o}{P_y}\right)$$

$$\zeta_2 = \frac{2}{\pi}\left(\frac{r-1}{r+1}\right)\left(1-\frac{X_y}{X_o}\frac{P_o}{P_y}\right)$$

$$\zeta_3 = \frac{\frac{2}{\pi}\left(\frac{r-1}{r+1}\right)\left(1-\frac{X_y}{X_o}\frac{P_o}{P_y}\right)}{2-\frac{X_yP_o}{X_oP_y}\left[1+\frac{2}{r+1}\left(\frac{X_oP_y}{X_yP_o}-1\right)\right]}$$

$$\zeta_4 = \frac{\frac{2}{\pi}\left(\frac{r-1}{r+1}\right)\left(\frac{X_o}{X_y}\frac{P_y}{P_o}-1\right)}{1+\frac{1}{2^{r-2}(r+1)}\left(\frac{X_oP_y}{X_yP_o}-1\right)}$$

FIG. 4.4 RAMBERG-OSGOOD TYPE FORCE-DEFORMATION RELATIONSHIP AND DIFFERENT DAMPING VALUES

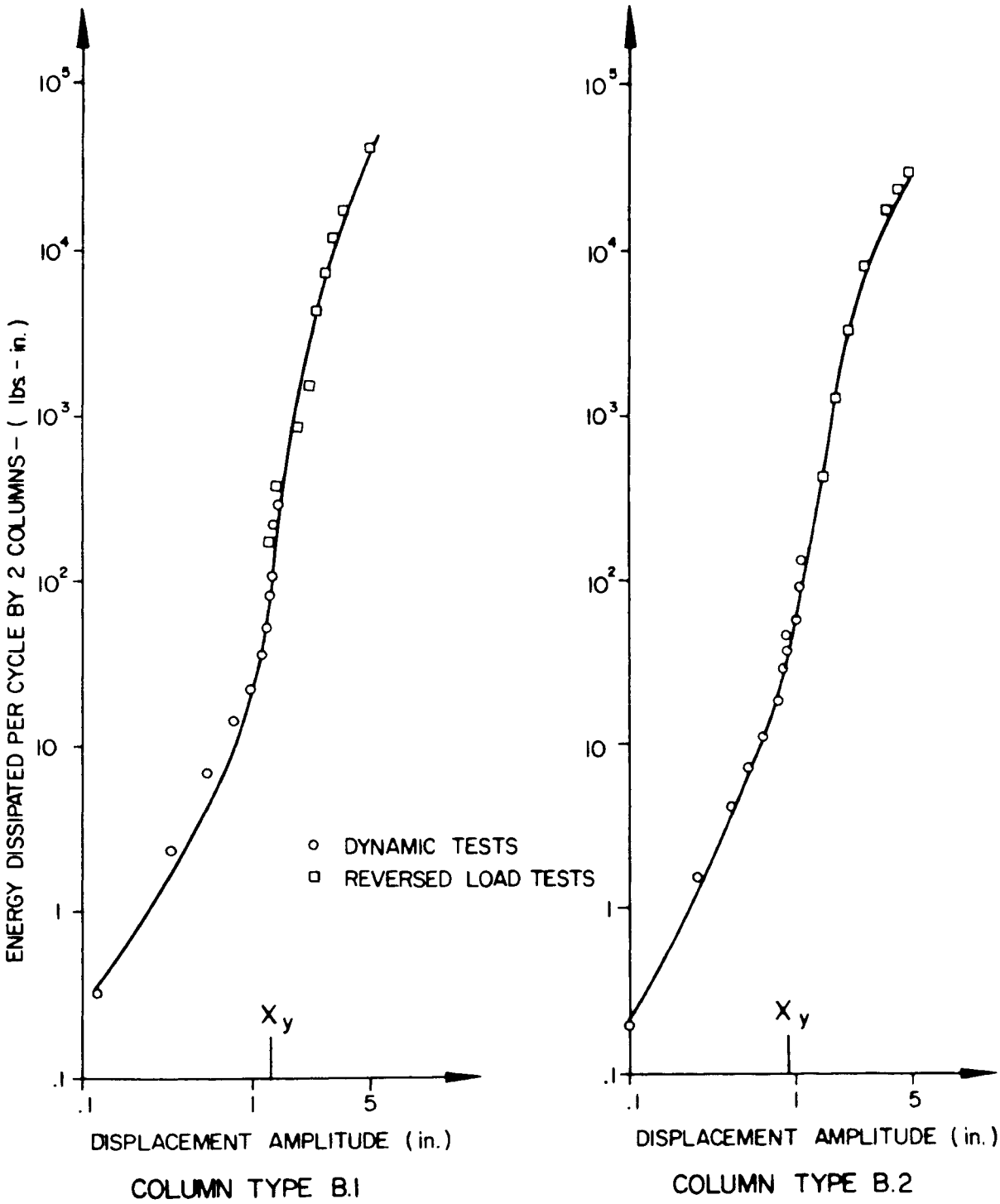

FIG. 4.3 ENERGY DISSIPATED IN REVERSED LOAD TESTS AND DYNAMIC TESTS

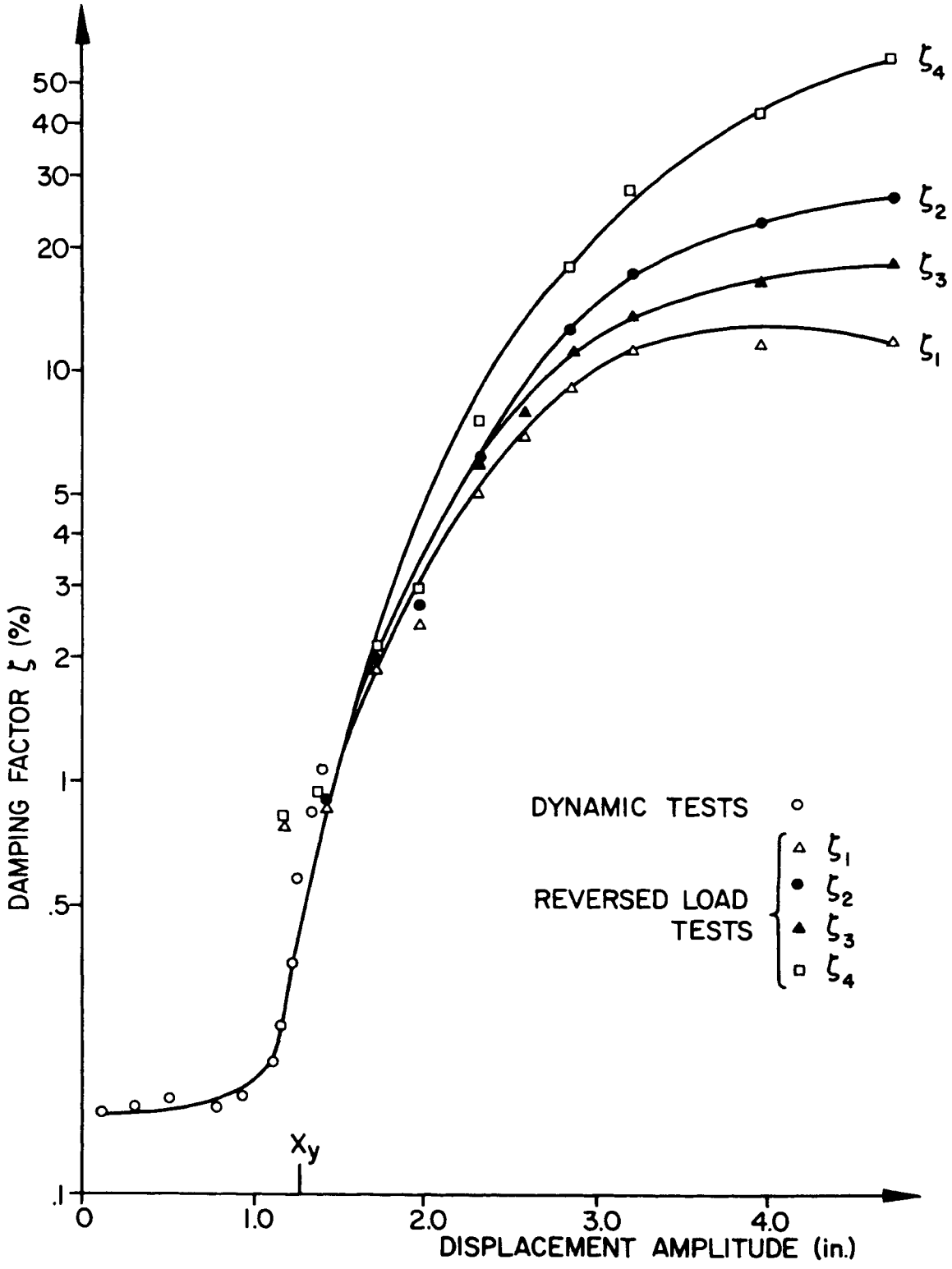

FIG. 4.5 DAMPING FACTORS FOR STRUCTURE NO. 6

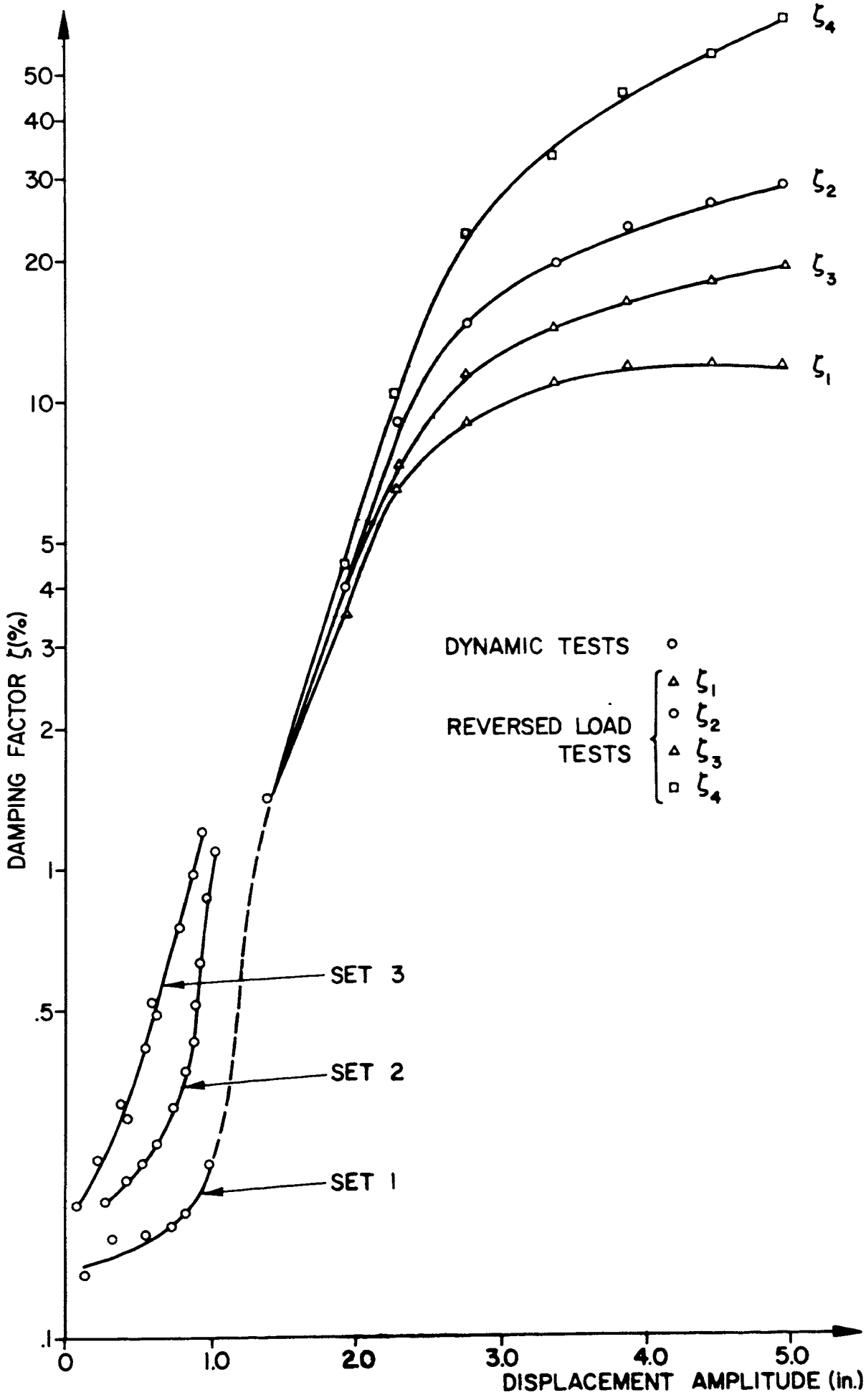

FIG. 4.6 DAMPING FACTORS FOR STRUCTURE NO. 7

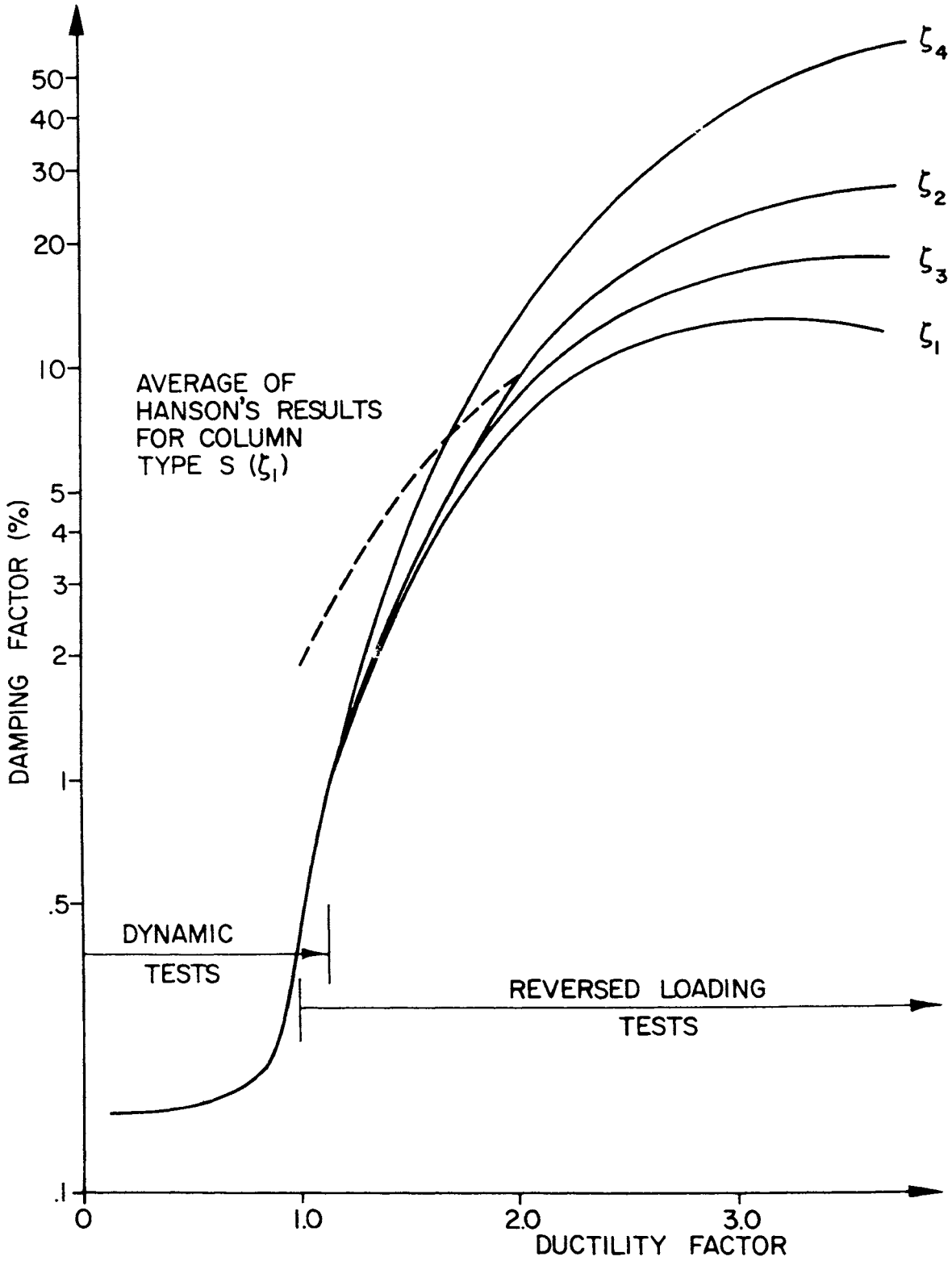

FIG. 4.7 COMPARISON OF DAMPING FACTORS FOR STRUCTURE NO. 6 AND HANSON'S STRUCTURE WITH COLUMNS OF TYPE S

EARTHQUAKE ENGINEERING RESEARCH CENTER REPORTS*

EERC 67-1 "Feasibility Study Large-Scale Earthquake Simulator Facility", by J. Penzien, J. G. Bouwkamp, R. W. Clough, Dixon Rea - September 1967.

EERC 68-1 Unassigned

EERC 68-2 "Inelastic Behavior of Beam-to-Column Subassemblages Under Repeated Loading", by V. Bertero, April 1968.

EERC 68-3 "A Graphical Method for Solving the Wave Reflection-Refraction Problem", by H. D. McNiven and Y. Mengi - April 1968.

EERC 68-4 "Dynamic Properties of McKinley School Buildings", by D. Rea, J. G. Bouwkamp, R. W. Clough - November 1968.

EERC 68-5 "Characteristics of Rock Motions During Earthquakes", by H. B. Seed, I. M. Idriss, F. W. Kiefer - September 1968.

EERC 69-1 "Earthquake Engineering Research at Berkeley", January 1969.

EERC 69-2 "Nonlinear Seismic Response of Earth Structures", by M. Dibaj and J. Penzien - January 1969.

EERC 69-3 "Probabilistic Study of the Behavior of Strucrures During Earthquakes", by P. Ruiz and J. Penzien - March 1969.

EERC 69-4 "Numerical Solution of Boundary Value Problems in Structural Mechanics by Reduction to an Initial Value Formulation", by Nestor Distefano and Jaime Schujman - March 1969.

EERC 69-5 "Dynamic Programming and the Solution of the Biharmonic Equation", by Nestor Distefano - March 1969.

EERC 69-6 "Stochastic Analysis of Offshore Tower Structures", by Anil Kumar Malhotra and Joseph Penzien - May 1969.

EERC 69-7 "Rock Motion Accelerograms for High Magnitude Earthquakes", by H. B. Seed and I. M. Idriss - May 1969.

EERC 69-8 "Structural Dynamics Testing Facilities at the University of California Berkeley", by R. M. Stephen, J. G. Bouwkamp, R. W. Clough, J. Penzien - August 1969.

EERC 69-9 "Seismic Response of Soil Deposits Underlain by Sloping Rock Boundaries", by Houshang Dezfulian and H. Bolton Seed - August 1969.

EERC 69-10 "Dynamic Stress Analysis of Axisymmetric Structures Under Arbitrary Loading", by Sukumar Ghosh and E. L. Wilson - September 1969.

EERC 69-11 "Seismic Behavior of Multistory Frames Designed by Different Philosophies", by James C. Anderson and V. Bertero - October 1969.

EERC 69-12 "Stiffness Degradation of Reinforced Concrete Structures Subjected to Reversed Actions", by V. Bertero, B. Bresler, Huey Ming Liao - December 1969.

EERC 69-13 "Response of Non-Uniform Soil Deposits to Travelling Seismic Waves", by H. Dezfulian and H. B. Seed - December 1969.

EERC 69-14 "Damping Capacity of a Model Steel Structure", by Dixon Rea, R. W. Clough and J. G. Bouwkamp - December 1969.

* All reports are for sale by the Clearinghouse for Federal Scientific and Technical Information, National Bureau of Standards, U. S. Department of Commerce, Springfield, Va. 22151, Price $3.00.

Committee of Structural Steel Producers • Committee of Steel Plate Producers

american iron and steel institute

150 East 42nd Street, New York, N.Y. 10017

(140) PS021

PRINTED IN U.S.A. 171/1